NOKIA MOBILE PHONES

November 16th, 1998

P.O. Box 86
Joensuunkatu 7E
FIN-24101 SALO
Finland

FEDERAL COMMUNICATIONS COMMISSION
Equipment Authorization Branch
7435 Oaklands Mills Road
Columbia, MD 21046

SAR TEST REPORT of Nokia 6185

Gentlemen,

Please find attached SAR test report of FCC ID: GMLNSD-3AX

For and on behalf of Nokia Mobile Phones Ltd.

Respectfully,

Jari Talkara
Engineering Manager, Antennas

Contents

		Page
1.	Description of the measurement	3
2.	Description of calibration by manufacturer	4
3.	List of standards	4
4.	Device list	5
5.	Equipment under test	6
5.1	Verification and results	6
5.2	Specification of Liquid	6
5.3	Specification of position with phone against generic twin phantom	7
5.4	The phone position against generic twin phantom	8
5.5	Results of SAR for 1g	9

Appendix 1	11
Appendix 2	12
Appendix 3	13
Appendix 4	14
Appendix 5	15
Appendix 6	16
Appendix 7	17
Appendix 8	18
Appendix 9	19
Appendix 10	20

1. Description of the measurement

This measurement was done by E-field scanning system for dosimetric assessments. It is robot-based system which allows automated E-field scanning in tissue simulating solutions. The measurements are based on the induced specific absorption rate (SAR) definition of relevant ANSI / IEEE standards. The dosimetric assessment system of Nokia Mobile Phones is manufactured by Prof. Niels Kuster at ETH (Schmid & Partner Engineering AG) in Switzerland, Europe.

The method used to determine the 1 gram average value of SAR is:

Initially a coarse scan is performed over the whole area on a 20 x 20 mm grid. From this coarse scan, the location at which the maximum value is measured is used as the centre for a second, more detailed scan. This second scan is based on a 3 dimensional grid of 4 x 4 x 7 points on a grid of 10 mm for 900 MHz band and grid of 5 x 5 x 7 points on a grid of 8 mm for 1800 MHz band . The average SAR values are computed using the 3D spline inter-polation algorithm. The 3D spline is composed on three one-dimensional splines with the "Not a knot" condition in the x, y and z directions (1), (2). The volume is integrated with the trapezoidal algorithm. 1000 points (10x10x10) are interpolated to calculate the average. All neighbouring volumes are evaluated until no neighbouring volume with a higher average is found.

(1) W. Gander, Computermathematik, Birkhauser, Basel, 1992

(2) W. H. Press, S. A Teukolsky, W. T. Vettering and B. P. Flannery, Numerical Recipes in C, The Art of Scientific Computing, second edition, Cambridge University Press, 1992

2. Description of calibration by manufacturer

The calibration of data acquisition electronics and probe was done by the manufacturer. (Appendix 3 and 7)

- the data acquisition unit is calibrated and tested using a FLUKE 702 Process Calibrator

- measurement uncertainty is less than ± 20% for various tissues simulating solutions and frequencies:
    - these calibration parameters were measured using a temperature probe developed by manufacturer
    - description of the probe calibration and examples of the evaluation are enclosed in Appendix 7

3. List of standards

ANSI/IEEE Std C95.1-1992
IEEE Standard for Safety Levels with Respect to Human Exposure to Radio Frequency Electromagnetic Fields, 3 kHz to 300 GHz

ANSI/IEEE Std C95.3-1992
IEEE Recommended Practice for the Measurement of Potentially Hazardous Electromagnetic Fields-RF and Microwave

4. Device list:

Automated E-field scanning system for dosimetric assessments System.
Calibration due August 1999. Technical data (Appendix 1)

Probe ET3DV4, SN: 1105, Recalibrated due August 1999
Technical data (Appendix 2)

DASY-dosimetric assessment system, DAE V2, SN: 213, Calibration due August 1999 (Appendix 3)

Industrial robot and Control unit, type STÄUBLI CS7 RX 90(CR)
NO:595148-01, Technical data (Appendix 4)

Generic Twin Phantom Version 3 (Appendix 6).

PC COMPAQ 466
laser printer QMS magicolor plus

Devices for preparation of the brain tissue simulating liquids
-General laboratory equipment for preparation of liquids
-Magnetic stirrer with heating plate IKA RET CV, SN:792708
-Scale Mettler Doleto, SN: 2114177678

HP 85070A Dielectric probe system
- network analyzer HP 8753B, SN:2716U00762, Calibration due March 1999
- cables
- probe stand
- dielectric probe kit NO: US33020242
- PC AST PREMMIA 4/66 d
- HP-IB 82335B (interface and software)

Dipole Validation kit for 900 MHz band, Schmid & Partner Engineering AG,
Typ: D900V2, SN: 003, Recalibrated/Verification due August 1999 and
Dipole Validation kit for 1800 MHz band, Schmid & Partner Engineering AG,
Typ: D1800V2, SN: 207, Recalibrated/Verification due August 1999
- signal generator ROHDE & SCHWARZ, 1038.6002.03 , Calibration due July 2000
- power meter, ROHDE & SCHWARZ, 857.8008.02, Calibration due November 1999
- amplifier ZHL-42 (SMA), 022488-RM:4152

5. Equipment under test

Unit: **NOKIA 6185**
FCC-ID: **GMLNSD-3AX**

5.1 Verification and results

Validation of the measurement system was made before measurement using the Validation kit. Appendix: 8 and 9

This validation measurement makes sure that the repeatability of SAR measurement value with careful positioning is better than 10 %.

On 900 MHz band error was < 3 % compared to the parameter of manufacturer SAR results (0.25W): 2.34 mW/g (1g) and 2.39 mW/g (1g).
On 1800 MHz band error was < 13 % compared to the parameter of manufacturer SAR results (0.25W): 9.28 mW/g (1g) and 10.5 mW/g (1g).
Appendix: 8 and 9

5.2 Specification of Liquid

The liquids were done using the "Recipe 900MHz " and "Recipe 1800MHz" for liquid of brain tissue at 900 MHz and 1800 MHz, respectively, and preparation bases on brochure. Appendix 5

900 MHz liquid was used with the 900 MHz validation kit measurement and 1800 MHz liquid was used with the 1800 MHz validation kit measurement.

The parameters was measured by liquid testing of HP85070A Dielectric probe system. The amounts of used liquids were 20 litres.

Liquid parameters εr *(Relative permittivity) and* σ *(Conductivity)* were measured by HP 85070A Dielectric probe system.

900 MHz:	εr	= 41.3	σ	= 0.86
824 MHz:	εr	= 42.1	σ	= 0.79
836 MHz:	εr	= 41.9	σ	= 0.80
849 MHz:	εr	= 41.8	σ	= 0.81
1800 MHz:	εr	= 40.3	σ	= 1.73
1850 MHz:	εr	= 40.1	σ	= 1.75
1880 MHz:	εr	= 40.0	σ	= 1.78
1910 MHz:	εr	= 39.8	σ	= 1.81

5.3 Specification of position with phone against generic twin phantom

The position of the phone relative to the head phantom is shown on page 8. The centre of the phone's earpiece is aligned such that it is co-axial with a mark on the phantom which represents the centre of the ear on the left side of the head.

Measurement was done with a Left-Hand (L.H.) side because the helix phone antenna is situated in the top right corner of the phone (viewed from the earpiece side). Therefore, the antenna is closer to the head in the measurement position using a L.H. side rather than a R.H. side. It is concluded that the L.H. side is worst case measurement position.

The test signal for SAR measurement was analog AMPS and a pulsed mode (TDMA)

The phone position against the head was in Normal phone position (for the IEEE Std C95.1-1991 (ANSI / IEEE) and FCC measurement). The angle between the reference line of the phone and the line connecting both auditory canal opening was 90°. The distance between the handset and the ear area of phantom head is 4 mm (page 8).

The used radio channels on 900 MHz band were: 991, 383 and 799.
The used radio channels on 1800 MHz band were: 25, 600 and 1175.
Peak TX power of analog AMPS and CDMA test signal ("Power" in the table of the paragraph 5.5) was measured from external antenna connector of the transceiver using power level 2. During the tests the battery was fully charged.

Ambient and "brain tissue" liquid temperature was 23 °C ± 1 °C.

5.4 The phone position against generic twin phantom

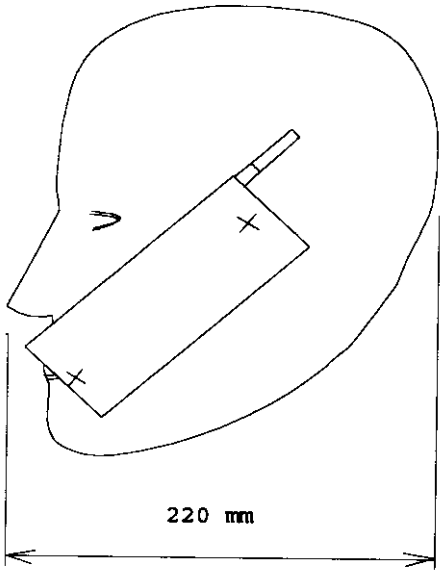

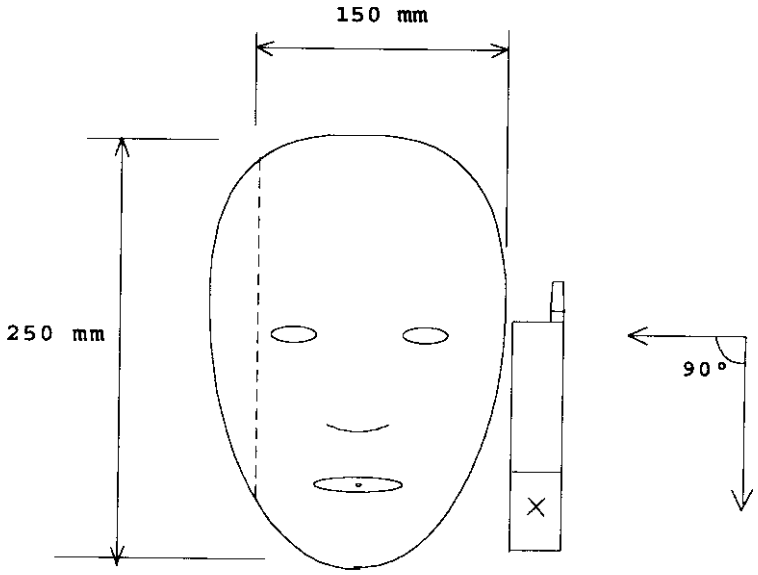

5.5 Results of SAR for 1g.

Appendix: 10

The plots in Appendix 10 are a graphical representation of the SAR values over the whole area being scanned.

Appendix 10, page 10 (nr:10), has sketch of the phone added on the plot for clarifying the position of the phone with respect to the measured SAR values.

The size of the area being scanned is sufficiently large to ensure that all possible regions of peak SAR are measured. This is indicated by the fact that the position of peak SAR is in the measured area, and the value of SAR reduces asymptotically in the x- and y- directions as the probe is moved towards the border of the measured area.

Analog mode AMPS

meas nr:	Phone position	Frequency MHz / channel	Power [dBm]	SAR (1g) [mW/g]
1	90°	824 / 991	25.5	1.24
2	90°	836 / 383	25.5	1.49
3	90°	849 / 799	25.5	1.53
FCC ID: GMLNSD-3AX MEASURED: 16.11.1998 / NMP		FCC limit		1.60 [mW/g] (ANSI/IEEE)

CDMA Cellular

meas nr:	Phone position	Frequency MHz / channel	Power [dBm]	SAR (1g) [mW/g]
4	90°	824 / 991	24.0	0.92
5	90°	836 / 383	24.0	1.02
6	90°	849 / 799	24.0	1.07
FCC ID: GMLNSD-3AX MEASURED: 16.11.1998 / NMP		FCC limit		1.60 [mW/g] (ANSI/IEEE)

CDMA PCS

meas nr:	Phone position	Frequency MHz / channel	Power [dBm]	SAR (1g) [mW/g]
7	90°	1850 / 2	22.5	1.14
8	90°	1880 / 1000	22.5	1.20
9	90°	1909 / 1998	22.5	1.00
FCC ID: GMLNSD-3AX MEASURED: 16.11.1998 / NMP		FCC limit		1.60 [mW/g] (ANSI/IEEE)

Jari Tele
1998-11-16

Appendix 1

pages 1 - 9

AUTOMATED E-FIELD SCANNING SYSTEM FOR DOSIMETRIC ASSESSMENTS

Automated E-Field Scanning System for Dosimetric Assessments

Thomas Schmid, Oliver Egger and Niels Kuster

Swiss Federal Institute of Technology
Zurich, Switzerland

Abstract— **The interest in accurate dosimetric measurements inside phantoms that simulate biological bodies has burgeoned since several regulatory commissions began calling for or recommending the testing for compliance with safety standards of low power devices . This paper presents a newly developed, robot-based system that allows automated E-field scanning in tissue simulating solutions. The distinguishing characteristics of the system are its high sensitivity and its broad dynamic range (1 μW/g to 100 mW/g) over the entire frequency range (10 MHz to over 3 GHz) used for mobile communications. The reproducibility of the dosimetric evaluations has been shown to be considerably better than ± 5%. This has been accomplished by the use of an improved isotropic E-field probe connected to amplifiers with extremely low noise and drift characteristics in conjunction with digital processing of the data. Special emphasis has been placed on system reliability, user-friendliness and graphic visualization of data.**

Keywords—

I. Introduction

The question of whether low power transceivers comply with current safety limits was first raised by Cleveland et al. [1]. Two years later the study of the absorption mechanism in the near field of sources revealed a direct contradiction of the exclusion clause for low power devices with basic safety restrictions [2]. Additional findings of the latter study relevant for this paper were:

- In the close near field, induced currents are mainly caused by the inductive coupling of the high frequency (HF) current distribution on the radiating structure with the biological body.
- The induced specific absorption rate (SAR) depends more on the actual design and the position of the radiating structure with respect to the body than on the inhomogeneity of the tissue.
- Devices with an input power of considerably less than 1 W might violate the basic safety limits for partial body exposure which are: 1.6 mW/g averaged over 1 g (ANSI/IEEE [3]), 2.0 mW/g averaged over 10 g tissue (CENELEC [4]) respectively.

These findings have been confirmed in the following by studies with partially homogeneous bodies exposed to dipole and helix antennas [5], [6] and by a study with largely inhomogeneous head phantoms [7].

Several recently published dosimetric studies on current mobile phones found spatial peak SAR values in the range of the safety limits for uncontrolled environments [8], [9], [10], [11], [12], [13]. Under certain conditions, these limits were exceeded [8], [11], [10], [13]. This caused some concern in the industry as the current trend towards miniaturization with shorter antennas is bound to lead to higher absorption if these issues are not carefully considered during the design process.

Taking various concerns and factors into consideration, individual type approval using dosimetric tests is the most sound approach for both the public as well as industry. As far back as 1992, the German Agency for Radiation Protection [14] recommended type approval for mobile communication devices. The FCC [15] has now taken a similar stance and is calling for the demonstration that the maximum SAR for PCS devices with output power of more than 100 mW complies with the ANSI/IEEE guidelines for SAR values.

Needless to say, such test procedures will lead to decisions with far-reaching economic consequences. It is therefore essential that the testing procedure meets the highest possible standards of accuracy, reproducibility, standardization and availability during the design procedure of new devices. A critical issue is the operating position of the device being tested. In case compliance must be demonstrated for the use of the device under all operational conditions [14], it is not sufficient to test the device by measurement or computation in one particular predefined position (e.g., normal position). Instead, the "worst case" exposure situation among all operational conditions must be tested. This "worst case" exposure situation can only be determined by varying the most relevant parameters such as the position of the device, the operational condition of the device (e.g., extended or retracted antenna), use by left or right handers, variations of head shape and the position of the hand holding the device.

As no system is yet available that satisfies all these requirements, several groups are currently engaged in developing numerical simulation tools or measurement systems for safety assessments of handheld transceivers.

Although anatomical details can now be represented with considerable detail, the numerical approach is fraught with serious difficulties: (1) As today's transceivers have been optimized with regard to size, weight and appearance, simple modelling of the transmitter as a metal box with antenna may not suffice, even if the geometry has been correctly discretized. The reason is that considerable HF currents may flow on internal substructures of the

Author's address: Swiss Federal Institute of Technology (ETH), CH-8092 Zurich, Switzerland – *Submitted to IEEE Transactions on Microwave Technology, January 1995, Accepted in July 1995*

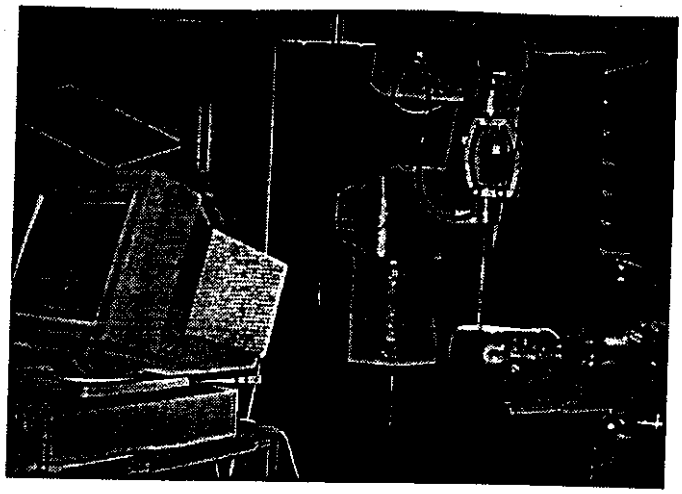

Fig. 1. Laboratory set up including robot, probe, data acquisition electronics, phantom and PC.

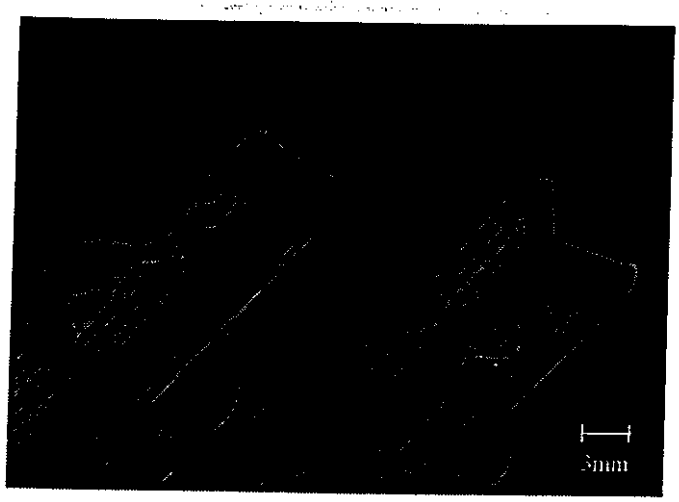

Fig. 2. Tips of the "triangular" (left) and the "rectangular" (right) probes. The tip shell has been removed.

transceivers which, in turn, can induce high SAR values. The HF coupling mechanisms of these internal structures are often not obvious and it can therefore be difficult to arrive at the appropriate numerical modelling. In addition, these effects can undergo considerable changes in the vicinity of the scatterer. (2) If compliance under all operational conditions is required, a number of simulations must be performed, which necessitate techniques that are efficient, largely independent of the grid orientations and which possess self-validating capabilities. (3) It may also be necessary to show that compliance is achieved despite manufacturing variations.

In contrast, an accurate and highly sensitive measurement set up would allow tests of randomly selected samples of a product whereas no modelling or alteration of the product being investigated would be necessary. The position of the device would be easily modified when seeking the worst case conditions. An important difference to numerical simulations is that only the system (including phantom) and not each measurement must be validated. As the location of the strongly local maximum is not known a priori, the SAR distribution in a larger volume of the exposed tissue must be scanned, requiring a large degree of mobility of the probe within the tissue. This in turn, restricts the possible complexity of the phantom.

This paper presents a system that enables the automated measurement of the absorption distribution as well as the assessment of the spatial peak SAR values inside any tissue simulating solution.

II. Laboratory Set Up

The SAR can be determined by measuring either the electric field (E) or the temperature rise ($\partial T/\partial t$) inside the exposed tissue.

$$SAR = \frac{\sigma}{\rho}E^2 = c\frac{\partial T}{\partial t} \qquad (1)$$

where σ is the conductivity, ρ the density and c the specific thermal constant of the tissue at the site of measurement.

In the set up shown in Figure 1, the SAR distribution is determined by measuring the electric field with miniaturized E-Field probes. Measuring the temperature rise in the simulated tissue does not provide sufficient sensitivity for compliance testing of consumer products [11]. However, this technique is used for the validation of the system as well as for the calibration of the probes (see section VIII).

Measurements are done in shell phantoms filled with tissue simulating solution. In the laboratory three types of shell phantoms are used:

- geometrically simple phantoms for calibration and numerical validation of the system
- simplified body and head phantoms to simulate worst-case conditions of exposure with real devices
- very detailed phantoms to investigate the effects of different tissue layers (skin, living bone, air cavities, etc.), different exposure conditions (device positions, hand effect, spectacle frames, etc.) and to validate the simplified phantoms.

The E-field probes are positioned by a 6-axis precision robot (Stäubli RX90) inside shell phantoms with a working range greater than 0.9 m and with a position repeatability that is better than ±0.02 mm (at constant temperature). Each probe incorporates an optical surface-detecting system, which permits the accurate positioning of the probe with respect to the phantom's surface. Basically the SAR distribution in any volume can be measured. The currently implemented compliance test involves firstly measuring the SAR on a coarse 3D-grid in a preselected volume. Afterwards a fine 3D-grid around the previously detected maximum is measured. The 1g or 10g-average SAR-values are interpolated from the fine-grid results. The procedure is completely automated and takes less then 15 minutes, which is well within the battery lifetime of standard communication devices.

III. Isotropic E-Field Probes

The most crucial components of the whole system are the E-field probes. The main requirements are:

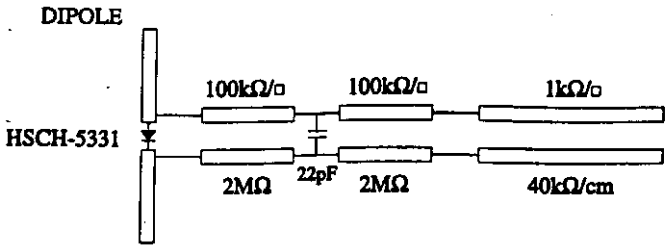

Fig. 3. Equivalent circuit representation of the probe.

- high sensitivity and linear response over a broad frequency range
- high spatial resolution
- isotropy in differing media
- low interaction with the measured field
- small in size

For optimal performance under different measuring conditions, two types of E-Field probes have been developed. The design with the triangular core (Figure 2) was selected for dosimetric measurements in liquids with high permittivity because of the smaller outline and the possibility of placing the surface detector in the center of the probe. The "rectangular" design (Figure 2) with one dipole parallel to the probe axis enables the separation of the field vector components corresponding to the coordinates of the probes, i.e., parallel and normal to the probe axis. This results in better omnidirectivity, especially in low-epsilon media [16]. However, the probe has an asymmetric core and a slightly bigger profile.

Each probe consists of three small dipoles (3mm) directly loaded with a schottky diode and connected with resistive lines to the data acquisition unit. The theory of this type of probe has been discussed previously in various publications (e.g., in [17]). While these papers describe the probe's characteristics by modelling the components (dipole-diode-line), they do not discuss the influence of the dielectric supporting materials of the probe, which can completely distort the theoretical dipole-characteristics. To further improve the directivity of the probes, special attention has been paid to these constructional problems.

A. Problem 1: Secondary Modes of Reception

An important part of most antenna design is to suppress secondary reception modes produced by the connecting lines, constructional asymmetries, etc. In the probes described above there are several possible secondary reception modes. One is produced by normal mode signals coupled into the resistive lines and rectified in the diode. These signals can be reduced by decreasing the spacing between the lines or by filtering techniques. Another mode is produced by common mode signals coupled into the lines and converted at the diode into normal mode signals by asymmetrical loading of the dipole halves due to constructional asymmetries (especially when measuring in the immediate proximity of metallic structures). As the source impedances of these modes have high resistive components, they are negligible at higher frequencies where the (mainly capacitive) impedances of the antenna and diode are much

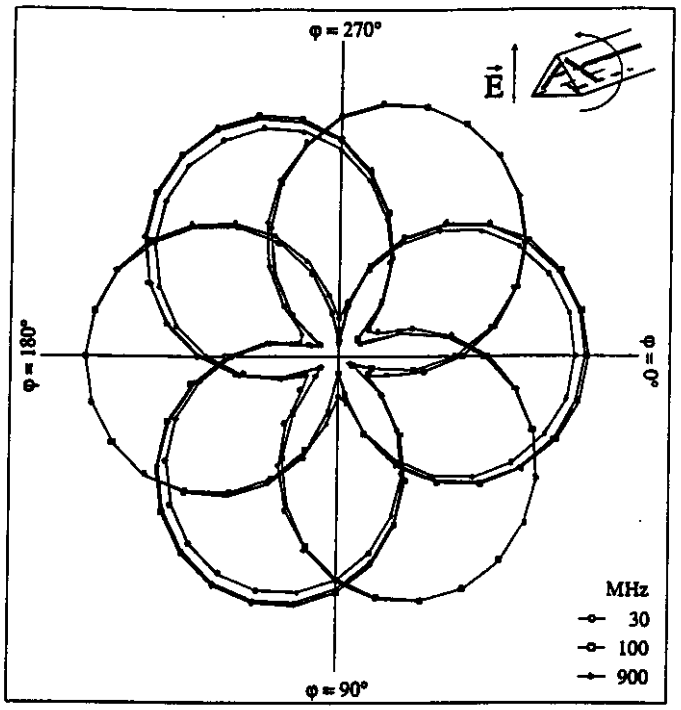

Fig. 4. Directivity diagram of the new probe in thick-film technique with the E-field normal to the probe axis. Measured using the TEM cell (ifi110) between 10 MHz and 900 MHz.

lower. At lower frequencies, however, these modes can become dominant and distort the ideal antenna characteristics (see Figure 5).

Other electromagnetic fields present in the laboratory can also be the source of such secondary signals, especially ELF fields produced by power lines or robot control signals. A carefully designed laboratory grounding system has proven to be of great importance for high probe sensitivity.

In order to suppress these modes and make the probe useful for frequencies down to 10 MHz, a distributed filter was introduced between the dipole and the resistive line (see Figure 3).

The thick-film technique was employed for the construction of the dipole and lines instead of the normally used thin-film technique. This permits the use of lines with different sheet resistances on the same substrate, and the production of much higher sheet resistances than manufacturable with the thin-film technique. Since the thick film layers are printed using silk screening, the structures are much coarser than those of thin-film probes.

In Figure 4 the directivity diagram normal to the probe axis of the "triangular" probe is shown between 10 MHz and 900 MHz. For comparison, Figure 5 shows the same diagram of the well known E-Field probe in thin film technology (50 μm line spacing and width) described in [17]. Apparently, the performance degeneration caused by direct coupling effects between dipole and line (TEM cell ifi110) could be significantly reduced by this new approach.

The high resistive decoupling of the diode from the detector circuit has another desired effect. The diode impedance has less influence on the timing characteristic of the detec-

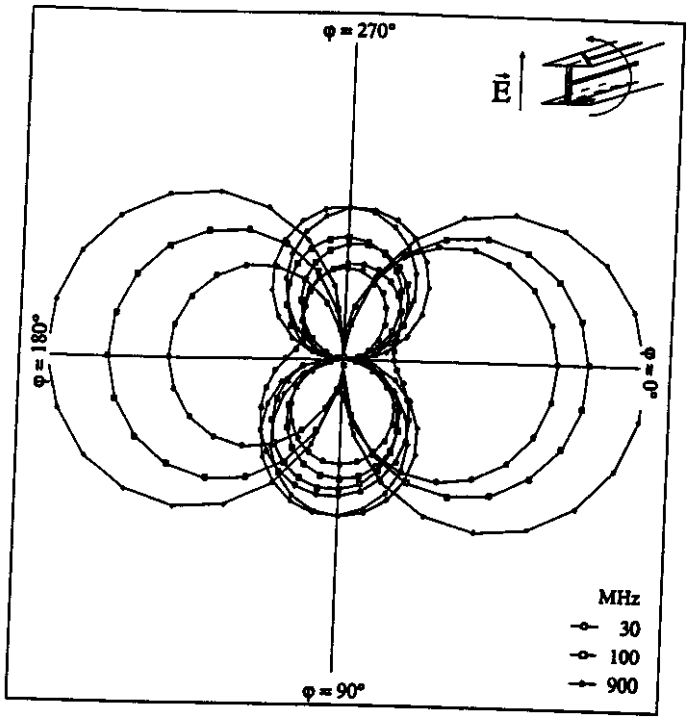

Fig. 5. Directivity diagram of the standard probe in thin-film technique with the E-field normal to the probe's axis. Measured using the TEM cell between 10 MHz and 900 MHz.

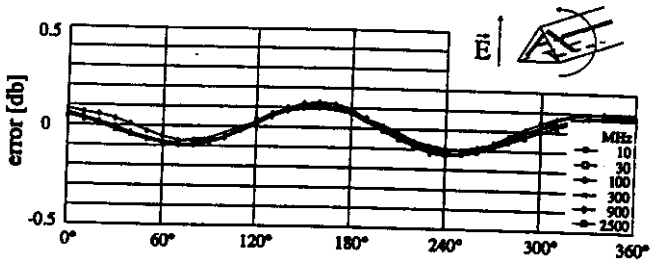

Fig. 6. Deviation from isotropy of the probe with triangular design in air, whereby the E-field was rotated in a plane normal to the probe axis. Measured using the TEM cell (ifi110) between 10 MHz and 900 MHz and the waveguide R26 at 2500 MHz.

tor circuit. This prevents the usual "peak detector characteristic" of diode detector probes for pulsed signals. In Figure 13, the rms response of this approach is tested for duty cyles of up to 100.

B. Problem 2: Influence of the Probe Materials on the Field

Any dielectric material around electric dipoles will have an effect on the local signal strength. It is obvious from the construction of these probes that the influence on E-field components normal to the probe axis will be different to those on E-Field components parallel to the probe axis. Furthermore, this difference in sensitivity depends on the surrounding media. This results in poor isotropy in planes that include the probe axis.

Figures 6 and 7 shows the deviation from isotropy of the probe with triangular design in air and brain simulating solution in a plane normal to the probe axis and in a plane through the probe axis, respectively.

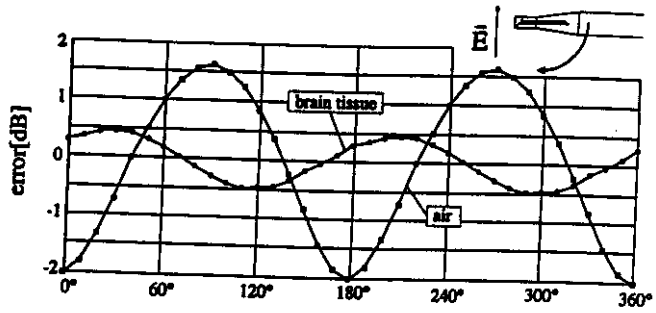

Fig. 7. Deviation from isotropy of the probe with triangular design in air at 2500 MHz (above an open waveguide R26) and in brain tissue equivalent solution (900MHz), whereas the E-field was rotated in a plane through the probe axis.

It can be clearly seen that the component of the E-field in the direction of the probe axis in air is much stronger than the component normal to the probe axis, while in solutions with high permittivity this effect is reversed, but to a much lesser extent. While this probe works well in solutions which simulate the electric properties of tissues with high water content, it proves to be unusable in air (unless the polarization of the E-Field is known in advance and the probe placed accordingly, i.e., normal to the field). This problem can be overcome in the following ways:

- By selecting material for construction with the same characteristics as the surrounding media. As such material must be easily mechanically processible, no such materials for air or for biological tissue are available.
- By adjusting the angular orientation of the dipoles in order to compensate for the different sensitivities along and normal to the probe axis. It follows that such a probe would only be usable in a single surrounding media.
- Another approach is to compensate for these effects by numerically weighting the dipole-signal input according to the field orientation with respect to the probe extension. This is only possible if the component of the E-field along the probe axis can be separated, i.e., if one of the probe's dipoles is aligned along the probe axis. This has been successfully accomplished in the "rectangular" design which is described in [16] (see also Figure 2). By simply introducing a media-dependent conversion factor for the signal of the component along the probe axis, the isotropy in air is better than ±0.5 dB in all directions and for all polarizations.

The probe with the triangular design was selected for dosimetric measurements for the following reasons:

- There was slightly better isotropy in planes normal to the probe axis due to the high degree of constructional symmetry in this plane.
- The slightly weaker isotropy in the other planes in solutions with high water content is not a significant drawback. The reason being that the components of the E-field along the probe axis, i.e., normal to the phantom surface, have been shown to be significantly smaller than components in other directions. This has

been predicted in [2] and is demonstrated in Figures 8 and 9. Hence, the maximum error introduced by this lack of isotropy is much less than the deviation of ±0.6 dB in Figure 7.

- The fact that the dipole orientation differs from the probe orientation is not a disadvantage because only the total field is of interest in dosimetric applications.
- The high degree of constructional symmetry improves the efficiency of the described filtering method for secondary reception modes. The frequency response at frequencies below 100 MHz is better than in the probe with the "rectangular" design.
- The triangular design is very compact and ensures a high spatial resolution. The distance between the dipole centers is less than 2 mm.
- The surface detection system (see Section V) is positioned in the center of the probe. This ensures excellent positioning accuracy even when the probe is not normal to the phantom surface.

C. Problem 3: Influence of the Probe on Inhomogeneous Fields

The disturbance caused by the probe on inhomogeneous fields depends not only on the probe material and geometry but also largely on the field itself. The influence of these effects must be investigated in each case. Figure 14 shows the results of SAR measurements in brain simulating solution near the shell of the phantom.

If the distance between the probe tip and surface of the phantom is less than 1 mm, the field distribution inside the probe tip differs due to short circuiting between the probe and the outside media, i.e., the measured values become too high. This error source is greater than the error caused due to scattering effects by the probe at the interface [18]. The problem can be solved by measuring the SAR at different distances from the surface and extrapolating the SAR values to the surface. (This extrapolation procedure is also necessary because of the separation of the dipole center from the probe tip).

Another source of error in inhomogeneous fields arises from the spacing between the dipole centers in the probe. Because each field component is measured at a slightly different location, discrepancies are to be expected where field magnitudes or directions change rapidly within the probe's dimensions. Because of the nature of the absorption mechanism [2], the field gradients induced by mobile phones operating at frequencies below 3 GHz have larger dimensions than the probe's diameter.

IV. Probe Construction

The probe consists of a two-shell construction. The core which holds the ceramic substrate is made entirely of the synthetic microwave material (STYCAST 0005) with a permittivity of 2.54 and a loss tangent of 0.0005. The tip of the outer shell is made of the same material and the main outer shell is made of common PMMA tubing. The core is centered at the tip and held in place with a spring at the connector end. A slight deformation of the outer shell does not effect the fragile core. The probe can be dismantled for repair. Between the core and the outer shell a sheet of very high resistivity is introduced to neutralize static charges on the exterior of the probe or in the measuring set up. The distance between the probe tip and the dipole center is 2.7 mm.

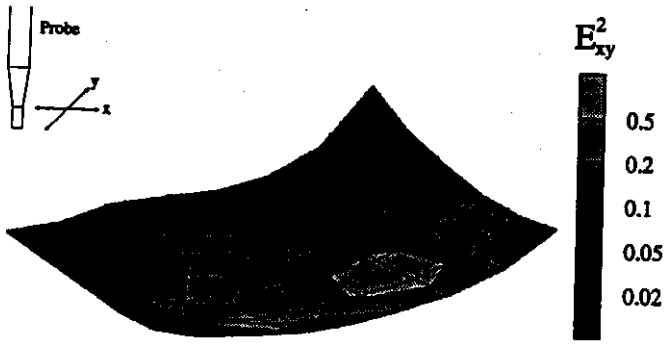

Fig. 8. Distribution of the SAR component normal to the probe axis in the shell phantom measured with a commercial mobile phone.

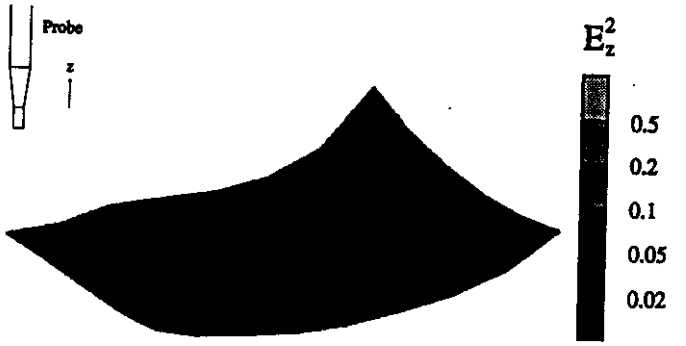

Fig. 9. Distribution of the SAR component in the shell phantom parallel to the probe axis measured with a commercial mobile phone.

The probe is connected with a precision 7-terminal connector to the acquisition unit. The counter part in the acquisition unit is flexibly mounted. If excess force is applied to the probe, the probe will give way and a touch detection logic in the acquisition unit will immediately stop the robot. A dielectric tube over the probe connector holds the probe flexibly at a second point 8 cm from the connector. This ensures very high accuracy in the positioning of the probe tip at all probe angles.

V. Surface Detection

The surface detection system included in the probes consists of an optical multifiber line. Half of the fibers are pulsed by an infrared LED, the other half are connected to a synchronized receiver. An object in the correlation area of the two fiber ends causes a coupling between transmitting and receiving fibers. When the probe is moved towards the surface, the reflected signal increases until it reaches a maximum approximately 1.2 mm from the surface, from where it decreases until the probe touches the surface. The location of the maximum is independent of the surface reflectivity and largely independent of the angle between the probe and the surface (see Figure 10). The complete set up gives a positioning accuracy of the probe

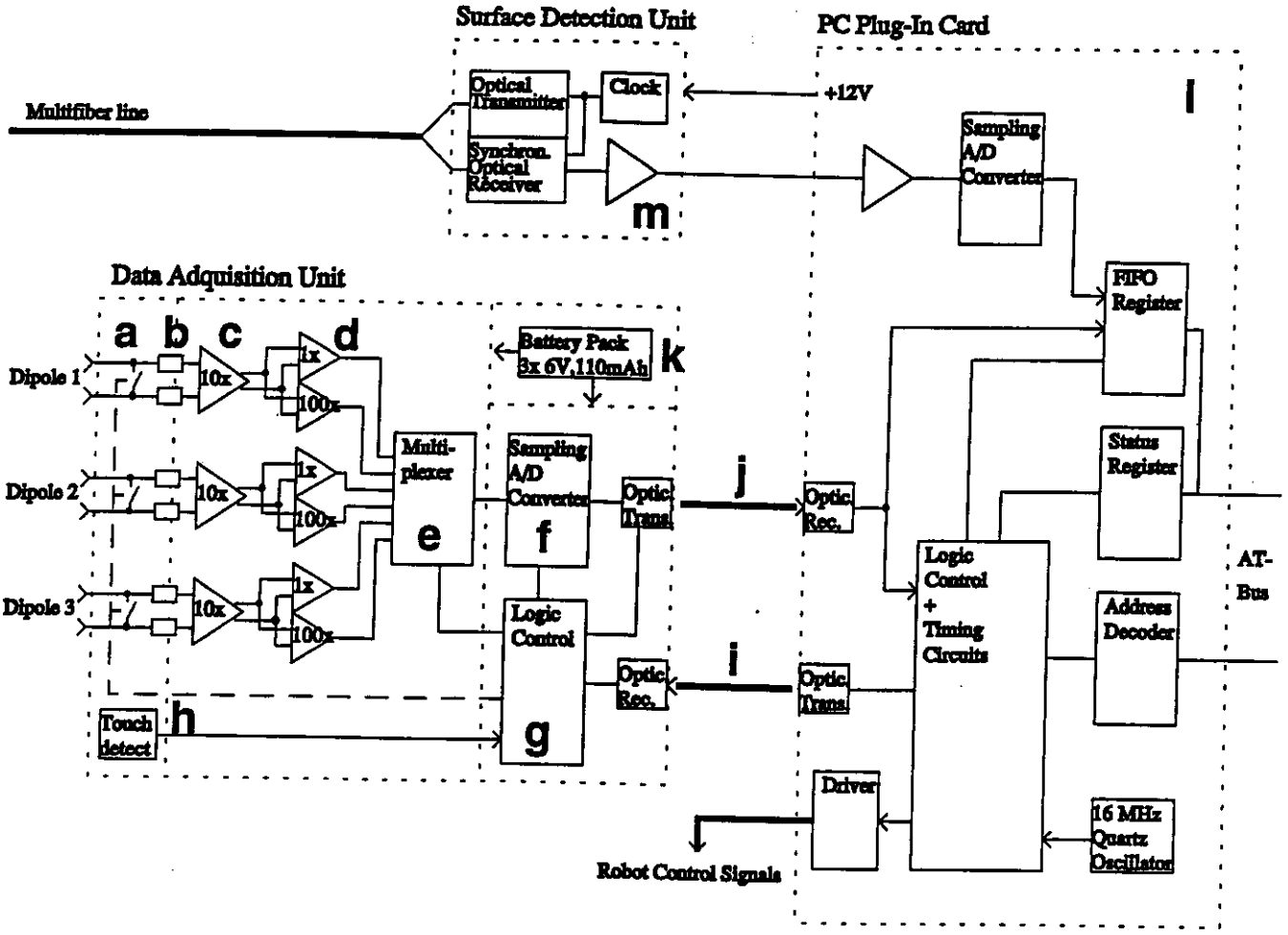

Fig. 11. Block diagram of the data acquisition hardware.

with respect to the surface of ±0.2 mm.

VI. Data Acquisition Electronics

The improved probe characteristics were obtained at the cost of increased demands on the signal amplifier. The probes have source impedances of 5 to 8 MΩ due to the high resistive lines and the decoupling filters. The rectified signals range from 1μV to 200 mV. High noise signals (especially induced signals from power lines) are to be expected.

The first unit of the data acquisition system is housed in a metal box of dimensions 68 x 57 x 46mm, is battery powered and is connected with fiber-optic links to the main data evaluation system. The system can therefore be used in situations where telemetric measurements are necessary.

Figure 11 shows the block diagram of the data acquisition system.

a. Pulse relays with low thermal voltage (<0.5 μV) for offset calibration.
b. Input filter to prevent HF-signals passing to the amplifier and being rectified in input nonlinearities.
c. Electrometer grade differential input amplifier (<0.1 pA bias current).
d. Second stage instrumentation amplifier with x1 / x100 gain.
e. Multiplexer to switch between channels and gain.
f. Fast 16 bit sampling AD-converter with serial output.
g. Control logic for power down mode, calibration cycle, channel selection, gain selection.
h. Touch logic with asynchronous transmission of touch state signal to instantly stop the robot's movement.
i. Optical up-link with 1 MHz clock, synchronization and control signals.
j. Optical down-link with serial data and state signals (low battery, touch, channel address,etc.).
k. Rechargable battery pack for 5 hours of operation.
l. Computer plug in card with main timing unit, data conversion of the serial E-Field data and state signals, data acquisition of the analog signal from the surface detection amplifier and fast digital link to the robot.
m. Optical transmitter/receiver for the surface detection system.

VII. Software

For ease and speed of measurements, a program has been written in C^{++} under Windows, to perform all involved tasks: Data acquisition, surface detection, robot control, administration of all calibration parameters of the system, evaluation and visualization of the measured data. Complex measuring tasks are available at the push of a button.

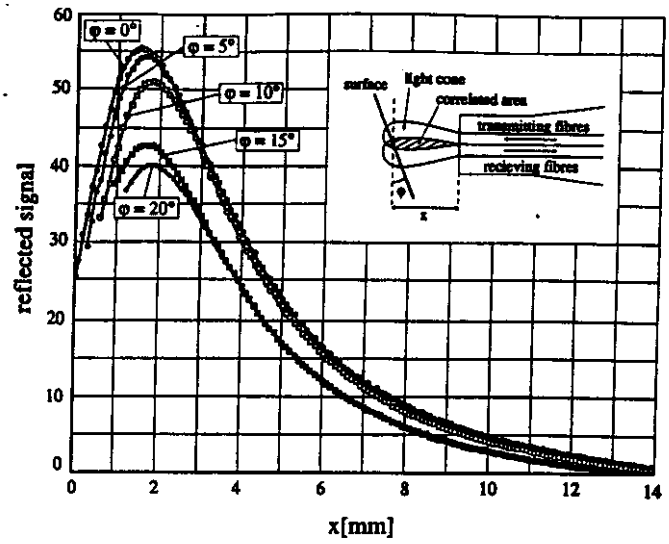

Fig. 10. Response of the surface detector as a function of the distance (x) from the surface.

A. Robot Control

The robot is completely controlled by the PC and its movements can be monitored on the screen. Some program modules are downloaded to the robot computer for faster response times.

Several measuring options permit complete measurements in user defined volumes, planes or along lines with or without surface detection. The measuring process is displayed on the screen. The filtered raw data from the data acquisition system is stored in data files together with all the calibration parameters. If a measurement is made with false parameters, it is possible to correct the parameters in the file and reevaluate the data.

B. Data Processing

The data acquisition system samples 7800 data sets per second, i.e., 2600 complete field measurements per second for 3D probes. The program reads and filters the incoming data during the measuring or surface detection cycles. Depending on the received signal strength, the program switches the gain of the amplifier unit and launches calibration cycles accordingly. The program calculates an accuracy estimate of the filtered signal and stops the measuring cycle upon reaching the desired accuracy. The measuring time per grid point (always a multiple of the power line period) varies with the desired accuracy and the received signal-to-noise ratio.

Figure 12 shows the deviation from linearity in function of the signal strength in V/m and the equivalent SAR values for brain tissue. The line with the empty symbole show the values before and those with the dark symbole those after numerical compensation of the diode compression. For low signal strengths, the measuring time was 10 seconds, for stronger signals 1 second.

Because of the low cutoff frequency the system cannot follow pulsed HF signals, but provides an average value of the rectified signal. As long as the signal strength stays

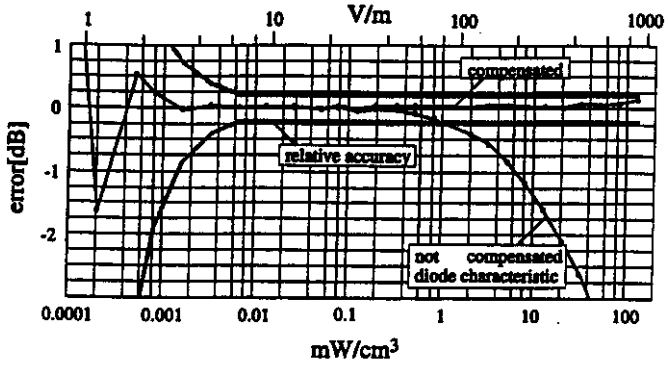

Fig. 12. Deviation from linearity. The line with the dark symbols are the values after compensation of the diode compression. The data was obtained from measurement at 900 MHz in the TEM cell (ifi 110).

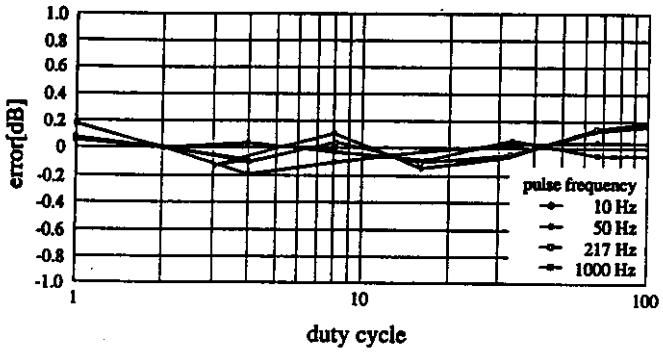

Fig. 13. Measured error between CW and pulsed signals with pulse frequencies between 10Hz and 1kHz and duty cycle between 1 and 100. Reference was a HP437B peak power meter.

within the square law range of the detector diode, the reading is the average of the absorbed power. If the peak signal strength is higher, the compression of the diode must be compensated. This is done automatically by the evaluation software depending on the duty cycle parameter. The system then calculates the peak power, compensates for the diode compression and gives the new average value.

Figure 13 shows the measured error between CW and pulsed signals with pulse frequencies between 10Hz and 1kHz and duty cycle between 1 and 100.

C. Data Visualization

The program evaluates the raw data with the calibration parameters and can produce two-dimensional or three-dimensional graphical output with interpolated isolines in different units (μV of rectified signal, V/m, SAR, power flow density, etc.). The total field strength of each of the dipole components can be separately plotted. SAR values can be numerically integrated over 1 g or 10 g of simulated tissue. Evaluated data can be exported to other file formats. Figures 8 and 9 demonstrate one of the various implemented graphical visualizations.

VIII. Calibration and Validation of the System

The system can be easily calibrated for air in known fields (far field of antennas or in TEM cells and wave

TABLE I

SYSTEM SPECIFICATIONS WITH ISOTROPIC E-FIELD.

frequency range	10 MHz to > 3 GHz	
dynamic range in tissue simulating solutions	1 μW/g to 100 mW/g	
linearity	< ±0.2 dB	
deviation from isotropy in tissue(triangular probe)		
- normal to probe axis	± 0.2 dB	probe.
- in all planes, all polarizations	± 0.8 dB	
variation with frequency	< ± 0.2 dB	
spatial resolution of SAR measurements	< 0.125 cm^3	
reproducibility of probe positioning	< ± 0.2mm	

Note: The rather large deviation from isotropy in all planes scarcely affects the accuracy of dosimetric assessments if the probe is positioned predominantely normal to the phantom surface.

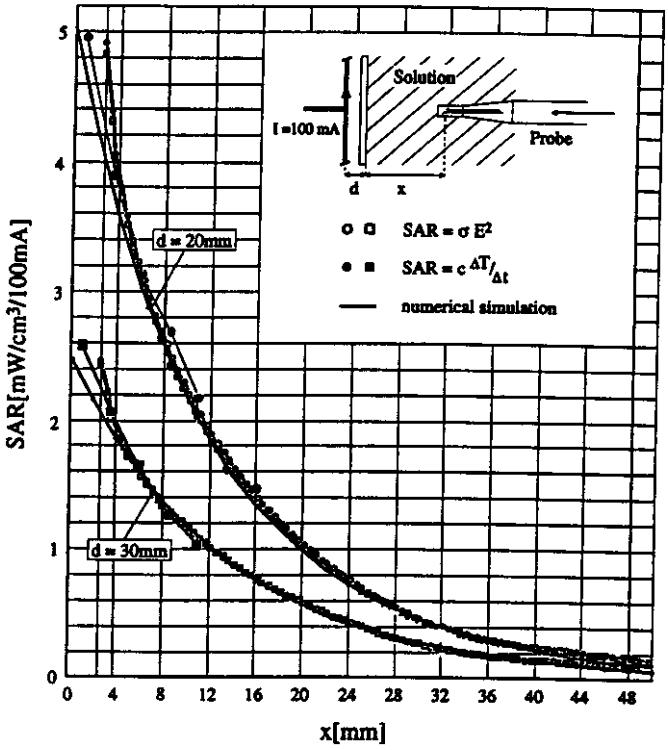

Fig. 14. Comparison of SAR values obtained by numerical simulation, measured temperature rise and E-field measurements for the same set up (plane phantom exposed to a half wave 900 MHz dipole parallel to the phantom's surface). The phantom was filled with brain equivalent solution (ϵ_r = 44, σ = 1.1 mho/m). All values are normalized to an antenna feedpoint current of 100 mA.

guides). In solutions, however, a conversion factor must be introduced to account for the different sensitivities of the probes in the solution. This conversion factor was obtained by comparing the measured values with those from numerical simulations. The simple set up was already used in [2] and consists of a standard half wave dipole below a half plane phantom.

To validate the result, the same set up was used with a 100 W amplifier and temperature measuring equipment. The fiber optical temperature probes have a diameter of less than 0.5 mm allowing true point measurements. However, high power is required because of the rather low sensitivity (> 10 mW/g). Figure 14 shows the results of the three evaluation methods at different distances from the transmitting dipole and the probe from the bottom of the phantom.

IX. CONCLUSION

The developed measurement system is a flexible, automated, time-efficient tool to assess SAR distributions in tissue simulating solutions. It is especially suited for compliance testing of handheld or body mounted devices with specific safety standards. Tests have shown an excellent reproducibility of the integrated peak SAR values of well within ±5% even when changing the starting measuring grid. The specifications of the system can be summarized as in Table I.

Although the main emphasis is now on the open phantom issue, several improvements are anticipated. For instance, extension of the system for general near field measurements used in antenna design, EMI, EMC.

ACKNOWLEDGEMENTS

The development of this scanning system was supported by the Federal Ministry of Posts and Telecommunications (Germany), Deutsche Telekom (Germany), Swiss Telecom PTT (Switzerland) and Mannesmann GmbH (Germany). The authors gratefully acknowledge the help of Mr. Klaus Meier, Mr. Martin Schmid, Mr. Jeroen de Keijzer, as well as valuable advice of Dr. Quirino Balzano and Mr. Oscar Garay.

REFERENCES

[1] Robert F. Cleveland and Whit T. Athey, "Specific absorption rate (SAR) in models of the human head exposed to hand-held UHF portable radios", *Bioelectromagnetics*, vol. 10, no. 1, pp. 173–186, Jan. 1989.

[2] Niels Kuster and Quirino Balzano, "Energy absorption mechanism by biological bodies in the near field of dipole antennas above 300 MHz", *IEEE Transactions Vehicular Technology*, vol. 41, no. 1, pp. 17–23, Feb. 1992.

[3] ANSI/IEEE C95.1-1991, *IEEE Standard for Safety Levels with Respect to Human Exposure to Radio Frequency Electromag-*

netic Fields, 3 kHz to 300 GHz, The Institute of Electrical and Electronics Engineers, Inc., New York, NY 10017, 1992.

[4] CENELEC CLC/SC111B, *Draft European Prestandard (prENV 50166-2, Human Exposure to Electromagnetic Fields High-Frequency : 10 kHz - 300 GHz*, CENELEC, Brussels, 1993, Draft, September, 1994.

[5] Niels Kuster, "Multiple multipole method for simulating EM problems involving biological bodies", *IEEE Transactions on Biomedical Engineering*, vol. 40, no. 7, pp. 611–620, July 1993.

[6] Niels Kuster, "Multiple multipole method applied to an exposure safety study", in *ACES Special Issue on Bioelectromagnetic Computations*, A.H.J. Fleming and K.H.Joyner, Eds., vol. 7, pp. 43–60. Applied Computational Electromagnetics Society, No. 2, 1992.

[7] Peter J. Dimbylow, "Finite-difference time-domain calculations of SAR in a realistic heterogeneous model of the head for plane-wave exposure from 600 MHz to 3 GHz", *Phys. Med. Biol.*, vol. 38, no. 12, pp. 361 – 368, 1993.

[8] Niels Kuster, Thomas Schmid, and Klaus Meier, "Untersuchungen der Absorption im extremen Nahfeld von Sendern", in *VDE-Fachbericht 45: Biologische Wirkungen elektromagnetischer Felder*, pp. 135–143. Verband Deutscher Elektrotechniker (VDE), Nov. 1993.

[9] Om P. Gandhi, J-Y. Chen, and D. Wu, "Electromagnetic absorption in the human head for cellular telephones", in *Proc. of the 14th Annual Meeting of the Bioelectromagnetic Society*, Copenhagen, Denmark, June 1994.

[10] Peter J. Dimbylow and S.M. Mann, "SAR calculations in an anatomically realistic model of the head for mobile communication transceivers at 900 MHz 1.8 GHz", *Phys. Med. Biol.*, vol. 39, no. 12, pp. 1537–1553, 1994.

[11] Klaus Meier, Oliver Egger, Thomas Schmid, and Niels Kuster, "Dosimetric laboratory for mobile communication", in *Proc. of the 9th Symposium on Electromagnetic Compatibility*, Zürich, Mar. 1995.

[12] A.H.J. Fleming, "A numerical estimate of SAR levels in a heterogeneous model of the head due to exposure by a mobile phone", in *Proc. of the 14th Annual Meeting of the Bioelectromagnetic Society*, Copenhagen, Denmark, June 1994.

[13] Michael A. Jensen and Yahya Rahmat-Samii, "EM interaction of handset antennas and a human in personal communications", *Proceeding of the IEEE*, vol. 83, no. 1, pp. 7–17, Jan. 1995.

[14] Strahlenschutzkommission,
"Empfehlung der Strahlenschutzkommission verabschiedet auf der 107. Sitzung am 12./13. Dezember 1991", in *Schutz vor elektromagnetischer Strahlung beim Mobilfunk*, SSK, Ed., pp. 3–18. Gustav Fischer Verlag, 1992.

[15] Federal Communication Commission, "Amendment of the commission's rules to establish new personal communication services", Tech. Rep. FCC 94-144, FCC, Washington, D.C. 20554, 1994.

[16] Thomas Schmid and Niels Kuster, "Near field scanning system", *IEEE Transactions on Microwave Theory and Techniques*, vol. 0, no. 0, pp. 000–000, Jan. 1995.

[17] Howard I. Bassen and Glen S. Smith, "Electric field probes – a review", *IEEE Transactions on Antennas and Propagation*, vol. 31, no. 5, pp. 710–718, Sept. 1983.

[18] Glen S. Smith, "The E-field probe near a material interface with application to the probing of fields in biological bodies", *IEEE Transactions on Microwave Theory and Techniques*, vol. 27, no. 3, pp. 270–278, Mar. 1979.

Appendix 2

pages 1 - 8

PROBE ET3DV4 SN: 1105

Schmid & Partner
Engineering AG

Staffelstrasse 8, 8045 Zurich, Switzerland, Telefon +41 1 280 08 60, Fax +41 1 280 08 64

Probe ET3DV4

SN:1105

Manufactured:	May 1995
Calibrated:	July 1997
Recalibrated:	August 1998

Calibrated for System DASY2

Introduction

The performance of all probes is measured before delivery. This includes an assessment of the characteristic parameters, receiving patterns as a function of frequency, frequency response and relative accuracy. Furthermore, each probe is tested in use according to a dosimetric assessment protocol. The sensitivity parameters (NormX, NormY, NormZ), the diode compresion parameter (DCP) and the conversion factor (ConvF) of the probe and some of the measurement diagrams are given in the following.

The performance of the individual probes varies slightly due to tolerances arising from the manufacturing process. Since the lines are highly resistive (several MOhms), the offset and noise problem is greatly increased if signals in the low μV range are measured. Accurate measurement below 10 μW/g are possible if the following precautions are taken. 1) check the current grounding with the *multimeter*[1], i.e., low noise levels, 2) compensate the current *offset*[1], 3) use long integration time (approx. 10 seconds), 4) *calibrate*[1] before each measurement, 5) persons should avoid moving around the lab while measuring.

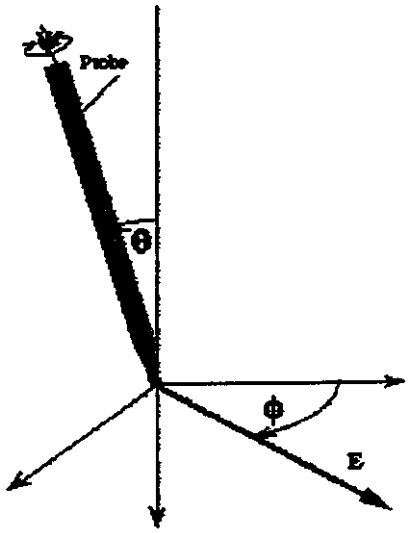

Fig. 1: Due to the field distortion caused by the supporting material, the probe has two characteristic directions, referred to as angle ψ and θ.

Since the field distortion caused by the supporting material and the sheath is quite high in the θ direction, the receiving pattern is poor in air. However, the distortion in tissue equivalent material is much less because of its high dielectricity. In addition, the fields induced in the phantoms by dipole structures close to the body are dominently parallel to the surface. Thus, the error due to non-isotropy is much better than 1 dB for dosimetric assessments.

The probes are calibrated in the TEM cell ifi 110 although the field distribution in the cell is not very uniform and the frequency response is not very flat. To ensure consistency, a strict protocol is followed. The conversion factor (ConF) between this calibration and the measurement in the tissue simulation solution is performed by comparison with temperature measurements and computer simulations. This conversion factor is only valid for the specified tissue simulating liquids at the specified frequencies. If measurements have to be performed in solutions with other electrical properties or at other frequencies, the conversion factor has to be assessed by the same procedure.

As the probes have been constructed with printed resistive lines on ceramic substrates (thick film technique), the probe is very delicate with respect to mechanical shocks.

Attention:

Do not drop the probe or let the probe collide with any solid object. Never let the robot move without first activating the emergency stop feature (i.e., without first turning the data acquisition electronics on).

[1] Feature of the DASY2 Software Tool.

DASY2 - Parameters of Probe: ET3DV4 SN:1105

Sensitivity in Free Space

NormX	1.51	$\mu V/(V/m)^2$
NormY	1.57	$\mu V/(V/m)^2$
NormZ	1.41	$\mu V/(V/m)^2$

Diode Compression

DCP X	41000	μV
DCP Y	41000	μV
DCP Z	41000	μV

Sensitivity in Tissue Simulating Liquid

450 MHz	ConvF X	6.6	extrapolated	ε_r = 48 ± 5%
	ConvF Y	6.6	extrapolated	σ = 0.50 ± 10% mho/m
	ConvF Z	6.6	extrapolated	(brain tissue simulating liquid)
900 MHz	ConvF X	6.0	± 10%	ε_r = 42.5 ± 5%
	ConvF Y	6.0	± 10%	σ = 0.86 ± 10% mho/m
	ConvF Z	6.0	± 10%	(brain tissue simulating liquid)
1500 MHz	ConvF X	5.3	interpolated	ε_r = 41 ± 5%
	ConvF Y	5.3	interpolated	σ = 1.32 ± 10% mho/m
	ConvF Z	5.3	interpolated	(brain tissue simulating liquid)
1800 MHz	ConvF X	4.9	± 10%	ε_r = 40.5 ± 5%
	ConvF Y	4.9	± 10%	σ = 1.659 ± 10% mho/m
	ConvF Z	4.9	± 10%	(brain tissue simulating liquid)

Sensor Offset

Probe Tip to Sensor Center	2.7	mm
Surface to Probe Tip	1.4 ± 0.2	mm

Receiving Pattern (ϕ), θ = 0°

f = 30 MHz, TEM cell ifi110

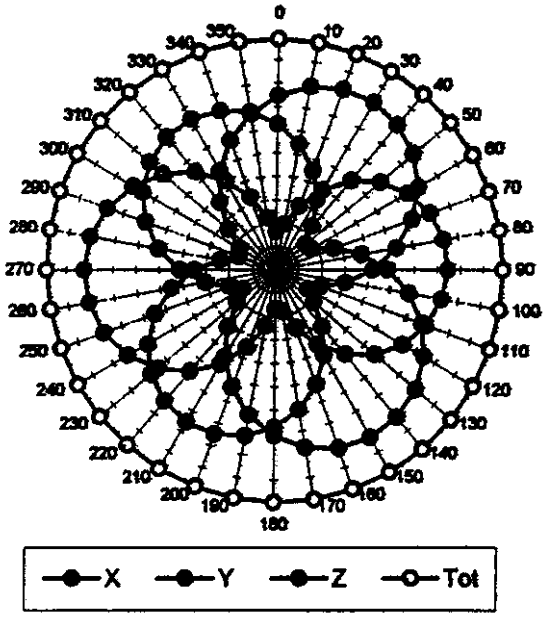

f = 100 MHz, TEM cell ifi110

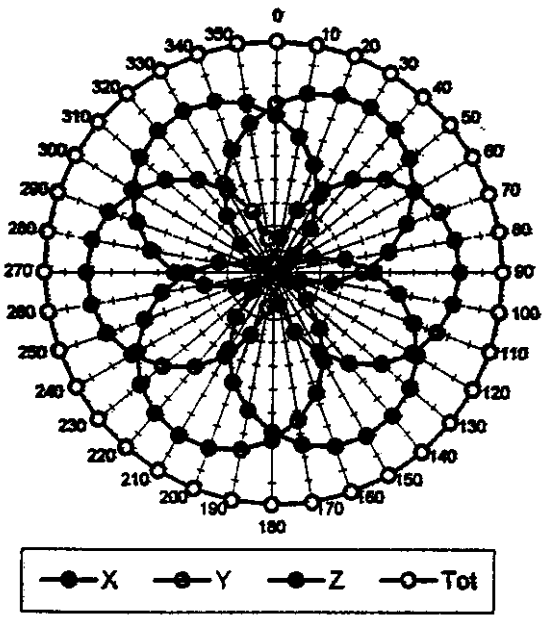

f = 300 MHz, TEM cell ifi110

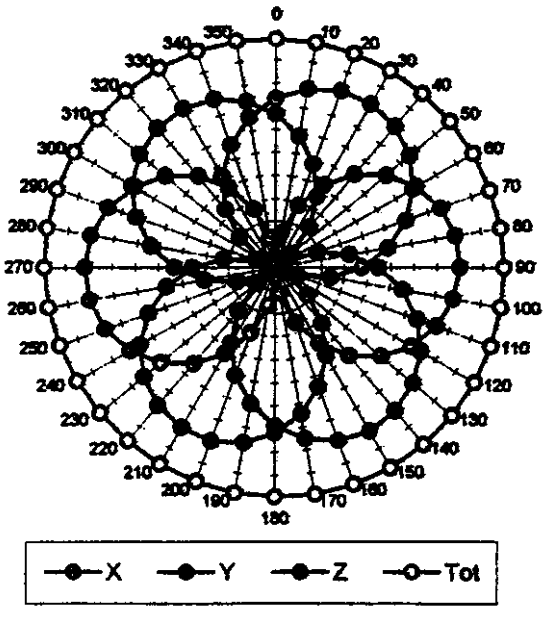

f = 900 MHz, TEM cell ifi110

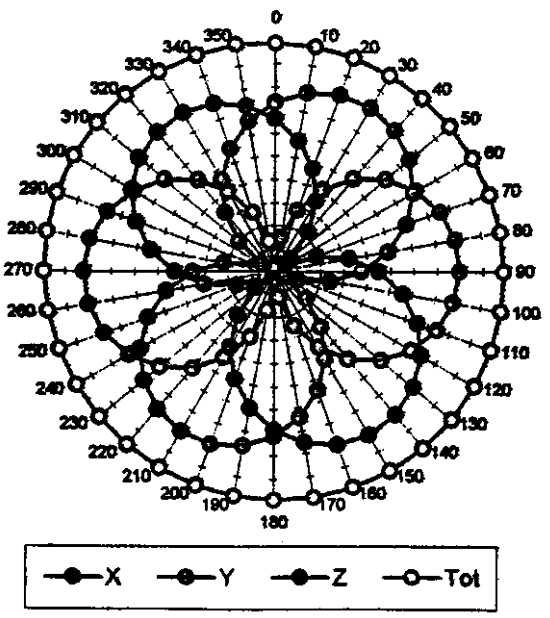

ET3DV4 SN:1105

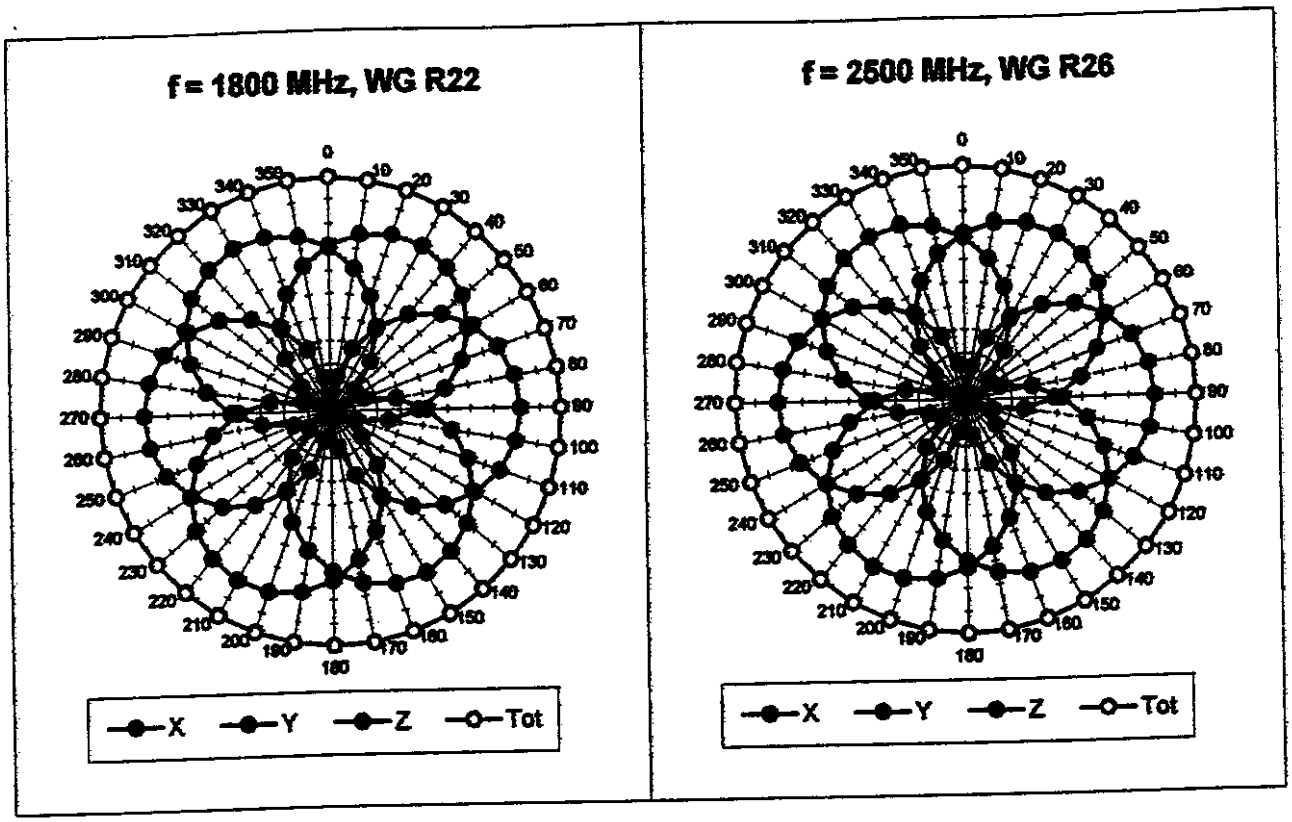

Isotropy Error (ϕ), θ = 0°

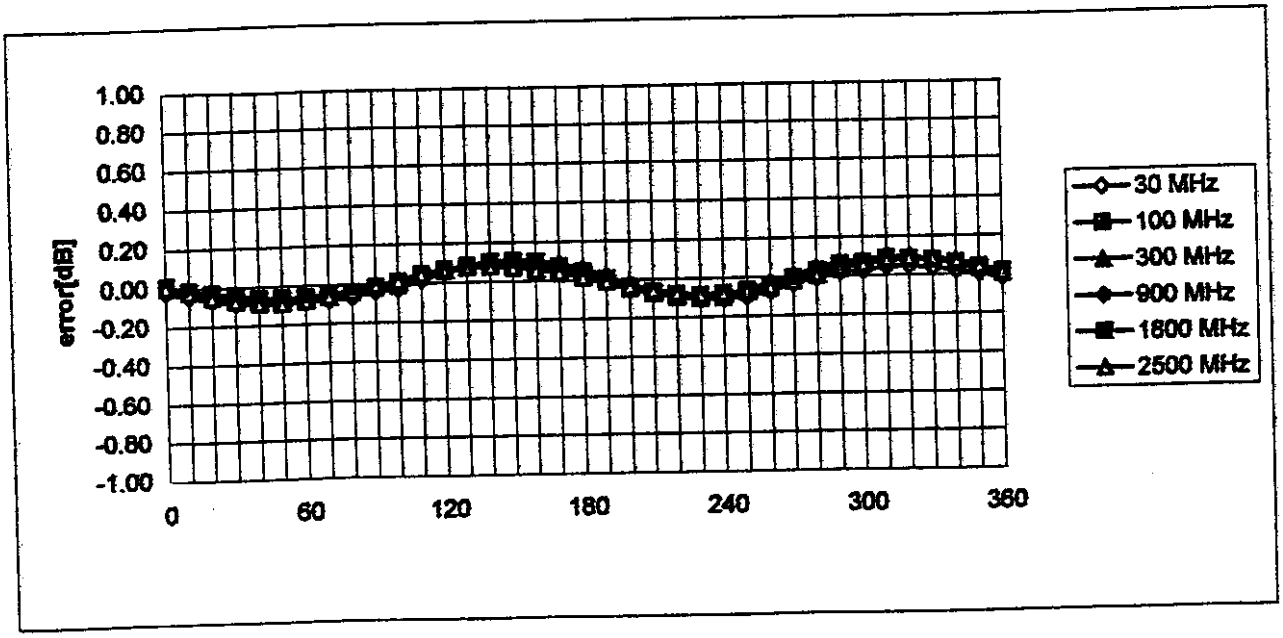

Frequency Response of E-Field

(TEM-Cell:ifi110, Waveguide R22, R26)

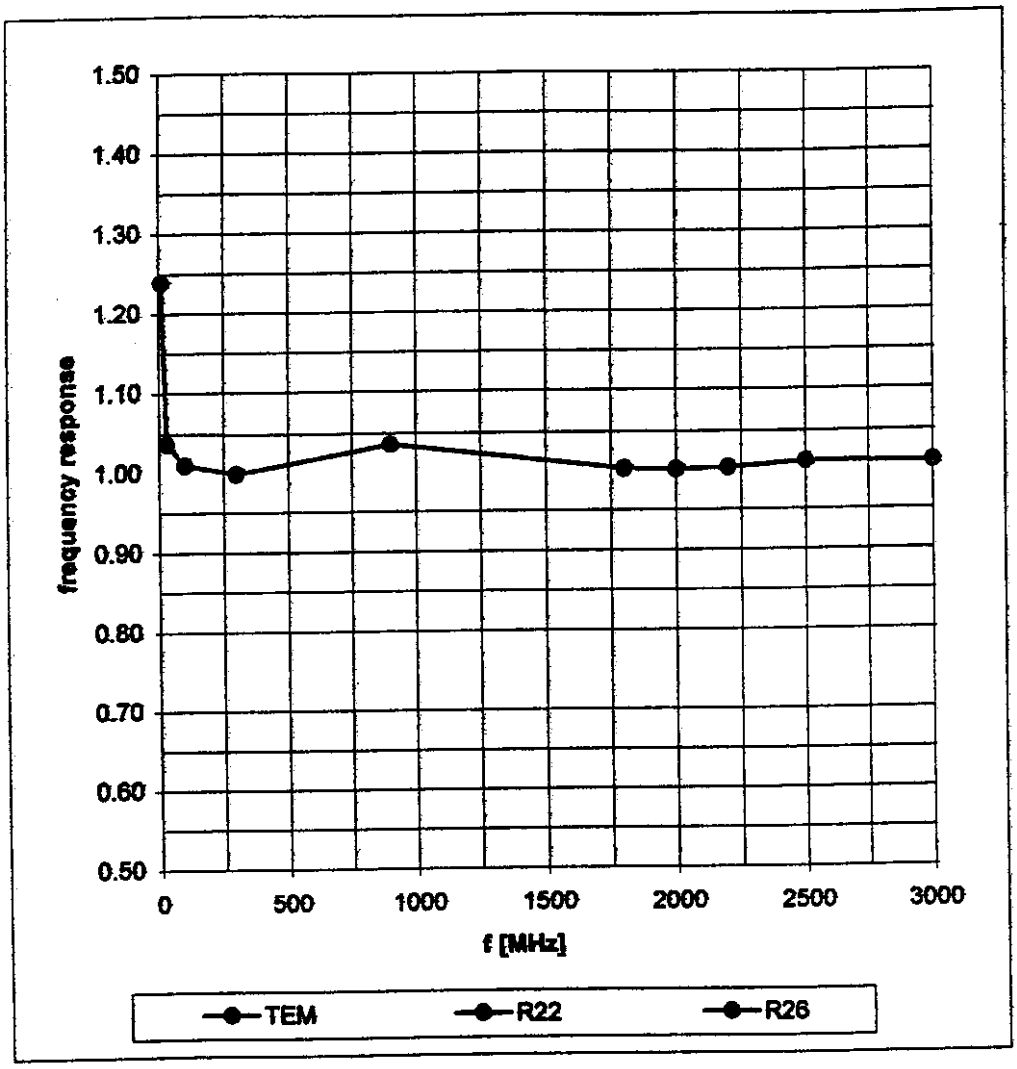

Dynamic Range f(SAR_{brain})

(TEM-Cell:ifi110)

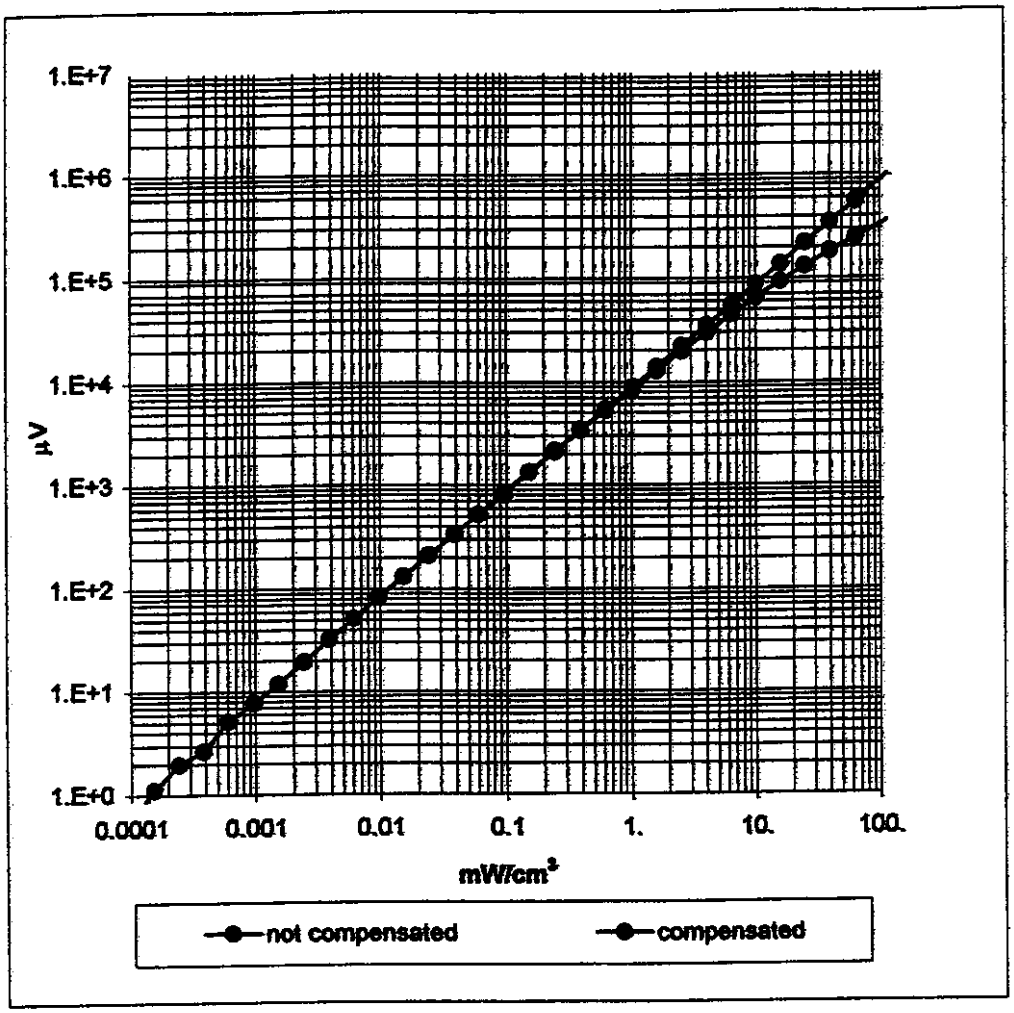

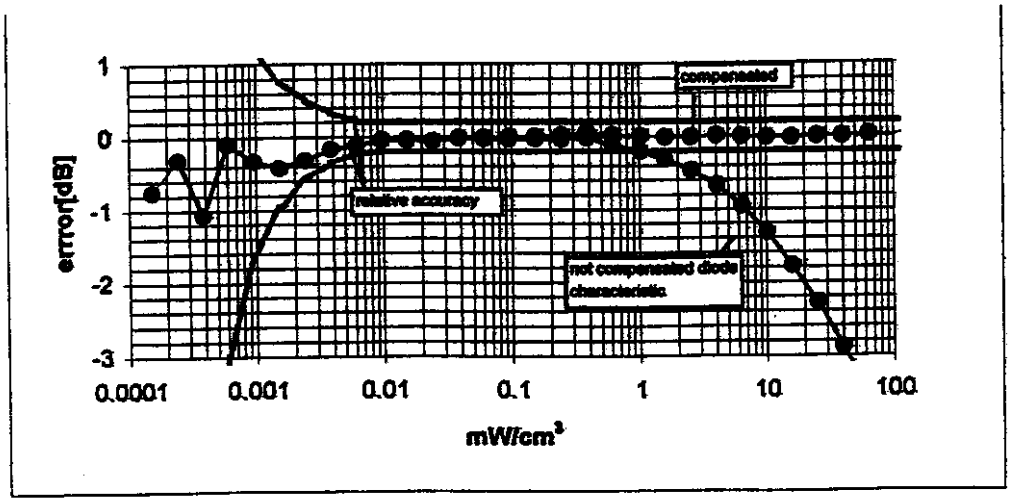

Conversion Factor Assessment

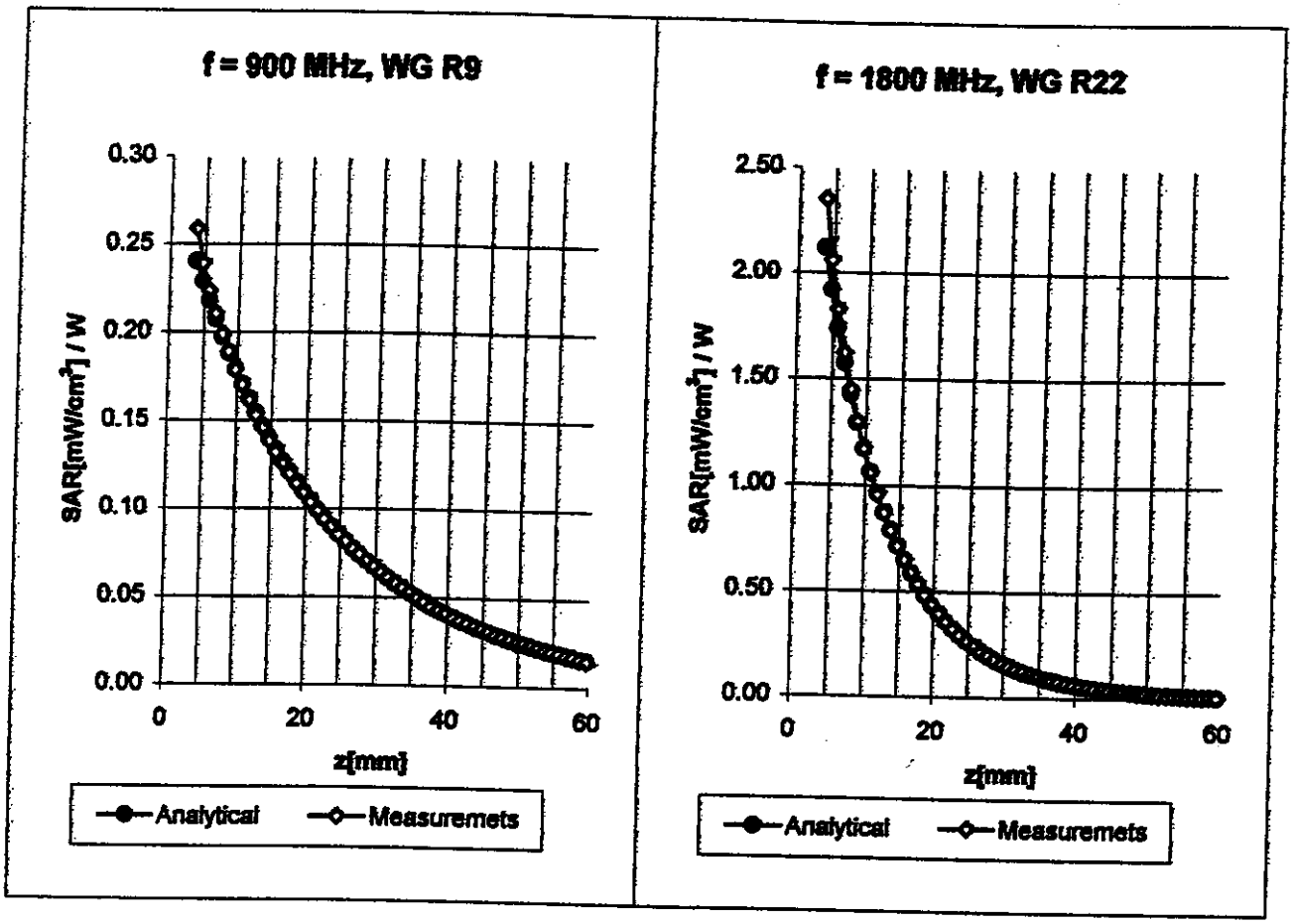

Receiving Pattern (ϕ)

(in brain tissue, z = 5 mm)

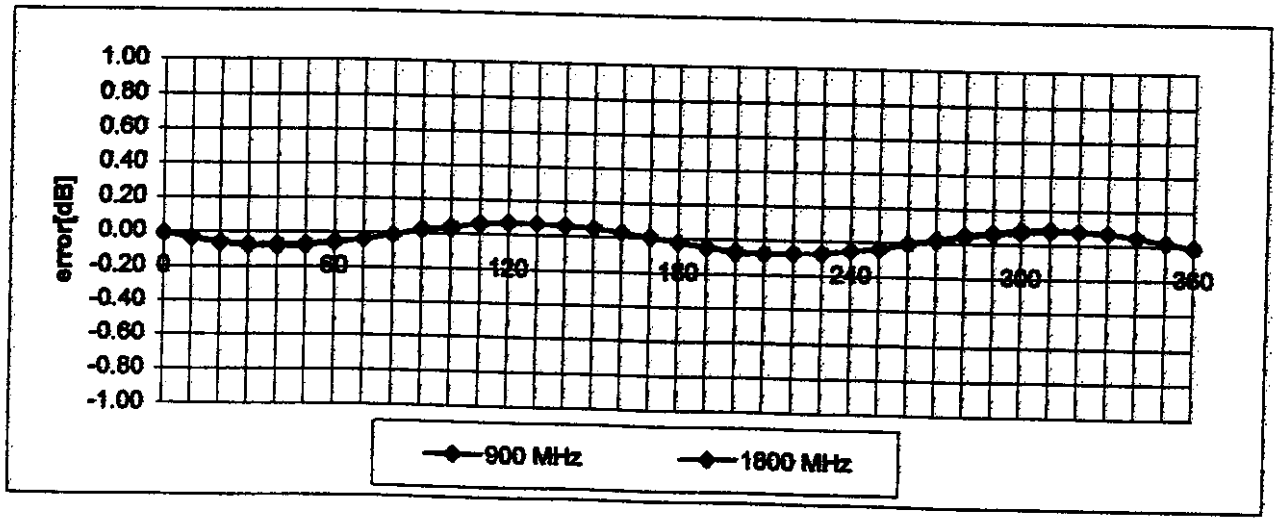

Appendix 3

pages 1 - 5

DASY- DOSIMETRIC ASSESSMENT SYSTEM CALIBRATION REPORT

DATA ACQUISITION ELECTRONICS

Schmid & Partner
Engineering AG

Staffelstrasse 8, 8045 Zürich, Switzerland, Telefon +41 1 280 08 60, Fax +41 1 280 08 64

DASY - DOSIMETRIC ASSESSMENT SYSTEM

CALIBRATION REPORT

DATA ACQUISITION ELECTRONICS

MODEL: DAE2

SERIAL NUMBER: 213

This Data Acquisition Unit was calibrated and tested using a FLUKE 702 Process Calibrator. Calibration and verification were performed at an ambient temperature of 23 ± 5 °C and a relative humidity of < 70%.

Measurements were performed using the standard DASY software for converting binary values, offset compensation and noise filtering. Software settings are indicated in the reports.

Results from this calibration relate only to the unit calibrated.

Calibrated by: M.Bruggmann

Calibration Date: 6.8.1998

DASY Software Version: DASY3 V1.0b

1. DC Voltage Measurement

DA - Converter Values from DAE

High Range:	1LSB =	6.1μV ,	full range =	400 mV
Low Range:	1LSB =	61nV ,	full range =	4 mV

Software Set-up: Calibration time: 3 sec Measuring time: 3 sec

Setup	X	Y	Z
High Range	400	400	400
Low Range	4	4	4
Connector Position	0°		

High Range	Input	Reading in μV	% Error
Channel X + Input	200mV	200484.8	0.24
	20mV	20052.84	0.26
Channel X - Input	20mV	-20044.08	0.22
Channel Y + Input	200mV	200692.8	0.35
	20mV	20070.9	0.35
Channel Y - Input	20mV	-20062.35	0.31
Channel Z + Input	200mV	200779.3	0.39
	20mV	20080.92	0.40
Channel Z - Input	20mV	-20071.6	0.36

Low Range	Input	Reading in μV	% Error
Channel X + Input	2mV	2004.037	0.20
	0.2mV	200.4825	0.24
Channel X - Input	0.2mV	-201.2267	0.61
Channel Y + Input	2mV	2010.955	0.55
	0.2mV	201.1715	0.59
Channel Y - Input	0.2mV	-201.258	0.63
Channel Z + Input	2mV	2011.045	0.55
	0.2mV	201.405	0.70
Channel Z - Input	0.2mV	-201.272	0.64

2. Common mode sensitivity

Software Set-up
Calibration time: 3 sec, Measuring time: 3 sec
Low Range

in µV	Common mode Input Voltage	High Range Reading	Low Range Reading
Channel X	200mV	-15.01851	-16.37388
	- 200mV	3.9423	5.190906
Channel Y	200mV	-5.942738	-12.73525
	- 200mV	8.959845	14.79019
Channel Z	200mV	-13.70552	-7.222769
	- 200mV	13.74889	1.222047

3. Channel separation

Software Set-up
Calibration time: 3 sec, Measuring time: 3 sec
High Range

in µV	Input Voltage	Channel X	Channel Y	Channel Z
Channel X	200mV	-	-2.15438	-3.630622
Channel Y	200mV	-3.786761	-	-2.68589
Channel Z	200mV	-11.63471	-3.185863	-

4. AD-Converter Values with inputs shorted

in LSB	Low Range	High Range
Channel X	15341.1	16472.43
Channel Y	17057.39	16493.9
Channel Z	15677.94	16476.23

5. Input Offset Measurement

Measured after 15 min warm-up time of the Data Acquisition Electronic.
Every Measurement is preceded by a calibration cycle.

Software set-up:

Calibration time:	3 sec
Measuring time:	3 sec
Number of measurements: 100,	Low Range

Input 10MΩ

in µV	Average	min. Offset	max. Offset	Std. Deviation
Channel X	-0.54654	-1.7898	0.5676	0.6451
Channel Y	-0.46657	-1.2647	0.56467	0.52184
Channel Z	-0.04984	-1.9876	1.0168	0.65748

Input shorted

in µV	Average	min. Offset	max. Offset	Std. Deviation
Channel X	-0.1067	-0.65465	0.46841	0.6577
Channel Y	-0.41078	-0.7414	0.4235	0.46574
Channel Z	0.4218914	-0.46771	0.5719	0.79841

6. Input Offset Current

in fA	Input Offset Current
Channel X	< 100
Channel Y	< 100
Channel Z	< 100

7. Input Resistance

	Calibrating	Measuring
Channel X	199.6 kΩ	20.2 MΩ
Channel Y	199.7 kΩ	20.2 MΩ
Channel Z	199.2 kΩ	20.2 MΩ

8. Low Battery Alarm Voltage

in V	Alarm Level
Supply (+ Vcc)	5.3 V
Supply (- Vcc)	-5.6V

9. Power Consumption

in mA	Switched off	Stand by	Transmitting
Digital Supply (VCC)	0.011	4.72	12.2
Analog Supply (+ Vcc)	0.003	9.89	9.94
Analog Supply (- Vcc)	0.1	-9.7	-9.8

10. Functional test

Touch async pulse 1	ok
Touch async pulse 2	na
Touch status bit 1	ok
Touch status bit 2	na
Remote power off	ok
Remote analog Power control	ok

Date: 6.8.98 Signature: M. Burgmann

Appendix 4

page 1

INDUSTRIAL ROBOT AND CONTROL UNIT

Appendix 4

page 1

INDUSTRIAL ROBOT AND CONTROL UNIT

Technical Data

General	Axes	6
	Drives	AC Brushless electric motors
	Control	Digital
	Positional Control	Absolute resolvers, non-volatile
	Coordinates	Cartesian, revolute
	Structure	Revolute
	Interconnecting cables	5 m (between arm and control unit)
Work envelope	Reach at tool flange	985 mm
	Reach at wrist center	900 mm
	Working volume	360° working volume in lefty or righty configuration
	Working range	Axis 1 - Axis 2 - Axis 3 - Axis 4 - Axis 5 - Axis 6 320° 275° 285° 540° 225° 540°
Load capacity	Nominal payload	6 kg
	Maximum payload	9 kg (at low speed)
	Tool Flange	ISO 9409 - 1 - A 40 Outside dia. 50 mm
Performance	Repeatability	± 0,02 mm (constant temperature)
	Maximum speed	9,8 m/s
	Cartesian speed	1,5 m/s
	Nominal speed	Axis 1 - Axis 2 - Axis 3 - Axis 4 - Axis 5 - Axis 6 240°/s 200°/s 286°/s 401°/s 320°/s 580°/s
Control unit	CPU	Motorola 68030
	FPU	Motorola 68882
	Programming	"V+" advanced programming language and/or teach pendant
	I/O interface	12 In/6 Out in standard version, expandable to 64 In/64 Out by 32 In/32 Out module 3 RS-232 serial ports 1 RS-422/485 serial ports
	Options	Analog inputs/outputs 10 m interconnecting cables (between arm and control unit)
	Memory capacity	RAM : 4 Mbytes, expandable to 8 Mbytes Hard disk : 40 Mbytes minimum Built in 3 1/2" disk drive, (1,44 Mbytes) IBM PC format
Work environment	Temperature	5 to 40° C (CEI 204-1)
	Humidity	< 90 % non condensing (CEI 204-1)
	Interference suppression	Incorporated
	Power supply	230, 400, 440, 480 V 3-phase 50/60 Hz - 4 kVA
Weight	Arm	105 kg
	Control unit	200 kg

STÄUBLI® UNIMATION

Deutschland
Stäubli-Unimation
Zweigniederlassung der Stäubli & Co GmbH
D-60437 Frankfurt-Niedereschbach
Tel. (69) 50 00 09-0
Fax (69) 50 00 09-22

España
Stäubli Española SA
E-08013 Barcelona
Tel. (93) 232 13 12
Fax (93) 232 43 74

France
Stäubli France SA
F-74210 Faverges
Tel. 50 65 60 60
Fax 50 65 61 30

Italia
Stäubli Italia SpA
I-20048 Carate Brianza/Milano
Tel. (362) 90 63 69
Fax (362) 90 70 39

Japan
Stäubli KK
J-Osaka 541
Tel. (6) 229 0787
Fax (6) 229 0795

North America
Stäubli-Unimation Inc
USA-Pittsburgh,
PA 15143-2305
Tel. (412) 741 1740
Fax (412) 741 1789

Schweiz
Stäubli AG
CH-8810 Horgen
Tel. (1) 725 25 11
Fax (1) 725 13 88

United Kingdom
Stäubli-Unimation Ltd
GB-Telford, Shropshire TF3 3BN
Tel. (952) 290 931
Fax (952) 29 00 57

Appendix 5

pages 1 - 3

BRAIN TISSUE SIMULATING LIQUIDS

Schmid & Partner
Engineering AG

Oberer Deutweg 59, CH-8400 Winterthur, Telefon +41 52 232 7272, Fax +41 52 232 7127

Brain Tissue Simulating Liquids

Preparation of the Liquids

Requirements:

- Scale
- Magneto Stirrer: Heating Plate, Magnetos (recommended).
- HP 85070A Dielectric Probe Kit (200MHz to 20GHz) plus mounting device and Network Analyser
- Canisters or "closed" jars to store the liquid (recommended)

Preparation:

1.) Heat the water to about 40° Celsius.

2.) Add salt and bactericide to water while stirring and wait until salt is disolved.

3.) Add about one third of the sugar. Keep stirring. Wait until sugar is disolved. Add the second third and when disolved add the final third. The liquid gains volume and thickens slightly.

4.) Keep stirring at maximum speed possible.

5.) When all the sugar is disolved, add the HEC. HEC is highly hygroscopic. It forms lumps when added to the liquid. Either "help" the magneto stirrer by stirring from outside or disolve all of the HEC first in another jar with a little bit of liquid using another stirrer. Add it then to the rest of the solution. Once HEC is added the liquid thickens considerably.

6.) During the whole process watch the temperature to prevent water evaporation.

7.) Once the liquid clears up pour it into canisters. Let it stand for a couple of hours before using it.

III Use

- When in the item (phantom models), monitor water evaporation.
- To minimze water evaporation cover the phantoms when not used. Do not store the liquid in the phantoms, rather store it in closed canisters.
- In case water has evaporated, you can add (warm) water to the liquid. Be sure that after stirring it is completely homogeneous.
- The liquid can be used for at least 3 months. After longer periods bacteria might grow that are resistant against the bactericide.

Recipe 900 MHz:

Water	40.1 %
Sugar	58.0 %
Salt (NaCl)	0.8 %
HEC (Hydroxyethylcellulosis)	1.0 %
Preservative Substance	

900 MHz: $\varepsilon_r = 42.5 \pm 5\%$ and $\sigma = 0.85 \pm 10\%$ mho/m

Recipe 1800 MHz:

Water	45.0 %
Sugar	53.9 %
HEC (Hydroxyethylcellulosis)	1.0 %
Preservative Substance	

1800 MHz: $\varepsilon_r = 41.0 \pm 5\%$ and $\sigma = 1.65 \pm 10\%$ mho/m

Parameters of Probe ET3DV4 SN:1105

NormX	1.53	$\mu V/(V/m)^2$
NormY	1.6	$\mu V/(V/m)^2$
NormZ	1.42	$\mu V/(V/m)^2$
DCP	43000	μV
ConvF(450MHz)	6.64 ± 10%	ε_r=47.2 ± 5%; σ=0.45 ± 10% mho/m[1]
ConvF(900MHz)	5.98 ± 10%	ε_r=42.5 ± 5%; σ=0.86 ± 10% mho/m[1]
ConvF(1800MHz)	4.85 ± 10%	ε_r=41.0 ± 5%; σ=1.7 ± 10% mho/m[1]
$d_{probe\_tip - center\_dipoles}$	2.7	mm
$d_{surface - probe\_tip}$	1.2 ± 0.2	mm

[1] Brain tissue simulating liquids

Appendix 6

pages 1 - 2

GENERIC TWIN PHANTOM
Version 3.

Version 3

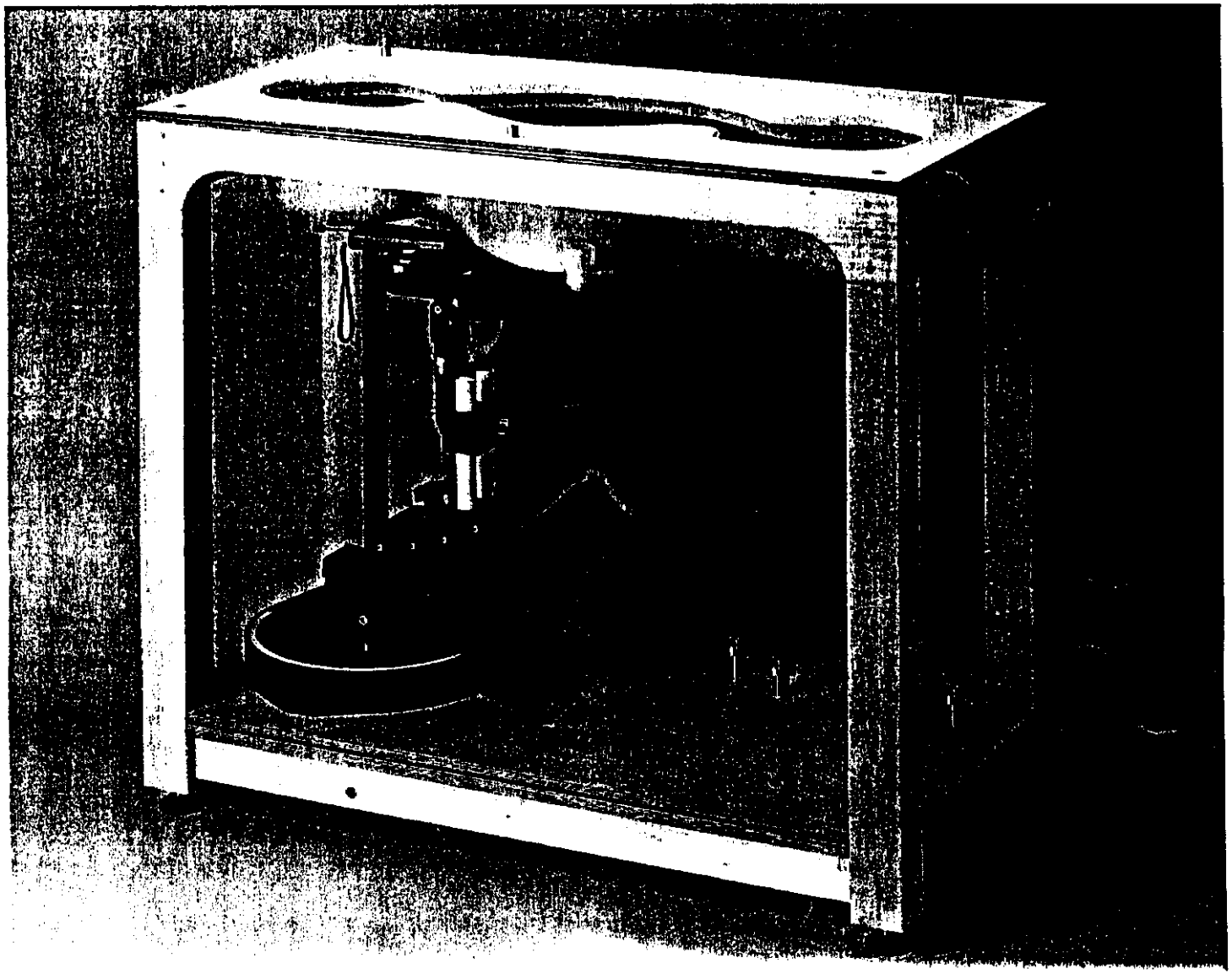

ADVANCED INFORMATION 7/96

OPTIMIZED PHANTOM WITH IMPROVED MOUNTING DEVICE FOR MTE

Summary

In cooperation with ETH Zurich, Schmid & Partner Engineering AG is currently developing a new phantom, as well as a new device for the mounting and positioning of handheld mobile telecommunications equipment (MTE). This new phantom setup will be optimized for compliance testing in accordance with CENELEC, ANSI/IEEE and NCRP requirements. It will have the following improvements compared to the current setup (Left/Right-Hand Torso V2.1 and Mounting Device for Transmitters V2.0):

Basis	The new phantom will be based on an anatomical study.
Shape	The shape of the new phantom will be designed to provide SAR values which are unlikely to be exceeded in the head of any user. Furthermore, the overestimation will be minimal.
Modeling of the Ear	The phantom will include a simple ear segment which represents the thickness of the pressed human ear.
Construction	The new phantom will also be made of fiberglass. However, the tolerance of the shell thickness will be substantially improved. The fiberglass shell will be integrated into a wooden table which will further improve the stability of the phantom.
Mounting Device	The mounting device for the MTE will allow accurate and repeatable placement of the device with respect to the positions defined in the latest CENELEC draft. The repeatability of the horizontal position shall be better than ±1 mm. It will be designed to be compatible with current MTE designs and anticipated future designs.
User-Friendliness	The phantom will also be more user-friendly, since left and right hand configurations and the device for mounting and positioning of the MTE will be combined in one setup, i.e., left and right hand measurements will be possible without exchanging phantoms. The minimum amount of simulation liquid to test MTE with operating frequencies above 800 MHz will be reduced.
Compatibility	The phantom will be fully compatible with the hardware and software of DASY2 as well as of DASY3. (DASY3 will be available in late Spring 97.)
Availability	The new phantom and the new device for the mounting and positioning of MTE will be commercially available in October 1996. The shape of the phantom will be available as a CAD data set on the Internet.

Appendix 7

pages 1 - 11

PROBE CALIBRATION

ETH Eidgenössische Technische Hochschule Zürich
Ecole polytechnique fédérale de Zurich
Politecnico federale di Zurigo
Swiss Federal Institute of Technology Zuri

Prof. Dr. Niels Kuster

Tel: +41 1 632 2737, Fax: +41 1 632 10

Institut für Feldtheorie
und Höchstfrequenztechnik
ETH Zürich
CH-8092 Zürich

Mr. Illkka Pankinaho
Nokia Mobile Phones
NMP/R&D
P.O. Box 86
FIN-24101 Salo
Finland

Zurich, 2 December 1995

Mobile Phone Certification

Dear Mr. ~~Pankinaho~~, ILKKA

In mid-September, we promised to send preprints of the paper which describes the calibration procedure we developed during the last months. We would appreciate any suggestions and comments, since a thorough calibration is fundamental to enforce the safety limits. In addition, we would like to take this opportunity to inform you about the newest developments towards finalizing the scientific and technical conditions for a type approval.

Uncertainties of Measurements: In connection with the calibration, we peformed an analysis which assessed the total uncertainty of SAR measurements in shell phantoms. The results are promising. The total uncertainty can be kept below ±20% at 900 MHz. A project to further reduce these uncertainties and to develop a standard calibration procedure has now been submitted to the EU program "Standards, Measurements & Testing."

Phantom: Another open issue is the verification that the absorption in homogeneous human phantoms represents well the actual spatial peak absorption in the user. In one study, in close cooperation with the research center of German Telekom, absorption induced in three numerical and three experimental phantoms were compared for the mobile communications frequency at 900 MHz. The various phantoms and our findings are briefly described in the attachment.

Requirements of a Certification Procedure: In connection with the recent WTR workshop in Rome, we defined the scientific pre-condition necessary to implement a certification procedure. The manuscript also reflects the requirements which were discussed within CENELEC's TC111 Working group on Mobile Telecommunications Equipment. Please find the manuscript in the attachment as well.

DASY: Schmid & Partner Engineering AG (SPEAG) has started the development of DASY3. Besides a general revision and extension of the DASY2 hardware and software, the main objectives of DASY3 are improved spatial resolution, improved precision and improved time efficiency. DASY3 will be largely compatible with DASY2, although some of the new functions will not be fully usable without minor hardware updates. SPEAG will keep you informed with respect to these developments.

The temperature probes which have been developed for the previously mentioned calibration study will soon be commercially available. The prototype showed a sensitivity of about <0.1 mK/s. It might be interesting to all DASY users that this probe will be fully compatible with DASY2, DASY3 and DASYmini. The active volume of about 1 mm3 is ideal for those laboratories which plan to do calibration or SAR measurements in very small structures.

Part of the industry was interested in a video of DASY2 to demonstrate the test procedure to their customers . Since we already had a video for other occasions, we adapted it to these requests and now have copies available. If you are interested, please return the enclosed form by mail or fax. If you want copies of any of the publications listed on that form, we would be happy to send you these copies as well.

If you have any questions regarding our activities in the area of mobile phone certification, please do not hesitate to contact me. For questions regarding the dosimetric assessment system DASY, I suggest you contact SPEAG directly (phone: +41 52 232 7272, FAX: +41 52 232 7127).

Yours sincerely

Prof. Dr. N. Kuster

Encl.

Broadband Calibration of E-Field Probes in Lossy Media

Klaus Meier, Michael Burkhardt, Thomas Schmid and Niels Kuster

Abstract— **A broadband calibration procedure for E-field probes that minimizes the overall uncertainties inherent in E-field measurements in lossy dielectric liquids has been developed. The analysis of the calibration requirements shows that probes that are symmetrical with respect to their axis greatly facilitate accurate calibration, since the calibration procedure can be divided into several discrete steps. Such a procedure is presented and analyzed with respect to its uncertainties. Absolute calibration is performed at three frequencies (450 MHz, 900 MHz and 1.8 GHz) and in different tissue-simulating liquids. The parameters obtained are verified by numerical simulations of the probe in the surrounding media. Such simulations allow the assessment of some of the calibration parameters with sufficient accuracy in cases where the experimental determination would be too tedious and time-consuming.**

I. Introduction

The interaction of high-frequency electromagnetic fields with biological matter has been the object of growing interest for several years. Miniature E-field probes have been developed to determine experimentally the induced electric field in actual tissue or tissue-simulating liquids.

In view of the phenomenal growth of the mobile communications market, the telecommunications industry has lately recognized the need to test its mobile telephones for compliance with today's safety limits. The key value for dosimetric assessments in general and compliance tests in particular is the maximum tolerable absorbed power per tissue mass in mW/g, known as the specific absorption rate (SAR). The local SAR can be determined experimentally by measuring either the induced electrical field strength or the temperature rise in tissue.

$$SAR = \frac{\sigma}{\rho}E^2 = c\frac{\partial T}{\partial t} \qquad (1)$$

where σ is the conductivity, ρ is the mass density and c is the specific heat of the tissue at the site of measurement.

Since measurements using thermal probes do not provide an adequate degree of efficiency and sensitivity for compliance-testing of consumer products, the research up until today has been focused on small isotropic E-field probes.

The original design of a miniaturized isotropic E-field probe for use in tissue-simulating liquids goes back to Bassen *et al.* [1] Recently the authors presented a new probe design [2] with significantly improved performance.

In view of the significance of, and the difficulties involved in, accurate calibration, surprisingly little has been published so far about broadband calibration of isotropic E-field probes in dielectric materials. In [3] a calibration procedure in an S-band waveguide at a single frequency of 2.45 GHz is described. However, the calibration uncertainties due to the dependence of the probe sensitivity on polarization, frequency, dielectric parameters of the surrounding media and spatial resolution have only been marginally addressed. In this paper these issues are analyzed and a calibration procedure enabling accurate calibration of the probes for a broad frequency range in two lossy dielectric liquids is described. A flexible setup has been chosen in order to study ways of minimizing the uncertainty of dosimetric assessments in the frequency range of mobile communications.

Submitted to IEEE Transactions on Microwave Technique and Technology - October 1995.

The authors are with the Swiss Federal Institute of Technology (ETH), CH-8092 Zurich, Switzerland.

II. E-Field Probe Design and Measurement Errors

The main requirements for E-field probes in any type of surrounding medium are:

- high degree of isotropy in various media;
- high sensitivity and linear response over a broad frequency range;
- high spatial resolution (small tip size); and
- low interaction with the measured field.

E-field probes with isotropic response can be achieved by the orthogonal positioning of three sensors that are sensitive to one E-field component each. Short dipoles or small E-field-sensitive crystals have these characteristics. In miniaturized E-field probes small dipoles with diode rectifiers are mainly used, because they offer the greatest sensitivity and have a linear response over a wide frequency range. A design with a triangular core was chosen for the new E-field probe. This design provides a small outline and shows a high degree of symmetry (Figure 1). The sensors themselves consist of three small dipoles (3 mm in length) directly loaded with a Schottky diode and connected via resistive lines to the data acquisition electronics.

In the following, a number of design problems of these probe types are mentioned; some of them apply to other probe types as well. A more detailed description of the probes is given in [2].

1.) *Secondary modes of reception:* Resistive lines are used to transmit the signal from the rectifier diodes to the evaluation electronics. The interaction of these lines with the field should be minimal. Nevertheless, RF signals can be picked up by the lines and detected and rectified by the diodes. These secondary reception modes appear mainly at lower frequencies, where the impedance of the dipole and the diodes is very high and can produce disturbed directivity characteristics. Special filtering techniques or high

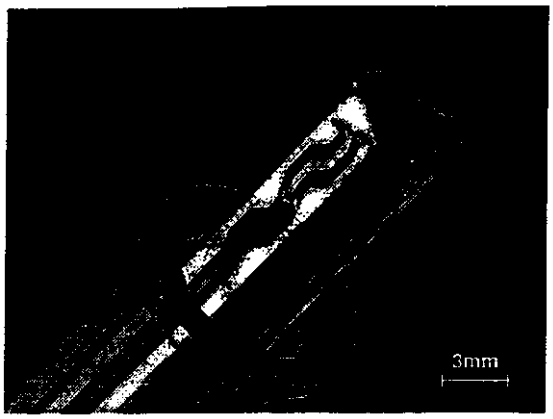

Fig. 1. Tip of the E-field probe. The tip encapsulation has been removed. One 3 mm long dipole and the diode can be seen. In the center of the core is the opening for a built-in optical proximity sensor.

ohmic lines can reduce this effect. [2]

2.) *Influence of the probe materials on the field:* Any dielectric material around electric dipoles can have an effect on the local signal strength inside the probe. It is obvious from the construction of these probes that the influence on E-field components normal to the probe axis will be different from that on E-field component parallel to the probe axis. Furthermore, this difference in sensitivity depends on the surrounding medium. This results in poor isotropy in planes along the probe axis. In [2], several methods are presented to compensate for these effects. In any case the directivity characteristic of the probe will be different in different media. This has to be taken into account when calibrating the probe in a specific medium.

3.) *Influence of the probe on nonhomogeneous fields:* The disturbance caused by the probe on nonhomogeneous fields depends both on the geometrical and material properties of the probe and on the nature of the field itself. The influence of these effects must be investigated in each case. Errors in SAR readings can occur when using the probe in the immediate vicinity of material discontinuities – for instance, when the probe approaches the surface of a shell phantom (see also Figures 6 to 9). By performing measurements at different distances from the surface and extrapolating to the surface, corrected SAR values for the vicinity of the surface can be obtained.

4.) *Spatial resolution:* Another source of error in nonhomogeneous fields arises from the spacing between the dipole centers in the probe. Since each field component is measured at a slightly different location, discrepancies are to be expected when the field's magnitude or direction varies greatly within the probe's dimensions. By turning the probe along its long axis, the measurement locations of the three sensors shift and a further isotropy error will occur.

Therefore, a calibration setup that minimizes these errors must be carefully chosen.

III. Calibration Requirements

The three output signals from an isotropic E-field probe with three orthogonally positioned sensors must be evaluated to give a reading that corresponds to the SAR at the measurement site *in the absence of the probe.* The relation between the field and the sensor signals depends on various factors:

- design and construction materials of the probe;
- electrical properties of the surrounding media;
- direction and polarization of the field;
- field gradient at the measurement site;
- RF characteristics of the antenna, the rectifying element and the transmission line;
- higher order modes or different reception modes in the probe;
- sensitivity of the rectifier; and
- characteristics of the evaluation circuit for the rectified signals.

Each calibration essentially attempts to describe these effects quantitatively, so that correct SAR values can be obtained under various measurement conditions. Furthermore, it is important to know the absolute uncertainty and the validity range of the calibration. To keep the number of calibration parameters and calibration measurements low, it is crucial to separate the above-listed influences and quantify them individually. An effective way must be found to reduce the effect of any possible further errors that can arise under various measurement conditions. The probe design is a deciding factor in this regard. For our dosimetric probes, a three-step calibration process has proven to be the most effective approach:

$$|E^2| = \sum_{i=1}^{3} \frac{f_i(V_i)}{\eta_i \gamma_i} \tag{2}$$

a) $f_i(V_i)$: The rectified signal of each sensor (V_i) is linearized. The linearization function depends on the characteristics of the rectifier and the evaluation circuit. It can be described as a function of the magnitude of the rectified signal and can be assessed easily by a power sweep of the exciting field. When the rectifying elements and evaluation channels are identical, the same function f ($f_i(V_i) = f(V_i)$) can be used for all sensors. In the case of amplitude-modulated signals, the timing characteristics of the evaluation circuit must also be taken into account, unless the signal stays within the "square law" region of the detector element, or the evaluation is rapid enough to keep pace with the modulation. For pulsed signals with a known crest factor, a simple correction formula can be given; for arbitrary modulations, however, a more sophisticated signal analysis is necessary.

b) η_i: These factors describe the absolute sensitivities of the probe sensors ($\mu V/(V/m)^2$) in air for which γ_i is equal to one. They depend on the probe construction materials, the sensor positioning and the RF characteristics of the sensor components. If detector diodes are used as rectifying elements, the parasitic capacitance, which is generally not precisely specified, influences the RF behavior.

Therefore, the factors η_i will be different for each sensor, even if the sensors are positioned in a symmetrical fashion. These factors can be assessed by standard probe calibration procedures (see Section IV). All error sources (isotropy, frequency linearity) must be investigated during this calibration in order to assess the calibration factors for an average measurement situation and to evaluate the error and validity range of the calibration. For broadband E-field probes, the calibration factors are independent of the frequency over a wide range (2 to 3 decades) and can thus be considered to be constants.

c) γ_i: These factors describe the ratio of the sensitivity of the probe sensors in different media to their sensitivity in air. These usually depend both on the surrounding material and the frequency and on the constructional materials and the design of the probe. They will be identical for each probe of the same type. In the case of symmetrical sensor positioning they will even be identical for each sensor ($\gamma_i = \gamma$). This implies that the (time-consuming) assessment of these calibration factors (see Sections V and VI) need to be done only once for each probe type, and not for each individual probe. γ will hereafter be called the "conversion factor".

The separation of the calibration factor in a probe and sensor dependent factor η_i and a probe type and situation-dependent conversion factor γ_i is an approximation that is based on various assumptions:

- The variation of the dipole impedance caused by the surrounding medium is the same for all sensors.
- The local E-field distribution in the area of the sensors inside the probe only depends in magnitude on the surrounding medium. In symmetrical probes this condition can be regarded more leniently.
- The constructional differences (manufacturing tolerances) between probes of the same type are small.

The validity of these assumptions depends largely on the probe's design. Measurements and simulations of our probes have established the feasibility of this calibration procedure. However, it is necessary to reassess the deviation from isotropy in liquid, since it may differ from air. (see Section II).

At higher frequencies and in lossy media, the fields have high gradients. If the gradient is significant within the probe's dimensions, a calibration reference point in the probe must be defined. The field gradient will result in further isotropy errors depending on the probe's alignment with respect to the direction of the field gradient. For the best calibration results, the calibration setup should be as close as possible to the actual measuring situation.

IV. Calibration in Air

To calibrate the probe in air, a well-defined measurement volume with an absolutely known and largely homogeneous electrical field is necessary. The field strength can be measured with a standard calibrated probe, if available; otherwise, it must be determined from power measurements. Several methods are used to produce such fields:

a) Far field of standard radiators: These calibrations are done in free space or in anechoic chambers. The open measurement area permits the positioning of the probe easily at any angle towards the field. The radiated power can be measured with high accuracy. Errors in the determination of the antenna gain and reflections limit the absolute accuracy of this calibration method to approximately ±0.5 dB.

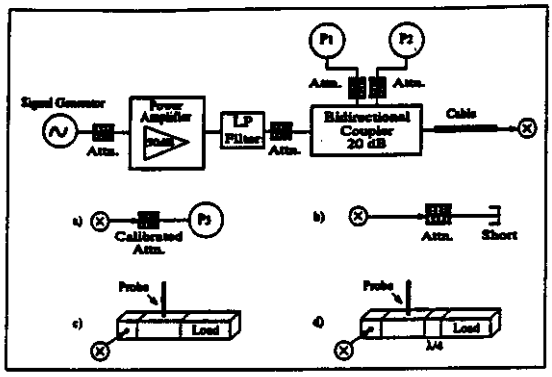

Fig. 2. Setup for calibration in waveguides (air). Measurements a and b to calibrate the power meters P_1 and P_2. P_3 is a high-precision meter. Probe measurements c and d with different distances to load.

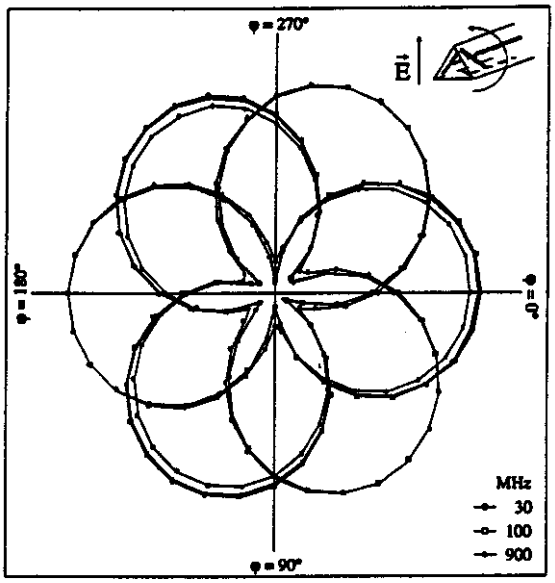

Fig. 3. Receiving pattern of the three orthogonally arranged dipoles after calibration in air. E-field is normal to the probe axis.

b) Near field of radiators: In the near field, it is not easy to determine the absolute field strength. However, the direction of the field vector is often determined by simple symmetry considerations. These fields can be used to measure the relative directivity of the probe when the field gradient is small compared to the probe dimensions.

c) TEM cells produce a homogeneous TEM wave in a limited volume ($\ll$ wavelength). The highest usable frequency is determined by the existence of higher-order propagation modes (200 MHz to 1.5 GHz, depending on the cell size). The power can be measured at the output of the cell. The accuracy is limited by cell impedance variations due to constructional inaccuracies. The discontinuities in the construction (edges, access openings) produce field deviations

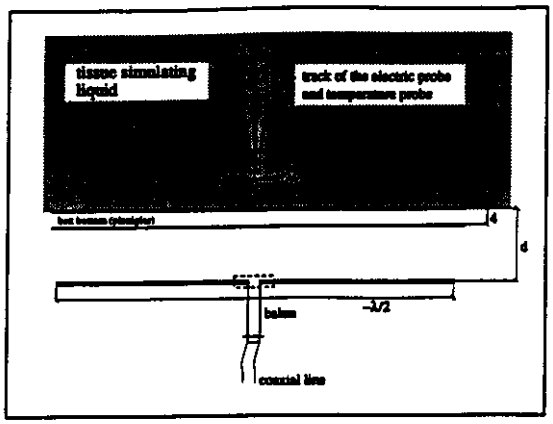

Fig. 4. Experimental setup. On the top is the Plexiglas box filled with the simulating liquid. At the bottom is the dipole. The temperature probes and the E-field probe are positioned directly above the dipole feedpoint.

from the theoretical TEM mode. An absolute accuracy of ±0.4 dB is possible.

d) GTEM cells have no discontinuities and can be used from DC to several GHz. The calibration volume can have dimensions of several wavelengths. The reflections from the built-in absorber and load produce standing waves, which limit the absolute accuracy of GTEM cells to ±1 to ±3 dB.

e) Waveguides produce well-defined fields in small volumes and a limited frequency band. With high-precision components (loads, lines, adaptors to coaxial lines) and error compensation, the field can be determined to be within ±2%. However, the influence of the probe itself on the field must be carefully investigated.

For the absolute probe calibration in air, we used methods c) and e). At frequencies over 1 GHz we measured in standard waveguides R22 and R26, with a setup according to Figure 2. The probe is rotated around its axis with a positioning accuracy at the probe tip of better than ±0.1 mm. Absolute accuracy of the calibration is given for an average in the directivity and lies within ±5% (The linearity over different frequencies and waveguides is better than ±2%.). At frequencies below 1 GHz, a TEM cell ifi110 was used for calibration (Figure 3).

The agreement in absolute value with the measurements in the waveguides is better than could be expected from the cell data (within ±3%). Waveguide measurements at 900 MHz will be performed to confirm this agreement. As the directivity for all rotational angles of the probe cannot be determined in waveguides, a near-field exposure situation was used. For higher frequencies, the center point over an open waveguide was chosen as the measurement site and, for lower frequencies, the field in the symmetry plane of highly symmetrical standard dipoles.

V. Calibration in Lossy Dielectric Liquids

A. Setup

To determine the conversion factor γ, a well-defined SAR distribution inside the dielectric material for which the probe must be calibrated is needed. Setups are preferred which allow the computation of the field inside the dielectric material analytically or by numerical simulations. One way would be a dielectric slab in a rectangular waveguide. Although the induced fields are well defined and can be determined easily if the emergence of spurious higher modes can be sufficiently suppressed, the setup is very narrow-banded.

Another setup used in [4] is the simulation of a dielectric half-space, which is exposed to a $\lambda/2$ dipole parallel aligned to the surface of this half-space (Figure 4). This configuration can be accurately simulated by using numerical techniques, since the SAR on the axis is predominantly proportional to the square of the antenna feedpoint current and not to the output power. However, experimentally, the feedpoint current can be assessed only with fairly large uncertainties of no better than ±10%.

Nevertheless this setup was chosen because:

- It is easy to build up and to handle.
- It provides much greater flexibility since a broad frequency range can be covered by the same setup.
- It is a good representation of the test situation implemented for dosimetric assessments of mobile communications devices [5].
- In lossy dielectric liquids, the local SAR values can be experimentally measured by small thermal probes according to equation (1) at high power levels.

The half-space is simulated by an acrylic glass box ($600\times300\times200\,\mathrm{mm}^3$) filled with the lossy dielectric liquid. The thickness of the acrylic glass box phantom is 4 mm. The dipoles are placed parallel to the dielectric surface at distances that are small compared to the dimensions of the box and to the distance from the floor. The floor is lined with absorbers.

The dipole used at 450 MHz is a Stoddard dipole 310 mm long, and at 900 MHz a high-precision dipole 147 mm long and 3.6 mm in diameter is used. In both cases, the dipoles are driven by an HP8656B generator and a broadband RF power amplifier (Kalmus Model 717C, 100 W output power). A bidirectional coupler HP775D monitors the forward and reflected power. The 1.8 GHz dipole is 73.5 mm in length and has a diameter of 2.25 mm. Losses along the coupler and the lines are taken into account.

In the following, the conversion factors γ for brain-simulating tissues at 450 MHz, 900 MHz and 1800 MHz are determined.

B. Brain Simulating Liquids

The simulating liquids for brain tissue at 450 MHz and 900 MHz consist of sugar, water, NaCl and Hydroxyethylcellulosis (HEC). [6] For brain tissue at 1.8 GHz, two different liquids were used. The first was based on a simple sugar-water solution without any salt (free ions). Nevertheless, the conductivity of such a solution was still higher than most recent data for living tissue [7] would suggest (Table I). At frequencies higher than 1 GHz, the bound sugar-water complexes begin to determine the conductivity level of the liquid. Therefore, in a second approach, sugar was replaced by butyldigol (2-(2-butoxyethoxy)ethanolbutyl),

TABLE I

DIELECTRIC PROPERTIES OF BRAIN TISSUE-SIMULATING LIQUIDS AT THE TESTED FREQUENCIES. AT 1.8 GHz, TWO LIQUIDS WERE USED: SUGAR-WATER SOLUTION (A) AND BUTYLDIGOL-WATER SOLUTION (B).

Frequency [MHz]	ϵ_r		σ [mho/m]	
450	47.0	±5%	0.43	±6%
900	40.0	±5%	0.87	±6%
1800A	40.5	±5%	1.75	±6%
1800B	41.5	±5%	1.25	±6%

which, when dissolved in water, shows smaller conductivity values. At the same ϵ_r value, the conductivity could be reduced from 1.75 to 1.25 mho/m. The electrical parameters were measured by an open coaxial method using the HP 85070A Dielectric Probe Kit. To verify the open coaxial method, we determined the electrical parameters using the slotted-line method. The agreement was within 4%. Table I gives an overview. The temperature dependence of the liquid's parameter was also checked. In the temperature range between 15° C and 30° C, a change of 5% was measured, which lies within the uncertainty of the permittivity measurement method.

The specific thermal constant c was determined using a simple calorimetric procedure with an accuracy of better than ±4%. The specific density ρ and c depend mainly on the ratio between sugar and water. For brain tissue-simulating liquids, c was determined to be 2.85 J/K/g ±4% with a specific density (ρ) of 1.30 g/cm^3 ±1%. Comparison of these values for c with data from literature shows considerable agreement. Gucker *et al.* measured 2.90 J/K/g for a similar aqueous sucrose solution. [8] The value for the brain tissue-simulating liquid which uses the sugar substitute Buthyldigol is 3.58 J/K/g (ρ = 0.98 g/cm^3 ±1%).

C. Temperature Probe

The measurement of the local SAR by temperature probes has the advantage that temperature is a scalar value. Small sensors can therefore be easily produced. Immunity of the temperature probes towards the HF fields must be guaranteed and can be achieved by optical probes or thermistor probes with high resistive lines. [9] The limited temperature sensitivity of theses sensors can be overcome by applying high power.

In this study, the nonmetallic temperature measurement system (SPEAG DASY2) was used to measure the temperature increase. The probe is based on an NTC temperature sensor connected to four resistive lines. [10] The noise level of this system is about 100 times less than that of the two comparable optical devices on the market (±0.001° C averaged over 0.1 s). The noise level for temperature rise measurement over a period of 10 s was found to be better than ±0.1 mK/s. At these high frequencies (450 MHz - 1.8 GHz) the absorption is very local – i.e., close to the feedpoint of the dipole and rapidly decreasing the further it penetrates the tissue. This causes strong temperature gradients inside the liquid. Thus, thermodynamic dissipation processes, such as convection, had to be monitored. The RF power was usually on for about 14 seconds. The corresponding linear temperature increase was evaluated by least-square. After every exposure period, the liquid was stirred until a thermodynamic equilibrium state was reached again before the RF power could be switched on again. The temperature increase in the liquid due to exposure to a 900 MHz field at two distances from the body is shown in Figure 5. The effects of convection were assessed by evaluating different time intervals and were found to be negligible within the first 10 s for sugar-water solution. The solution based on Buthyldigol had considerably lower viscosity, so that the evaluation time had to be reduced to 5 s.

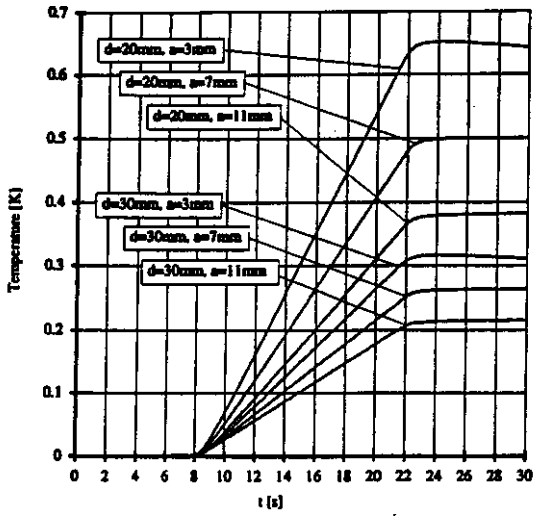

Fig. 5. Temperature increase measured during RF exposure to a 900 MHz field. The power input was 43 dBm. d = dipole distance from the simulating liquid; a = sensor distance from the acrylic glass bottom.

A robot positioned the temperature probe in the liquid by moving it from the top, like the E-field probes, towards the bottom of the box. The disturbance of the probe holder has proven to be negligible.

TABLE II

CONVERSION FACTOR γ, WHICH DESCRIBES THE INCREASE OF SENSITIVITY IN BRAIN TISSUE-SIMULATING LIQUIDS AT THE TESTED FREQUENCIES.

Frequency [MHz]	ϵ_r	σ [mho/m]	γ	
450	47.0	0.43	6.7	±10%
900	40.0	0.87	6.0	±10%
1800A	40.5	1.65	4.8	±10%
1800A	41.0	1.25	4.8	±10%

D. Results

The conversion factor γ was determined by comparing the SAR values measured by the temperature probe and by the E-field probe. The measurement points were located on a line normal to the Plexiglas bottom above the dipole

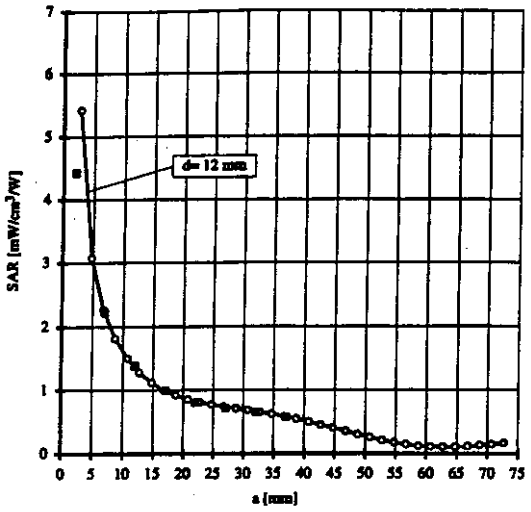

Fig. 6. SAR assessed by E-field (small empty symbols) and temperature measurement (big full symbols) at 450 MHz in brain-simulating liquid (ϵ_r = 47.0 and σ=0.43 mho/m). The SAR was normalized on 1 Watt input power. The frequency was set to 450 MHz. The dipole distance from the body was 12 mm. The conversion factor γ was determined to 6.7 ±10%.

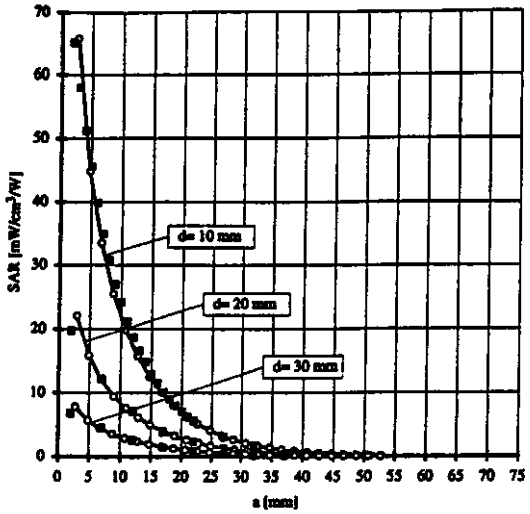

Fig. 8. SAR assessed by E-field (small empty symbols) and temperature measurement (big full symbols) at 1.8 GHz in brain-simulating liquid (ϵ_r = 40.5 and σ=1.75 mho/m). The SAR was normalized on 1 Watt input power. The dipole distances from the body were 10 mm, 20 mm and 30 mm. The conversion factor γ was determined to 4.8 ±10%.

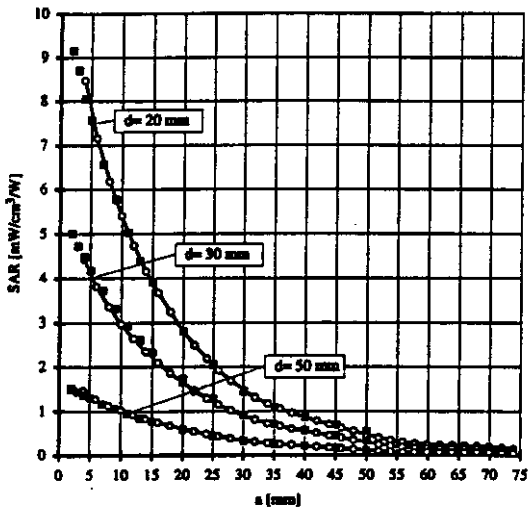

Fig. 7. SAR assessed by E-field (small empty symbols) and temperature measurement (big full symbols) at 900 MHz in brain-simulating liquid (ϵ_r = 40.0 and σ=0.87 mho/m). The SAR was normalized on 1 Watt input power. The dipole distances from the body were 20 mm, 30 mm and 50 mm. The conversion factor γ was determined to 6.0 ±10%.

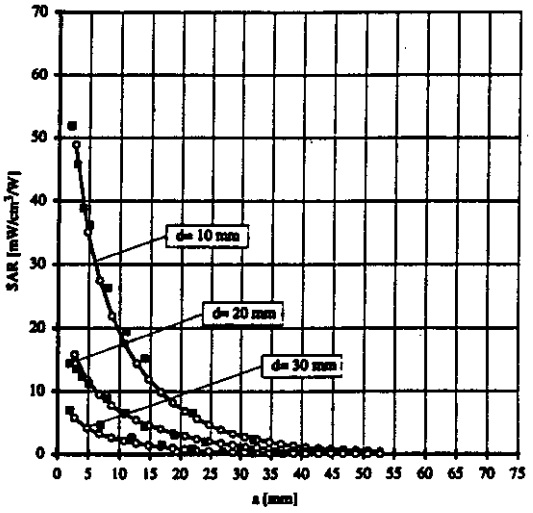

Fig. 9. SAR assessed by E-field (small empty symbols) and temperature measurement (big full symbols) at 1.8 GHz in brain-simulating liquid (ϵ_r = 41.0 and σ=1.25 mho/m). The SAR was normalized on 1 Watt input power. The dipole distances from the body were 10 mm, 20 mm and 30 mm. The conversion factor γ was determined to 4.8 ±10%.

feedpoint (Figure 4). These measurements were repeated at different power levels, at different distances of the RF source from the body and at different frequencies (Figures 6 to 9). The conversion factor was assessed by a least-square procedure considering all measured values. The results for the various tissues are summarized in Table II.

The accuracy of the conversion factor γ is mainly determined by the uncertainties in determining the correct electromagnetic and thermal properties of the tissue-simulating liquid. Using the "slot line" and "open coaxial" methods to determine the conductivity of the liquid introduces an uncertainty of about ±6%. The specific heat of the liquid can be assessed to an accuracy of about ±4%. The E-field probe yields another ±3%. Adding the uncertainty of the positioning of the E-field probe (±1%), of the temperature probe (±2%), and of the power meters (±1%) leads to a total uncertainty of less than ±10%.

VI. Numerical Studies

Three objectives led us to use numerical techniques to simulate the probe embedded in lossy dielectric materials: 1) to study methods to improve the isotropy of the probes [2]; 2) to assess the spatial resolution; and 3) to determine the conversion factor γ computationally, since numerical

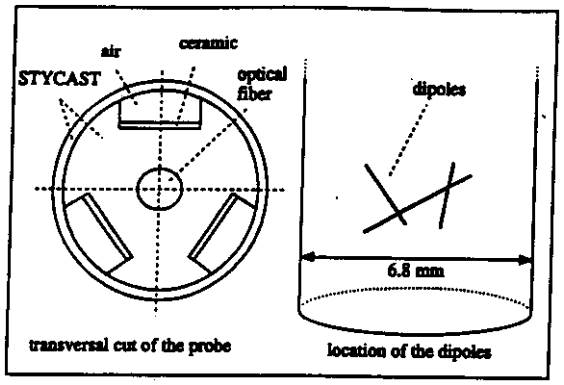

Fig. 10. Computer simulation model: transversal cut of the probe and location of the dipoles.

techniques are less tedious than the experimental approach.

To obtain a deeper insight into the behavior of the conversion factor, two numerical program packages based on two different techniques were used. This had the advantage of the possible cross-validation of the results obtained by both techniques, each of which has its strengths in different areas.

The first one is the 3D MMP software package developed at the Swiss Federal Institute of Technology (ETH). It is a frequency domain boundary technique suited for 2D and 3D scattering problems within piecewise linear, homogeneous and isotropic domains. Details are given in [11] and [12]. The second software package, "MAFIA", was developed at the Technische Hochschule Darmstadt (THD), Germany. The method used is based on the finite integration technique (FIT) and is very similar to an FDTD approach. Details are given in [13] and [14].

A. Modeling of the probe

To study the field distribution inside the probe depending on the electrical parameters of the surrounding media, different discretizations of the E-field probe were chosen. A transversal cut of the probe and a perspectival view with the location of the dipoles inside the probe is shown in Figure 10. Different discretizations with increasing complexity have been compared:

a) The simplest numerical representation of the probe is a simple homogeneous, lossless cylinder 6.8 mm in diameter with a relative permittivity of 2.54. This corresponds to the electrical properties of the microwave material utilized (STYCAST 0005) to build the core of the probe. The length of the cylinder is 15 mm, which has proven to be long enough to study the fields induced in the probe tip. MMP could only be used for this simple homogeneous model of the probe. In MMP, the modeling required about 550 matching points at the boundary of the two domains and 9 multipole expansions. As expected, the maximum errors (<10%) appeared on the matching points at the corners of the probe. In order to minimize these errors and to use a minimal number of expansion functions, the edge of the probe was slightly rounded. About 90,000 voxels were needed to model the whole computational domain within MAFIA, about 5,000 of which were needed for the probe itself. Problems occur at the outer boundaries when using open-boundary conditions and assuming the whole computational domain to be of a lossy material, as in the case of biological tissue. Nevertheless, in choosing a long computational domain in the direction of the wave propagation vector and in considering that the attenuation over one wavelength is very slight, the influence of possible reflected waves was assumed to be less than 3%.

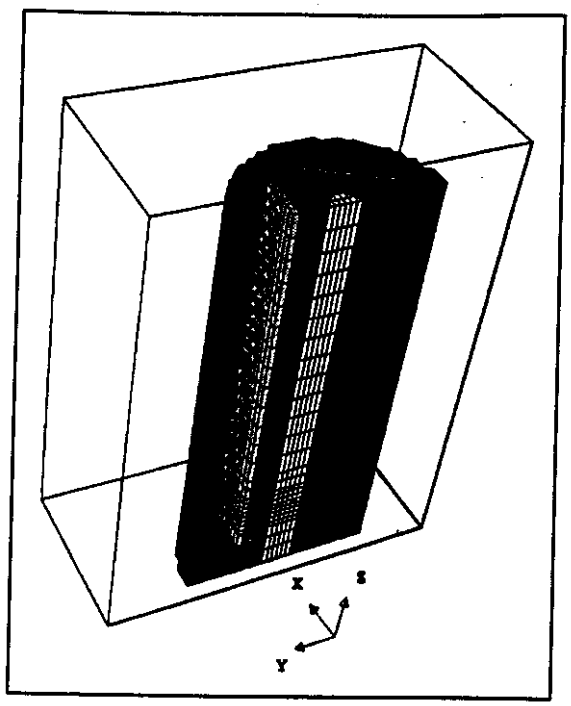

Fig. 11. Computer simulation model: complex model of the probe for the MAFIA simulation tool.

b) A more complex model simulated the optical fiber in the center of the core. The fiber was discretized as a smaller homogeneous cylinder 1 mm in diameter with a relative permittivity of 5 in the center of the STYCAST cylinder.

c) Additional details were incorporated in a further model by the modeling of the three air holes (Figure 10).

d) In the most complex model, three ceramic sheets on which the dipoles and lines are printed were simulated as well (Figure 11). This leads to a discretization with 210,000 voxels, about 37,000 of which were needed for the probe itself.

In all the models the dipoles were not simulated. The conversion factor can be calculated by integrating the electric field at the location of the dipoles, firstly with biological tissue surrounding the structure and then with air around it:

$$\gamma = \frac{\sum_{i=1}^{3} \left(\int_{Dipole_i} \vec{E}\vec{ds}(in\ tissue) \right)^2}{\sum_{i=1}^{3} \left(\int_{Dipole_i} \vec{E}\vec{ds}(in\ air) \right)^2} \qquad (3)$$

As the reference value, the E-field at the location of the dipole center in the absence of the probes was chosen.

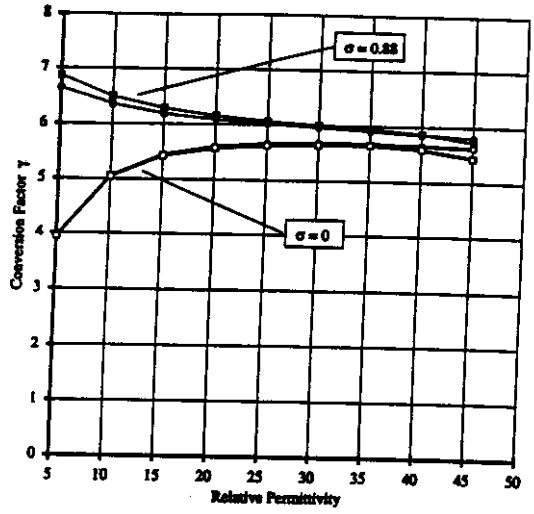

Fig. 12. Simulation: conversion factor at 900 MHz as a function of the relative permittivity of the biological tissue. Done for absorbing biological tissue and nonabsorbing tissue. MAFIA modeling are displayed by squares, MMP modeling by circles.

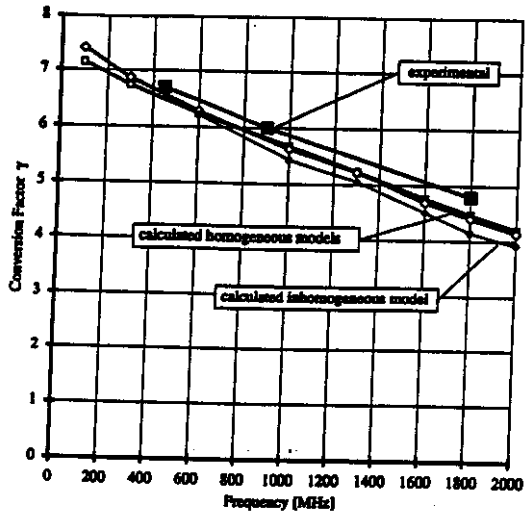

Fig. 14. Experimentally assessed conversion factor for brain tissue-simulating liquid in comparison with the values obtained from numerical simulation for homogeneous (empty symbols) and non-homogeneous (filled symbols) modelings of the probe.

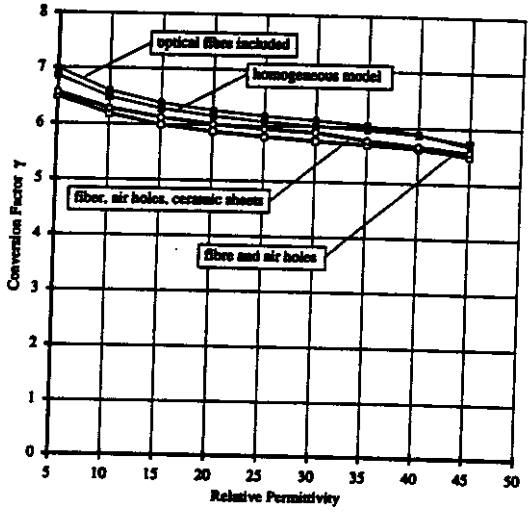

Fig. 13. Simulation: conversion factor as a function of the relative permittivity of the biological tissue for different MAFIA models. The conductivity is 0.88 mho/m, the frequency 900 MHz.

B. Results of the Simulations

The simulations with the simple homogeneous models were performed for different dielectric properties of the probe's surrounding medium. Figure 12 shows the dependence of the probe's conversion factor as a function of the relative permittivity. The frequency of the excitation was set to 900 MHz. These calculations were made for absorbing biological tissue and for nonabsorbing tissue.

The conductivity of the lossy material corresponds to the value used for the experimental investigations (0.88 mho/m, see below). The influence of the conductivity of the lossy material becomes less important for a larger real part of the complex permittivity. Within a wide range of relative permittivities (of biological tissue), the conversion factor or, in other words, the sensitivity of the probe changes by less than 10%. This is even true when changing the conductivity of the biological tissue within a certain range. However, for small real parts of the complex permittivity, the influence of the conductivity on the conversion factor is strong. A comparison of the results of the two methods (MMP and MAFIA) reveals that the difference is less than 1% for the nonabsorbing material and between 1% and 3% for the absorbing material.

In Figure 13, the results for different MAFIA models are compared. The results of the homogeneous model are the same as discussed before. The conductivity was again chosen to be 0.88 mho/m and the frequency 900 MHz. The effect of the optical fiber inside the probe can be neglected.

For the more complex model with an optical fiber, ceramic sheets and air holes, γ is about 6% lower than for the homogeneous model. Additional simulations which neglected the ceramic sheets or the air holes revealed that the air holes are responsible for the drop in the conversion factor.

In Figure 14, the frequency dependence of γ is shown for the homogeneous models of MMP and MAFIA and the more complex MAFIA model.

The homogeneous models simulated with MMP and MAFIA are in close agreement with each other. Again, the values for the more complex modeling are slightly lower than those for the homogeneous modeling. In contrast to these findings, the experimentally determined conversion factors are larger than those of the simulations. The reason lies in the fact that even the most complex modeling involves many simplifications of the structure of the real probe. In addition, the electrical parameters of the probe material were not measured, but were taken from the literature. The most important effect is most likely to be the change of the dipole capacitance, which depends on the surrounding media and could not be considered in the simulations. This effect is expected to be more significant for probe designs in which the dipoles are positioned closer to

the surrounding medium.

VII. Conclusions

A procedure has been presented that allows an absolute calibration of the probes for dosimetric assessments with an accuracy of better than ±10%. The chosen approach has the advantage that the calibration setup closely corresponds to that of the actual dosimetric assessments performed with the scanner described in [5]. Thus, further considerations with regard to polarization are not required. If such studies are needed, the techniques described in [5] can be used. Numerical techniques have proven to be adequate to assess the conversion factor γ if a precision of only ±20% is sufficient for this probe. For other probe designs, the uncertainties of the numerically determined conversion factors might be considerably larger.

VIII. Acknowledgments

We gratefully acknowledge the help of Mr. Oliver Egger, Ms. Katja Poković and Mr. Jeroen de Keijzer for their support in this study.

References

[1] H. I. Bassen and G. S. Smith, "Electric field probes – a review," *IEEE Transactions on Antennas and Propagation*, vol. 31, pp. 710–718, Sept. 1983.

[2] T. Schmid and N. Kuster, "Novel E-field probes for close near field scanning," *IEEE Transactions on Vehicular Technology*. submitted.

[3] D. Hill, "Waveguide technique for the calibration of miniature implantable electric-field probes for use in microwave-bioeffects studies," *IEEE Transactions on Microwave Theory and Techniques*, vol. 30, pp. 92–99, Jan. 1982.

[4] N. Kuster and Q. Balzano, "Energy absorption mechanism by biological bodies in the near field of dipole antennas above 300 MHz," *IEEE Transactions on Vehicular Technology*, vol. 41, pp. 17–23, Feb. 1992.

[5] T. Schmid, O. Egger, and N. Kuster, "Automated E-field scanning system for dosimetric assessments," *IEEE Transactions on Microwave Theory and Techniques*, vol. 43, Jan. 1996. in press.

[6] G. Hartsgrove, A. Kraszewski, and A. Surowiec, "Simulated biological materials for electromagnetic radiation absorption studies," *Bioelectromagnetics*, vol. 8, pp. 29–36, Jan. 1987.

[7] C. Gabriel , Personal Communication.

[8] F. Gucker and F. Ayres, "The specific heats of aqueous sucrose solutions," *American Journal of Chemistry*, vol. 59, pp. 447–452, Mar. 1937.

[9] M. Burkhardt, K. Poković, M. Gnos, T. Schmid, and N. Kuster, "Numerical and experimental dosimetry of petri dish exposure setups," *Bioelectromagnetics*, 1996. submitted.

[10] R. R. Bowman, "A probe for measuring temperature in radio-frequency-heated material," *IEEE Transactions on Microwave Theory and Techniques*, vol. 24, no. 1, pp. 43–45, 1976.

[11] Ch. Hafner and L. H. Bomholt, *The 3D Electrodynamic Wave Simulator*. New York: John Wiley & Sons Inc., 1993.

[12] N. Kuster, "Multiple multipole method for simulating EM problems involving biological bodies," *IEEE Transactions on Biomedical Engineering*, vol. 40, pp. 611–620, July 1993.

[13] T. Weiland, "Maxwell's grid equations," *Frequenz 44*, no. 1, 1990.

[14] CST GmbH, Lautenschlaegerstr. 38, D 64289 Darmstadt, *The MAFIA collaboration, User's Guide Mafia Version 3.x.*

Appendix 8

pages 1 - 12

DIPOLE VALIDATION KITS

Schmid & Partner
Engineering AG

Staffelstrasse 8, 8045 Zurich, Switzerland, Telefon +41 1 280 08 60, Fax +41 1 280 08 64

DASY

Dipole Validation Kit

Type: D900V2

Serial: 003

Manufactured: August 1995
Calibrated: August 1998

1. Measurement Conditions

The measurements were performed in the flat section of the new generic twin phantom (shell thickness 2mm) filled with brain simulating sugar solution of the following electrical parameters at 900 MHz:

Relative Dielectricity	**42.8**	± 5%
Conductivity	**0.85 mho/m**	± 5%

The DASY3 System (Software version 1.0a) with a dosimetric E-field probe ET3DV4 (SN:1302, Conversion factor 5.5) was used for the measurements.

The dipole was mounted on the small tripod so that the dipole feedpoint was positioned below the centre marking of the flat phantom section and the dipole was oriented parallel to the body axis (the long side of the phantom). The standard measuring distance was 15mm from dipole centre to the solution surface. The included distance holder was used during measurements for accurate distance positioning.

The coarse grid with a grid spacing of 15mm was aligned with the dipole. The 5x5x7 fine cube was chosen for cube integration. Probe isotropy errors were cancelled by measuring the SAR with normal and 90° turned probe orientations and averaging. The dipole input power (forward power) was 250mW ± 3 %. The results are normalised to 1W input power.

2. SAR Measurement

Standard SAR-measurements were performed with the phantom according to the measurement conditions described in section 1. The results have been normalised to a dipole input power of 1W (forward power). The resulting averaged SAR-values are:

averaged over 1 cm^3 (1 g) of tissue:	**9.36 mW/g**
averaged over 10 cm^3 (10 g) of tissue:	**6.16 mW/g**

Note: If the liquid parameters for validation are slightly different from the ones used for initial calibration, the SAR-values will be different as well. The estimated sensitivities of SAR-values and penetration depths to the liquid parameters are listed in the DASY Application Note 4: 'SAR Sensitivities'.

3. Dipole Impedance and return loss

The impedance was measured at the SMA-connector with a network analyser and numerically transformed to the dipole feedpoint. The transformation parameters from the SMA-connector to the dipole feedpoint are:

Electrical delay:	**1.416 ns**	(one direction)
Transmission factor:	**0.993**	(voltage transmission, one direction)

The dipole was positioned at the flat phantom sections according to section 1 and the distance holder was in place during impedance measurements.

Feedpoint impedance at 900 MHz:	Re{Z} = **49.9 Ω**
	Im {Z} = **3.4 Ω**
Return Loss at 900 MHz	**-29.6 dB**

4. Handling

The dipole is made of standard semirigid coaxial cable. The centre conductor of the feeding line is directly connected to the second arm of the dipole. The antenna is therefore short-circuited for DC-signals.

Do not apply excessive force to the dipole arms, because they might bend. If the dipole arms have to be bent back, take care to release stress to the soldered connections near the feedpoint; they might come off.

After prolonged use with 100W radiated power, only a slight warming of the dipole near the feedpoint can be measured.

alidation Dipole D900V2 SN:003, d = 15mm

equency: 900 [MHz]; Antenna Input Power: 250 [mW]
neric Twin Phantom; Flat Section; Grid Spacing: Dx = 20.0, Dy = 20.0, Dz = 10.0
obe: ET3DV5 - SN1302/DAE3; ConvF(5.50,5.50,5.50); Brain 900 MHz: σ = 0.85 [mho/m] ε_r = 42.8 ρ = 1.00 [g/cm^3]
bes (2): Peak: 3.56 [mW/g] ± 0.05 dB, SAR (1g): 2.34 [mW/g] ± 0.05 dB, SAR (10g): 1.54 [mW/g] ± 0.05 dB, (Worst-case extrapolation)
netration depth: 13.1 (11.9, 14.6) [mm]
werdrift: 0.00 dB

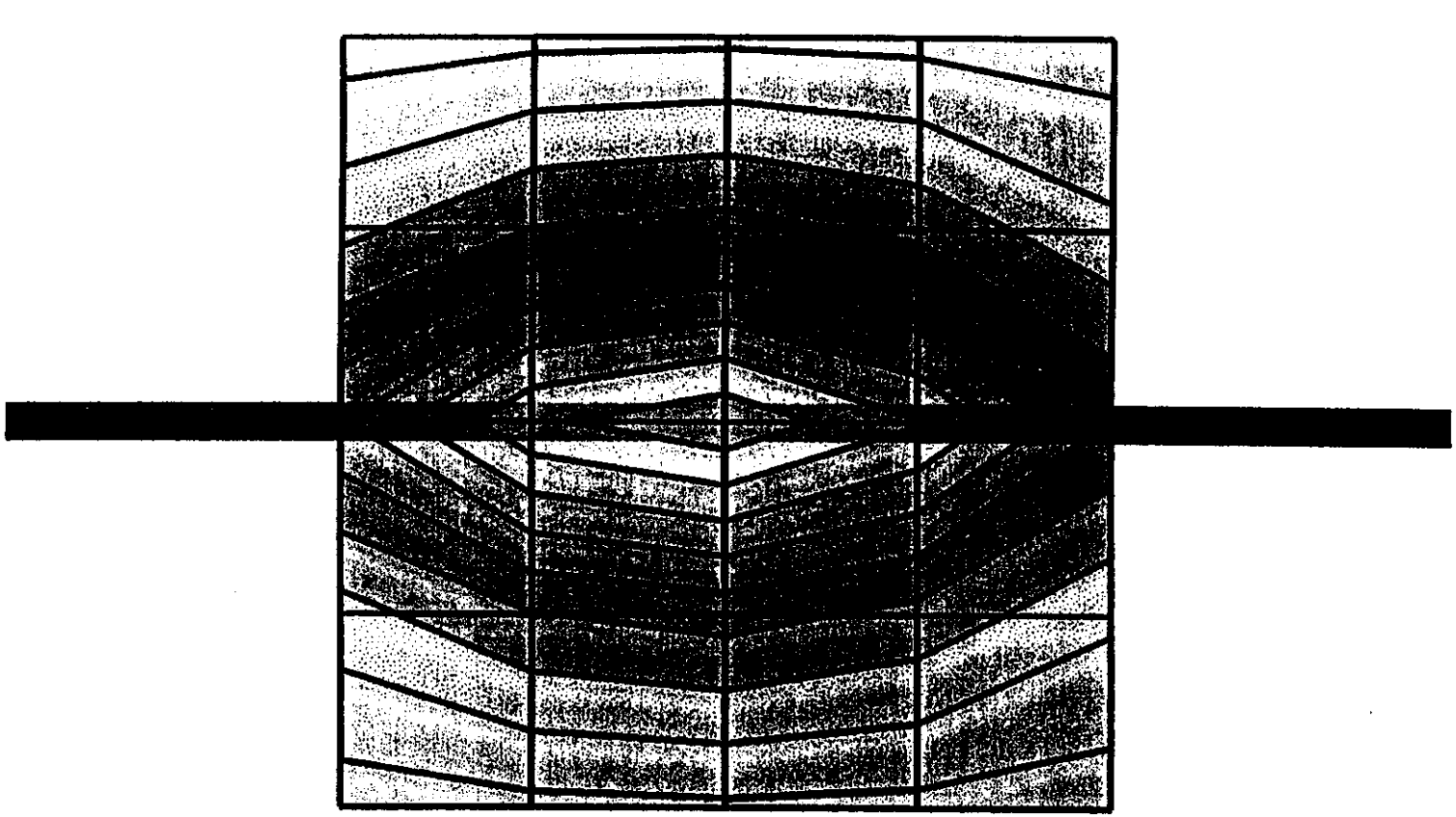

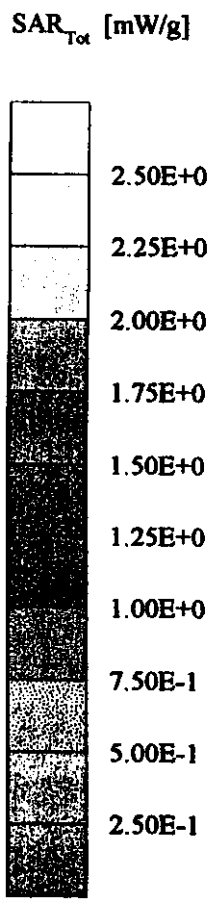

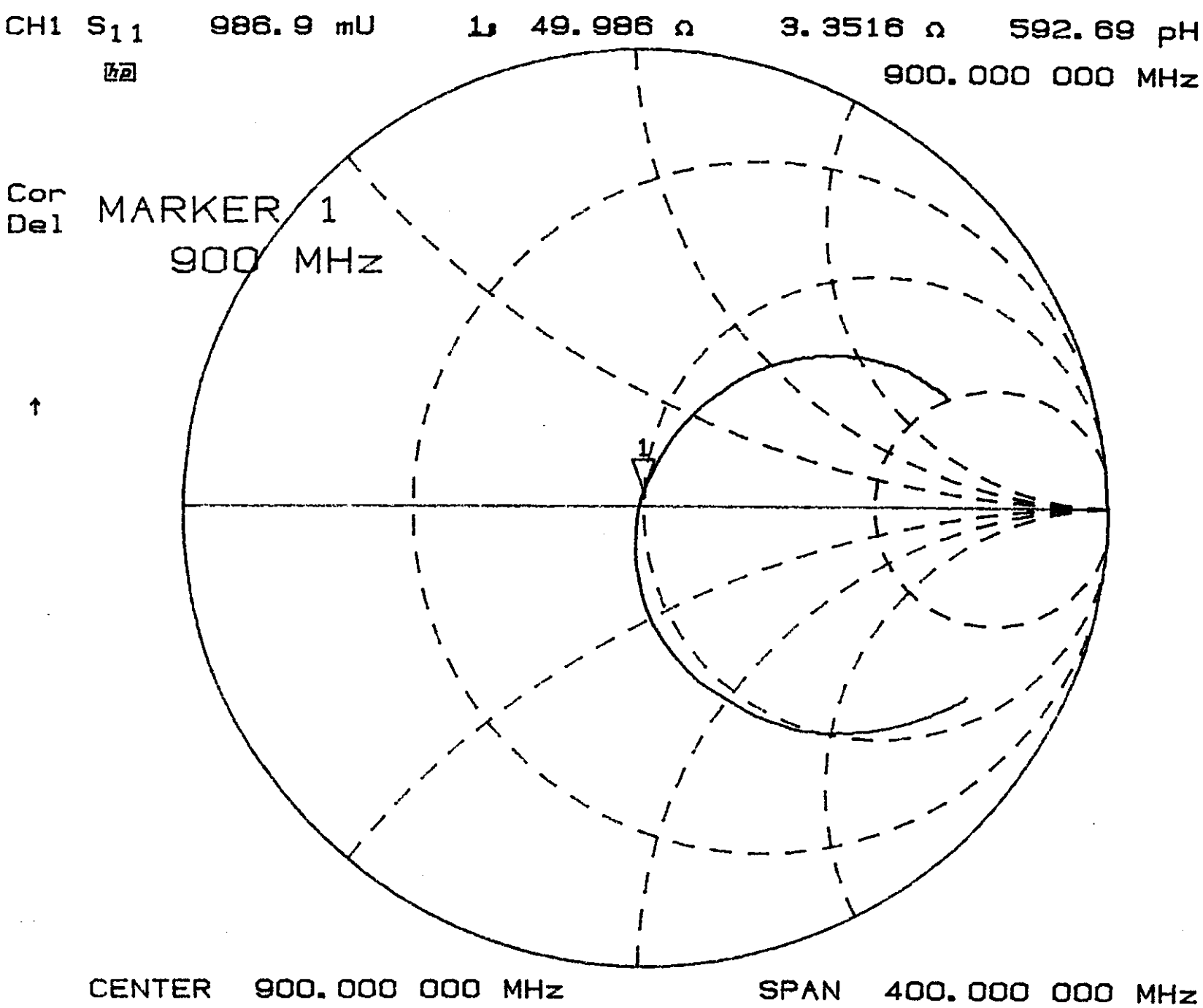
CH1 S11 986.9 mU 1: 49.986 Ω 3.3516 Ω 592.69 pH
900.000 000 MHz
Cor
Del
MARKER 1
900 MHz
CENTER 900.000 000 MHz
SPAN 400.000 000 MHz

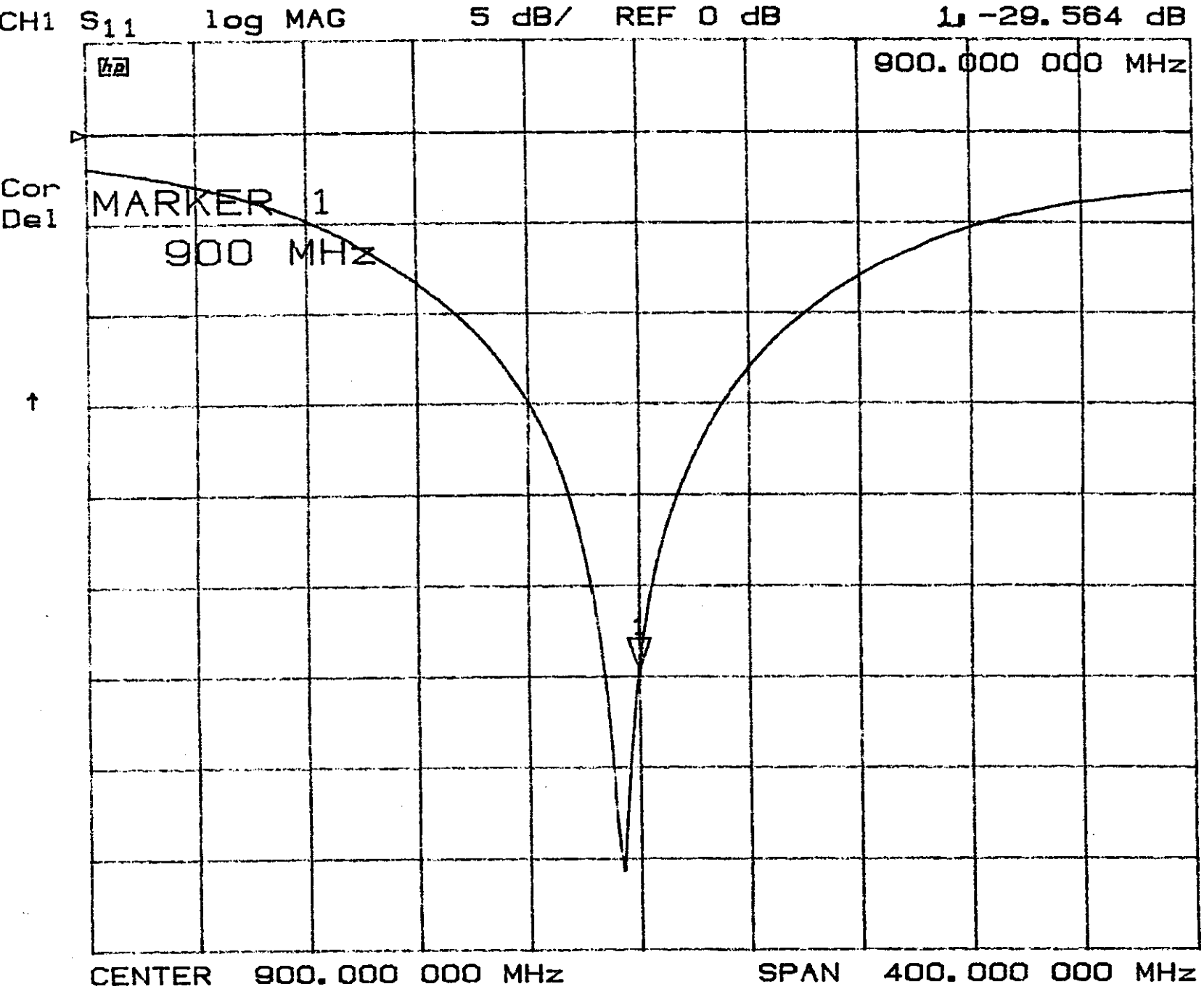
CH1 S11 log MAG 5 dB/ REF 0 dB 1 -29.564 dB
900.000 000 MHz
Cor
Del
MARKER 1
900 MHz
CENTER 900.000 000 MHz
SPAN 400.000 000 MHz

Schmid & Partner
Engineering AG

Staffelstrasse 8, 8045 Zurich, Switzerland, Telefon +41 1 280 08 60, Fax +41 1 280 08 64

DASY3

Dipole Validation Kit

Type: D1800V2

Serial: 207

Manufactured: July 1997
Calibrated: August 1998

1. Measurement Conditions

The measurements were performed in the flat section of the new generic twin phantom (shell thickness 2mm) filled with brain simulating sugar solution of the following electrical parameters at 1800 MHz:

Relative Dielectricity	**40.1**	± 5%
Conductivity	**1.65 mho/m**	± 10%

The DASY3 System (Software version 3.0b) with a dosimetric E-field probe ET3DV4 (SN:1302, conversion factor 4.6) was used for the measurements.

The dipole feedpoint was positioned below the centre marking and oriented parallel to the body axis (the long side of the phantom). The standard measuring distance was 10mm from dipole centre to the solution surface. The included distance holder was used during measurements for accurate distance positioning.

The coarse grid with a grid spacing of 15mm was aligned with the dipole. The 5x5x7 fine cube was chosen for cube integration. Probe isotropy errors were cancelled by measuring the SAR with normal and 90° turned probe orientations and averaging. The dipole input power (forward power) was 250mW ± 3 %. The results are normalised to 1W input power.

2. SAR Measurement

Standard SAR-measurements were performed with the head phantom according to the measurement conditions described in section 1. The results (see figure) have been normalised to a dipole input power of 1W (forward power). The resulting averaged SAR-values are:

averaged over 1 cm^3 (1 g) of tissue:	**37.1 mW/g**
averaged over 10 cm^3 (10 g) of tissue:	**18.5 mW/g**

Note: If the liquid parameters for validation are slightly different from the ones used for initial calibration, the SAR-values will be different as well. The estimated sensitivities of SAR-values and penetration depths to the liquid parameters are listed in the DASY Application Note 4: 'SAR Sensitivities'.

3. Dipole Impedanc and return loss

The impedance was measured at the SMA-connector with a network analyser and numerically transformed to the dipole feedpoint. The transformation parameters from the SMA-connector to the dipole feedpoint are:

Electrical delay:	**1.236 ns**	(one direction)
Transmission factor:	**0.971**	(voltage transmission, one direction)

The dipole was positioned at the flat phantom sections according to section 1 and the distance holder was in place during impedance measurements.

Feedpoint impedance at 1800 MHz:	Re{Z} = **49.9 Ω**
	Im {Z} = **-1.5 Ω**
Return Loss at 1800 MHz	**- 36.0 dB**

4. Handling

The dipole is made of standard semirigid coaxial cable. The centre conductor of the feeding line is directly connected to the second arm of the dipole. The antenna is therefore short-circuited for DC-signals.

Do not apply excessive force to the dipole arms, because they might bend. If the dipole arms have to be bent back, take care to release stress to the soldered connections near the feedpoint; they might come off.

After prolonged use with 40W radiated power, only a slight warming of the dipole near the feedpoint can be measured.

idation Dipole D1800V2 SN:207, d = 10mm

ency: 1800 [MHz]; Antenna Input Power: 250 [mW]
ic Twin Phantom; Flat Section; Grid Spacing: Dx = 20.0, Dy = 20.0, Dz = 10.0
: ET3DV5 - SN1302/DAE3; ConvF(4.60,4.60,4.60); Brain 1800 MHz: σ = 1.65 [mho/m] ε_r = 40.1 ρ = 1.00 [g/cm^3]
s (2): Peak: 18.1 [mW/g] ± 0.02 dB, SAR (1g): 9.27 [mW/g] ± 0.03 dB, SAR (10g): 4.63 [mW/g] ± 0.04 dB, (Worst-case extrapolation)
ration depth: 7.2 (7.0, 7.8) [mm]

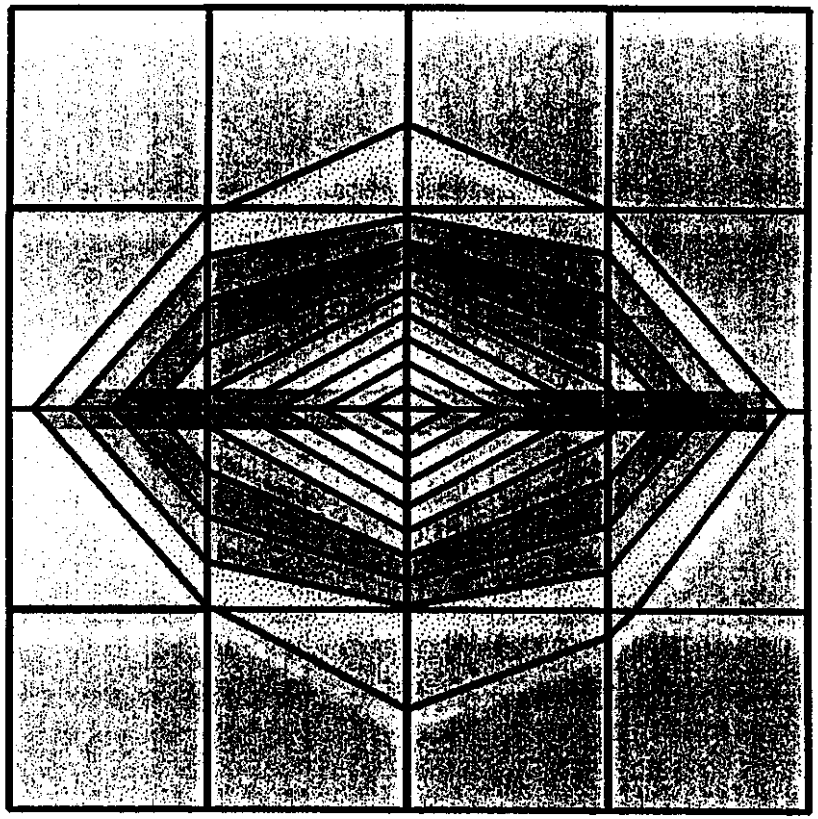

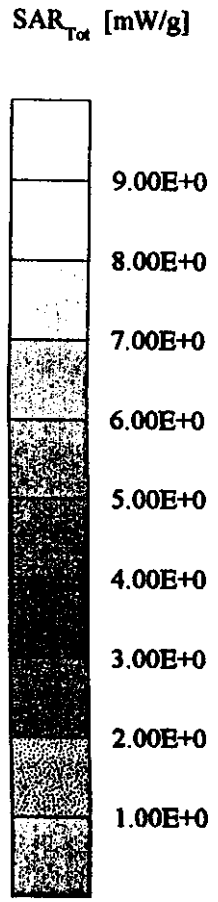

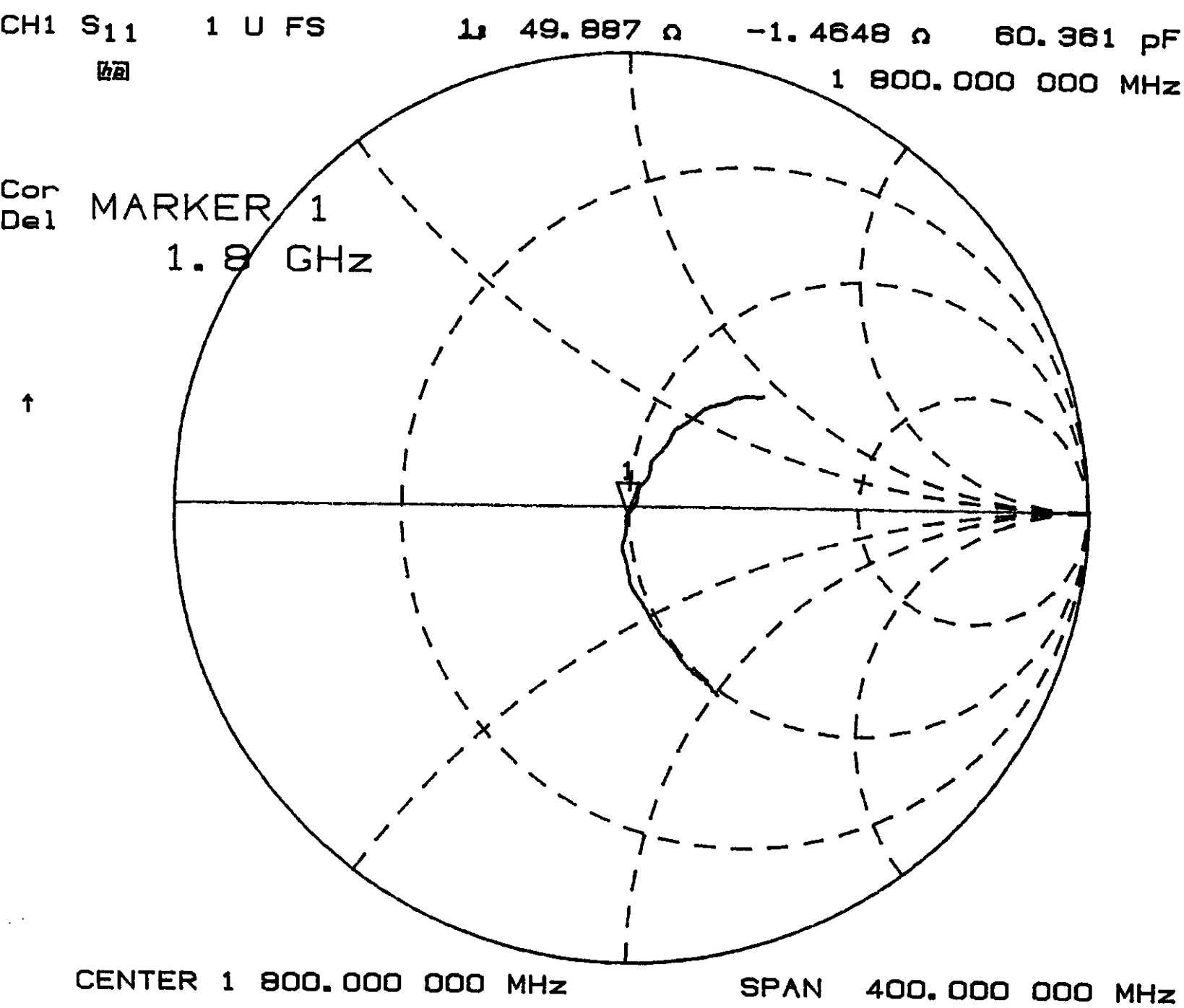
CH1 S11 1 U FS
1: 49.887 Ω -1.4648 Ω 60.361 pF
1 800.000 000 MHz
Cor
Del
MARKER 1
1.8 GHz
CENTER 1 800.000 000 MHz
SPAN 400.000 000 MHz

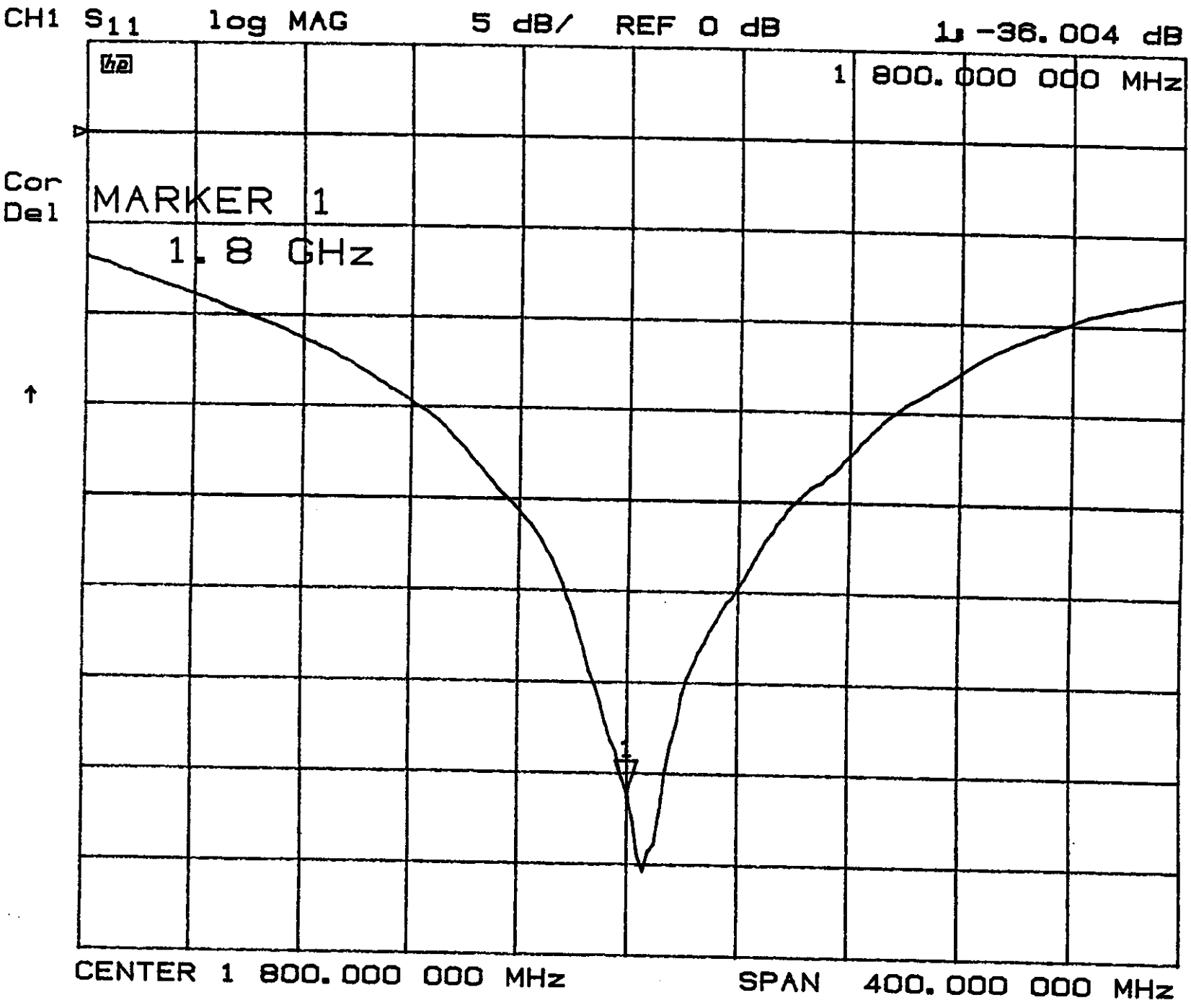
CH1 S11 log MAG 5 dB/ REF 0 dB
1 -36.004 dB
1 800.000 000 MHz
Cor
Del
MARKER 1
1.8 GHz
CENTER 1 800.000 000 MHz
SPAN 400.000 000 MHz

Appendix 9

pages 1 - 2

VERIFY WITH DIPOLE VALIDATION KITS

Verify with Validation Kit (D900V2 SN:003) / Generic flat phantom / f = 900 MHz / Pin = 250 mW / d = 15 mm / 1998-11-16th/NMP, file: val900.mea

σ = 0.86 [mho/m] ε_r = 41.3 ρ = 1.00 [g/cm^3]

Coarse Grid Dx = 20.0 Dy = 20.0 Dz = 5.0 [mm]

SAR [mW/g] Max: 2.35

SAR (1g): 2.39 [mW/g] SAR (10g): 1.55 [mW/g]

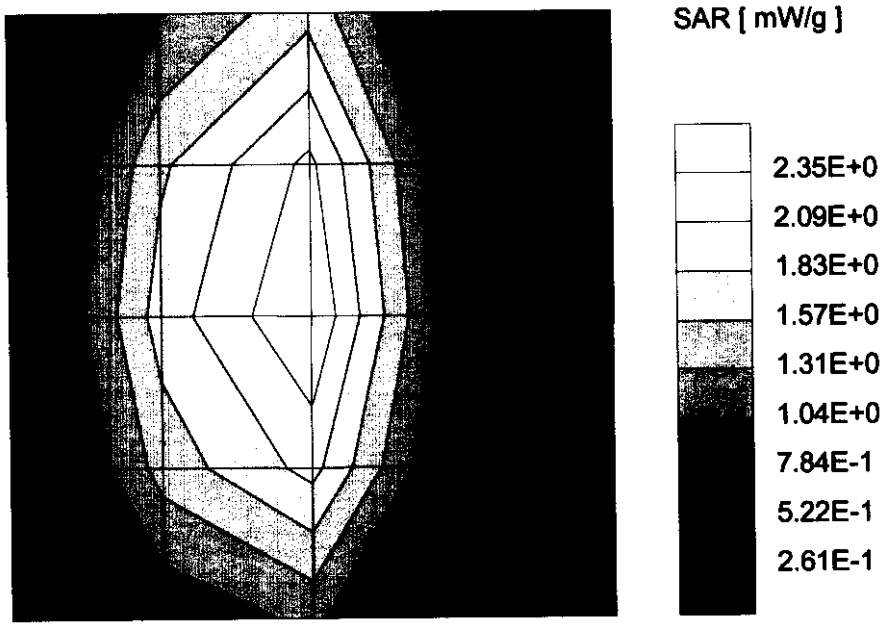

Verify with Validation Kit (D1800V2 SN:207) / Generic flat phantom / f = 1800 MHz / Pin = 250 mW / d = 10 mm / 1998-11-16th/NMP, file: valid.mea

σ = 1.73 [mho/m] ε_r = 40.3 ρ = 1.00 [g/cm^3]

Coarse Grid Dx = 20.0 Dy = 20.0 Dz = 5.0 [mm]

SAR [mW/g] Max: 9.21

SAR (1g): 10.5 [mW/g] SAR (10g): 5.30 [mW/g]

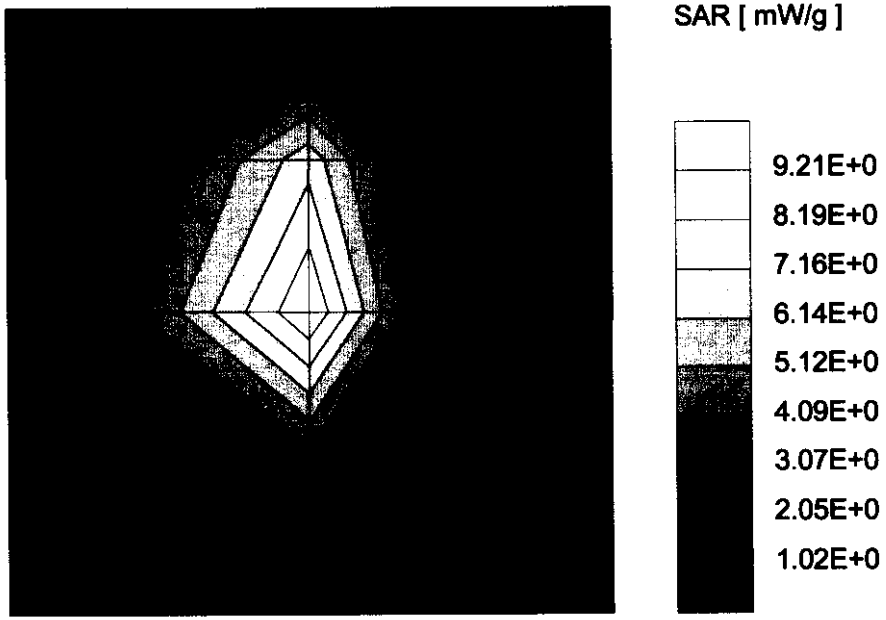

Appendix 10

pages 1 - 10

SAR MEASUREMENT RESULTS

Nr 1, Type: NSD-3AX, Amps mode, Channel 991 (824MHz), Phone position 90°, Measured 1998-11-16th/NMP, file: fca90l.mea

σ = 0.79 [mho/m] ε_r = 42.1 ρ = 1.00 [g/cm^3]

Coarse Grid Dx = 20.0 Dy = 20.0 Dz = 5.0 [mm]

SAR [mW/g] Max: 1.24

SAR (1g): 1.24 [mW/g] SAR (10g): 0.820 [mW/g]

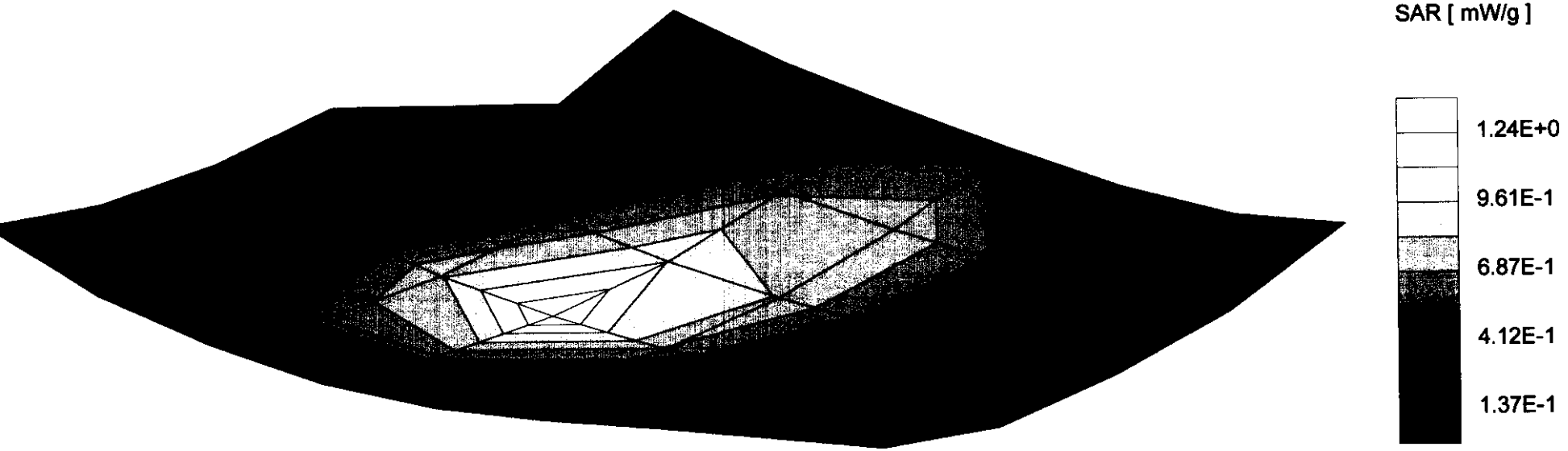

Nr 2, Type: NSD-3AX, Amps mode, Channel 384 (836MHz), Phone position 90°, Measured 1998-11-16th/NMP, file: fca90m.mea

σ = 0.80 [mho/m] ε_r = 41.9 ρ = 1.00 [g/cm^3]

Coarse Grid Dx = 20.0 Dy = 20.0 Dz = 5.0 [mm]

SAR [mW/g] Max: 1.48

SAR (1g): 1.44 [mW/g] SAR (10g): 0.954 [mW/g]

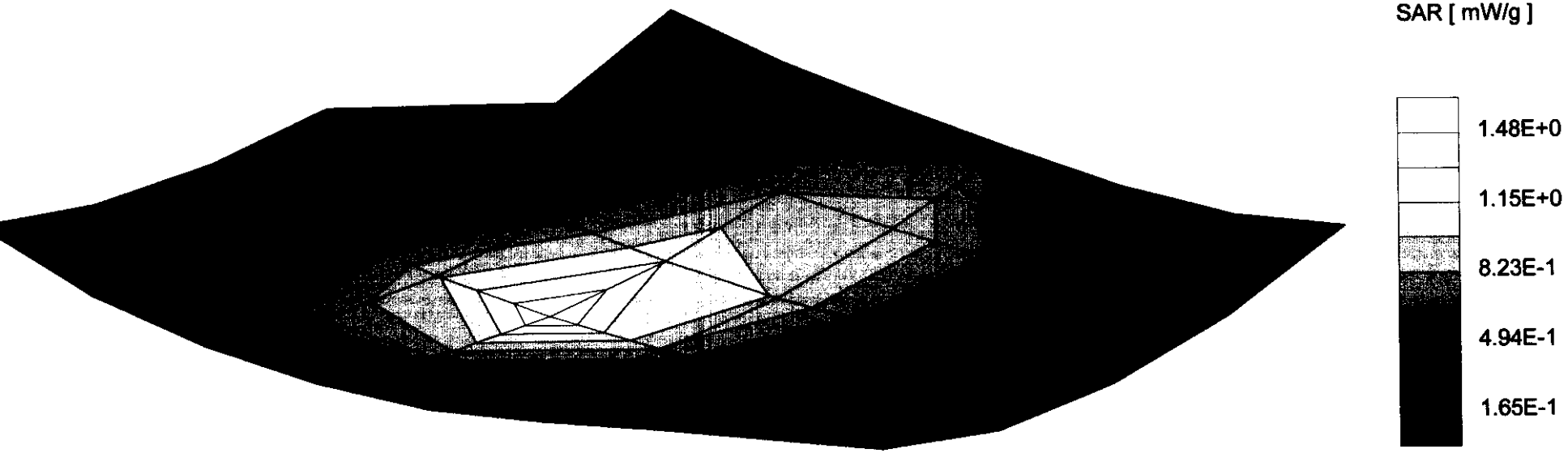

Nr 3, Type: NSD-3AX, Amps mode, Channel 799 (849MHz), Phone position 90°, Measured 1998-11-16th/NMP, file: fca90h.mea

σ = 0.81 [mho/m] ε_r = 41.8 ρ = 1.00 [g/cm^3]

Coarse Grid Dx = 20.0 Dy = 20.0 Dz = 5.0 [mm]

SAR [mW/g] Max: 1.57

SAR (1g): 1.53 [mW/g] SAR (10g): 1.00 [mW/g]

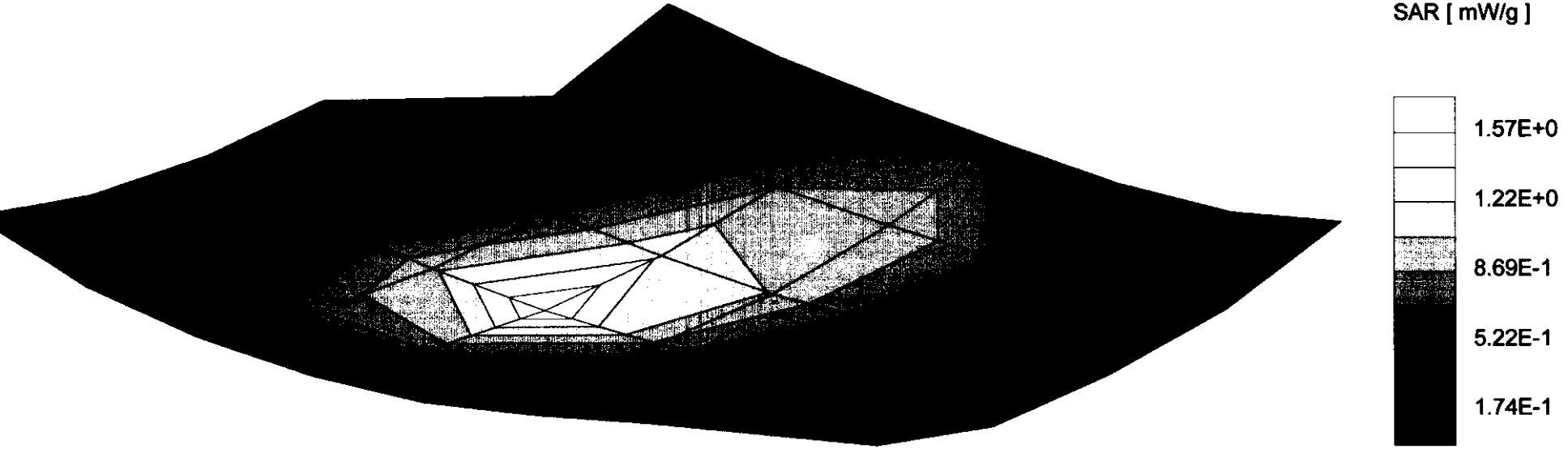

Nr 4, Type: NSD-3AX, CDMA Cellular, Ch. 991 (824MHz), Phone position 90°, Measured 1998-11-16th/NMP, file: ccf90l.mea

σ = 0.79 [mho/m] ε_r = 42.1 ρ = 1.00 [g/cm^3]

Coarse Grid Dx = 20.0 Dy = 20.0 Dz = 5.0 [mm]

SAR [mW/g] Max: 0.90

SAR (1g): 0.924 [mW/g] SAR (10g): 0.618 [mW/g]

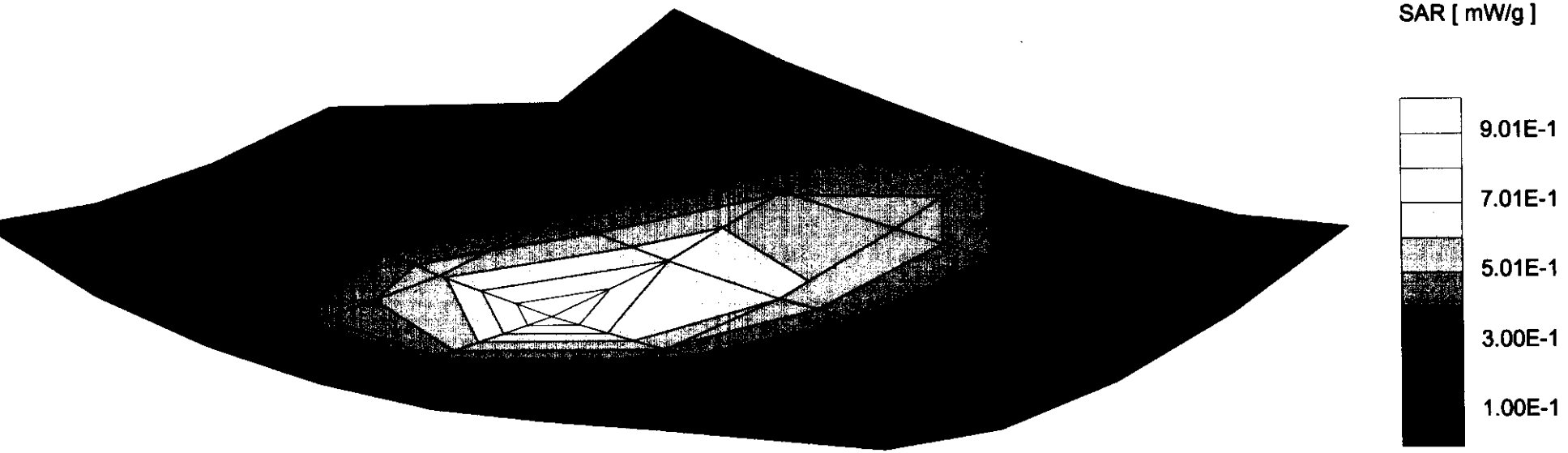

Nr 5, Type: NSD-3AX, CDMA Cellular, Ch. 384 (836MHz), Phone position 90°, Measured 1998-11-16th/NMP, file: ccf90m.mea

σ = 0.80 [mho/m] ε_r = 41.9 ρ = 1.00 [g/cm^3]

Coarse Grid Dx = 20.0 Dy = 20.0 Dz = 5.0 [mm]

SAR [mW/g] Max: 1.05

SAR (1g): 1.02 [mW/g] SAR (10g): 0.672 [mW/g]

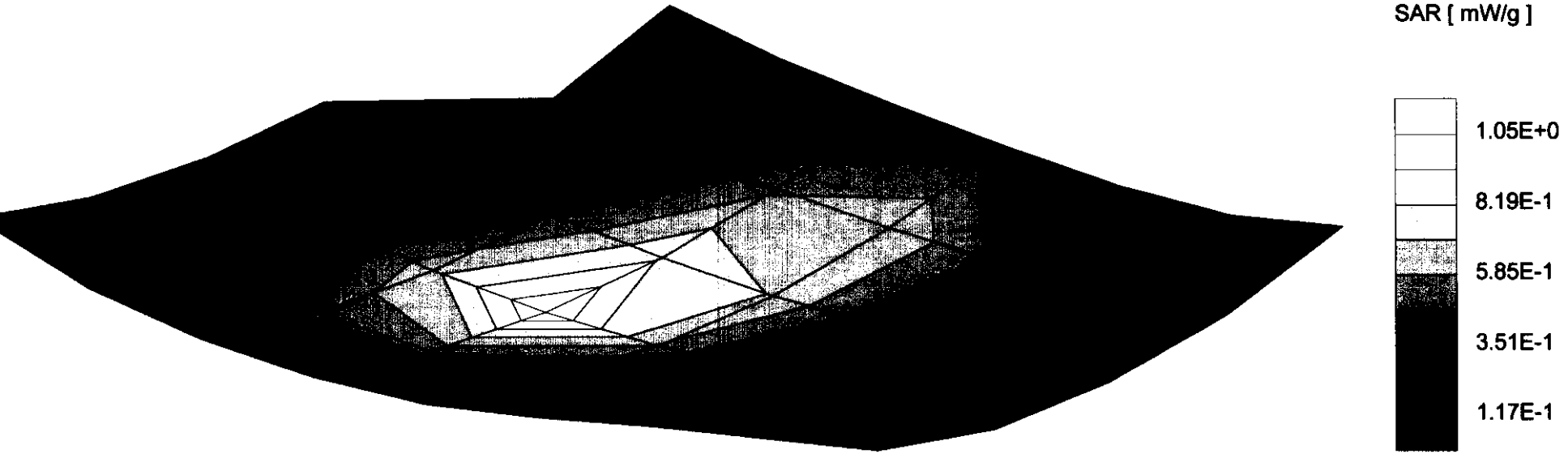

Nr 6, Type: NSD-3AX, CDMA Cellular, Ch. 799 (849MHz), Phone position 90°, Measured 1998-11-16th/NMP, file: ccf90h.mea

σ = 0.81 [mho/m] ε_r = 41.8 ρ = 1.00 [g/cm^3]

Coarse Grid Dx = 20.0 Dy = 20.0 Dz = 5.0 [mm]

SAR [mW/g] Max: 1.00

SAR (1g): 1.07 [mW/g] SAR (10g): 0.698 [mW/g]

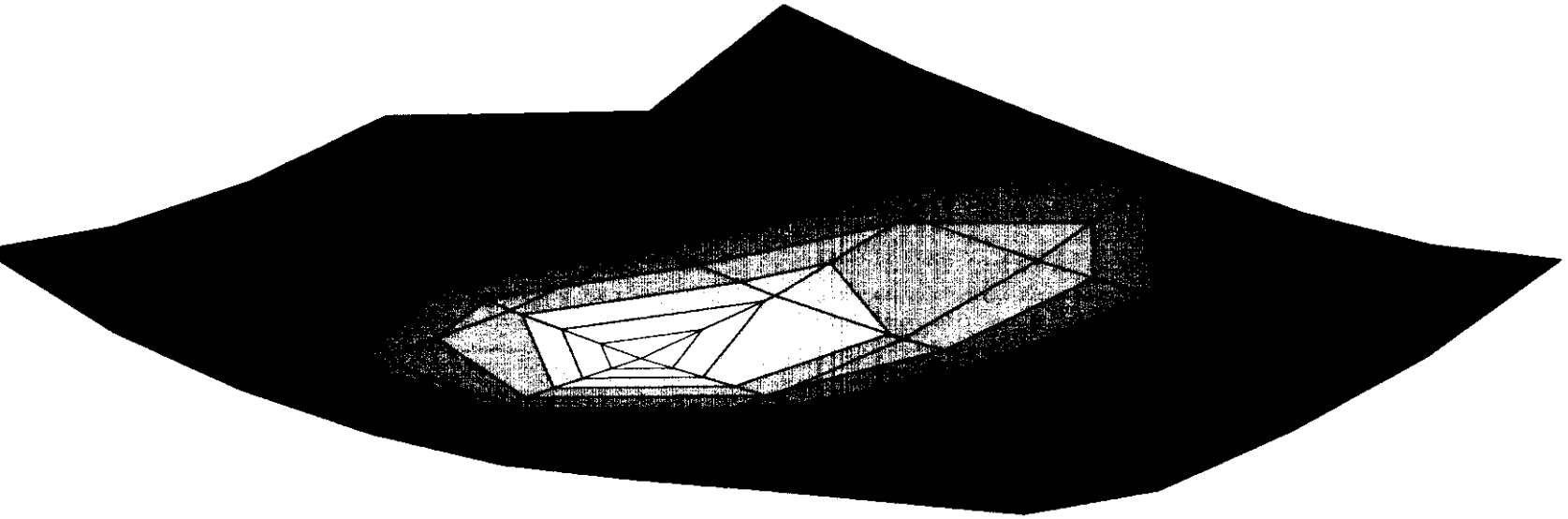

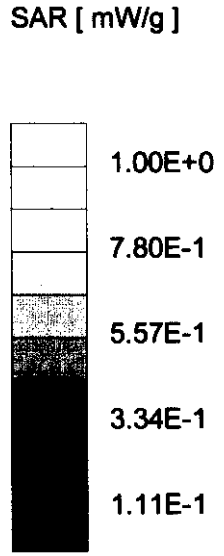

Nr 7, Type: NSD-3AX, CDMA Pcs, Channel 25 (1850MHz), Phone position 90°, Measured 1998-11-16th/NMP, file: fcp90l.mea

σ = 1.75 [mho/m] ε_r = 40.1 ρ = 1.00 [g/cm^3]

Coarse Grid Dx = 20.0 Dy = 20.0 Dz = 5.0 [mm]

SAR [mW/g] Max: 1.17

SAR (1g): 1.14 [mW/g] SAR (10g): 0.639 [mW/g]

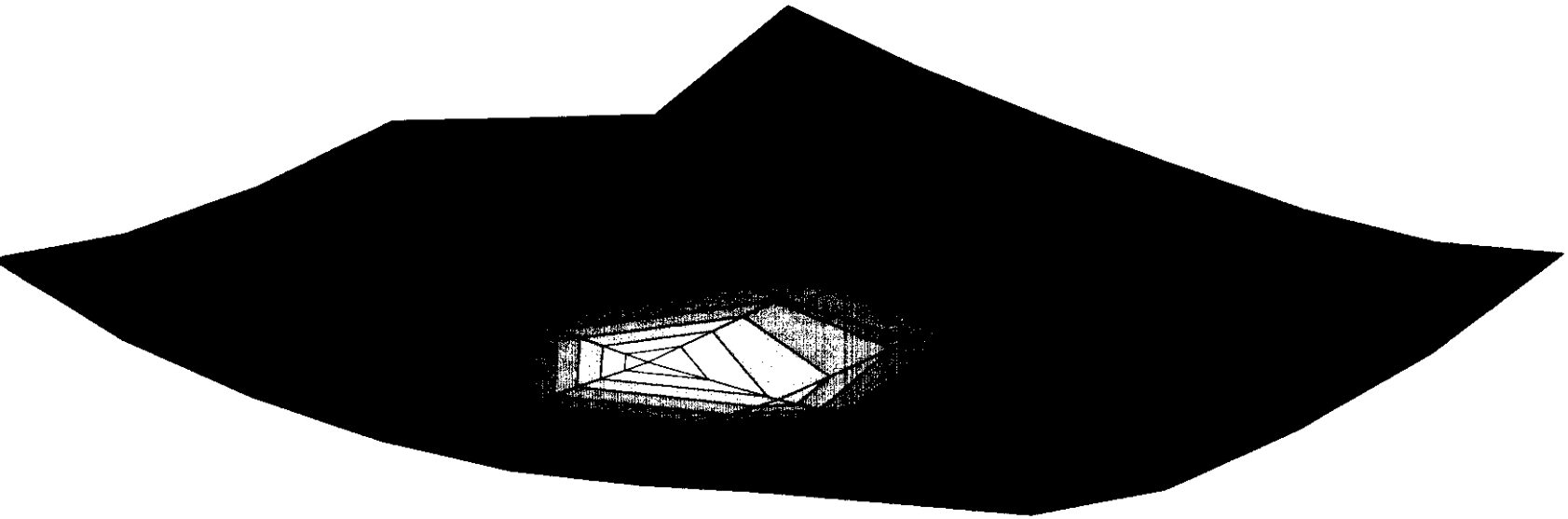

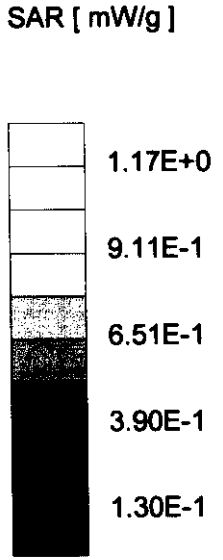

Nr 8, Type: NSD-3AX, CDMA Pcs, Channel 600 (1880MHz), Phone position 90°, Measured 1998-11-16th/NMP, file: fcp90m.mea

σ = 1.78 [mho/m] ε_r = 40.0 ρ = 1.00 [g/cm^3]

Coarse Grid Dx = 20.0 Dy = 20.0 Dz = 5.0 [mm]

SAR [mW/g] Max: 1.26

SAR (1g): 1.20 [mW/g] SAR (10g): 0.665 [mW/g]

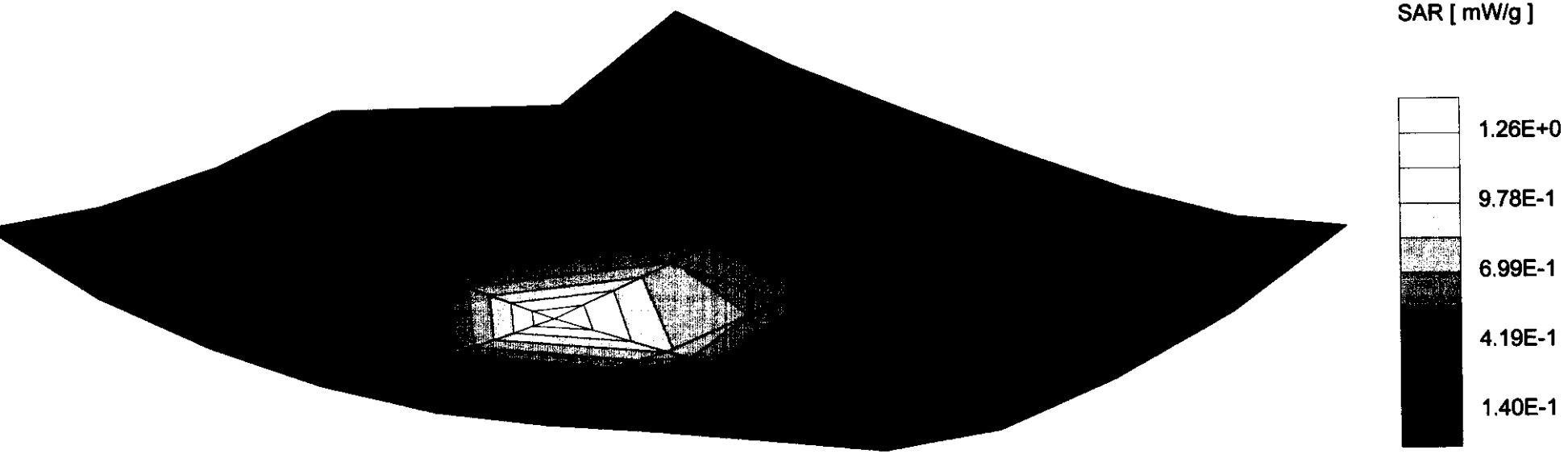

Nr 9, Type: NSD-3AX, CDMA Pcs, Channel 1175 (1909MHz), Phone position 90°, Measured 1998-11-16th/NMP, file: fcp90h.mea

σ = 1.80 [mho/m] ε_r = 39.8 ρ = 1.00 [g/cm^3]

Coarse Grid Dx = 20.0 Dy = 20.0 Dz = 5.0 [mm]

SAR [mW/g] Max: 1.20

SAR (1g): 0.995 [mW/g] SAR (10g): 0.554 [mW/g]

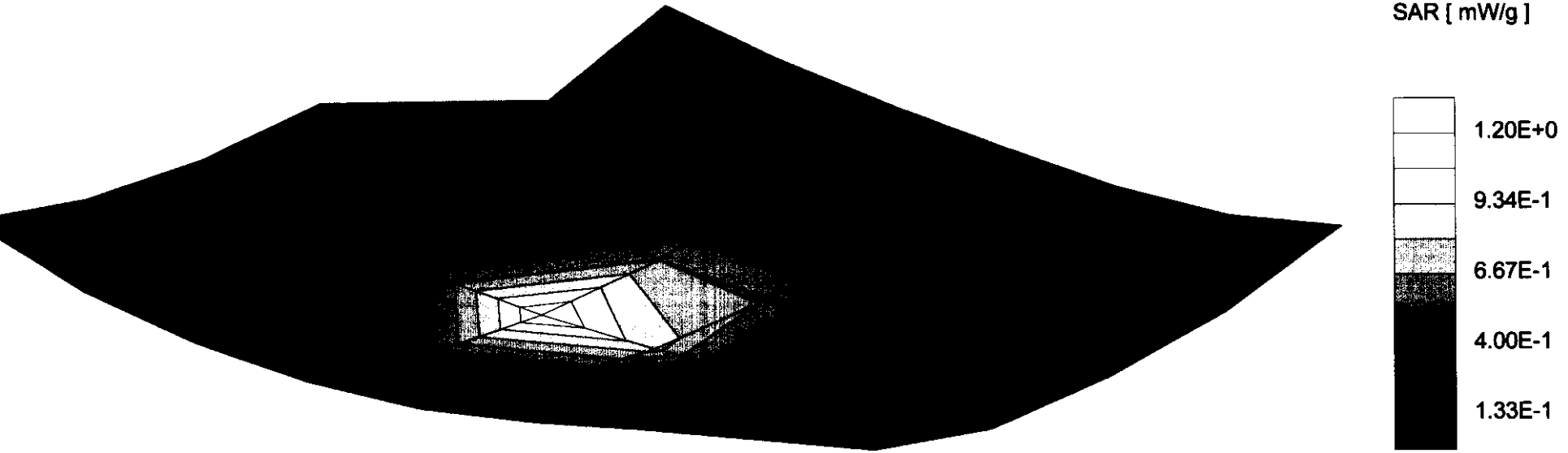

Nr 10, Type: NSD-3AX, Amps mode, Channel 991 (824MHz), Phone position 90°, Measured 1998-11-16th/NMP, file: fca90l.mea

σ = 0.79 [mho/m] ε_r = 42.1 ρ = 1.00 [g/cm^3]

Coarse Grid Dx = 20.0 Dy = 20.0 Dz = 5.0 [mm]

SAR [mW/g] Max: 1.24

SAR (1g): 1.24 [mW/g] SAR (10g): 0.820 [mW/g]